FINAL TECHNICAL REPORT

INVESTIGATION OF DUAL POLARIZATION LASER MODULATION

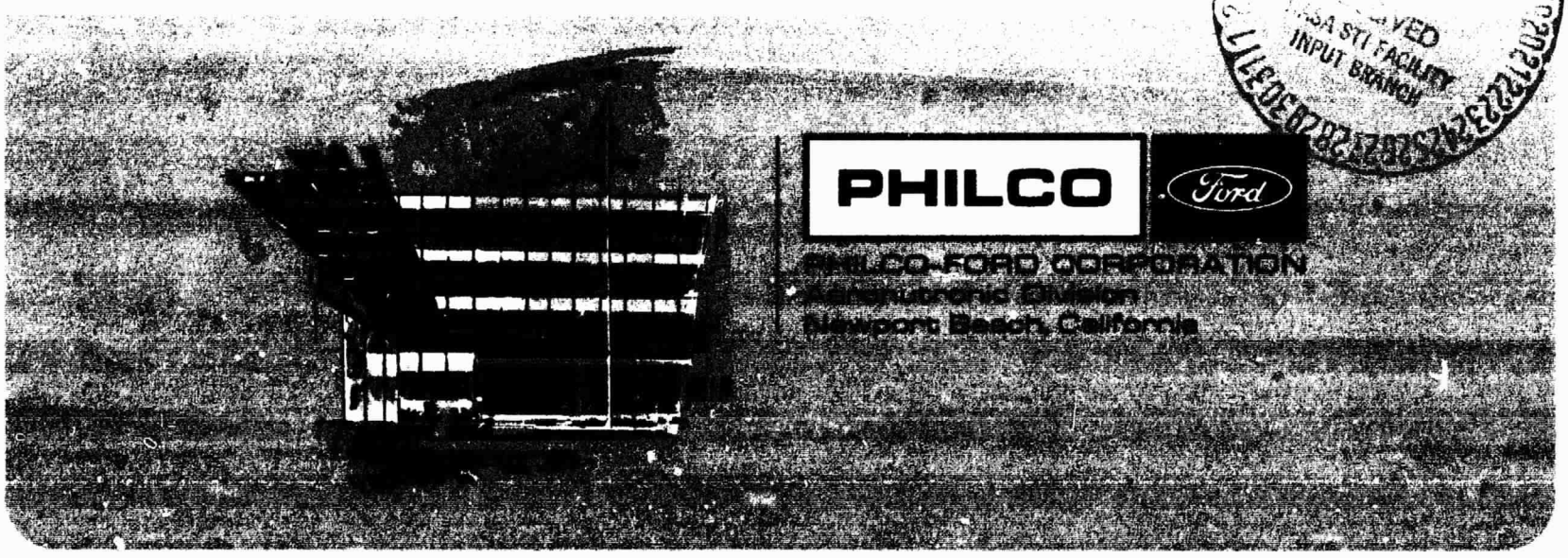

NASA CR 92484

Report No.: U-4559

FINAL TECHNICAL REPORT

INVESTIGATION OF DUAL POLARIZATION LASER MODULATION

Prepared for: NASA Manned Spacecraft Center

Under Contract: NAS-~~9~~7420

Prepared by: W. M. Doyle, W. D. Gerber, and M. B. White
Philco-Ford Corporation
Aeronutronic Division
Newport Beach, California

25 October 1968

Approved by: Paul M. Sutton

Paul M. Sutton, Manager
Physics and Chemistry Laboratory

CONTENTS

LIST OF ILLUSTRATIONS

LIST OF ILLUSTRATIONS (cont)

LIST OF ILLUSTRATIONS (cont)

LIST OF ILLUSTRATIONS (cont)

SECTION I

INTRODUCTION AND SUMMARY

This report covers a one year research program aimed at determining the applicability of the Dual Polarization laser to wide band optical communication. A major part of this program has been devoted to a study of the bandwidth capabilities of a frequency modulated Dual-Polarization laser. Experiments were carried out with 1.15μ and 3.39μ He-Ne lasers, modulation frequencies of up to 20 MHz, and fm bandwidths of up to 130 MHz. The results indicate that the achievable bandwidths are considerably greater than would be anticipated on the basis of the static laser characteristics and that the limitations which do occur are of a type which would have a minimal effect on the operation of an fm communication system. Additional He-Ne experiments demonstrated the active frequency stabilization of the modulated DP laser and determined the effect of modulation on the stabilization characteristics.

In addition to the He-Ne studies mentioned above, a program was undertaken to determine the applicability of the various Dual-Polarization techniques to the CO_2 laser. Although the insufficient mechanical stability of our laser prevented a detailed study of frequency modulation, the results were generally very promising and indicated the possibility of achieving both DPFM and DP frequency stabilization with a considerable range of subcarrier frequencies.

During the course of our experiments it became apparent that a polarization modulation version of the DP system might offer an even greater modulation sensitivity than that obtainable with the fm version. This possibility is particularly significant for CO_2 systems for which highly sensitive modulator materials are not available. Accordingly, we undertook to demonstrate DP Polarization Modulation of a CO_2 laser. It

was found that DPPM could be achieved very easily without requiring frequency stabilization. Modulation was effected at frequencies ranging from zero to 5 MHz with varying degrees of sensitivity. At 1.5 MHz, for example, a drive of 14 Vrms was sufficient to produce over 50% modulation. Reduction of the residual cavity birefringence should further greatly reduce the required drive.

SECTION 2

DUAL POLARIZATION LASER PRINCIPLES

The operation of the Dual Polarization Laser is based on the fact that the presence of a birefringent element in an appropriately designed otherwise isotropic laser cavity causes each cavity resonance to split into two components corresponding to orthogonal polarization states and having a frequency separation proportional to the magnitude of the birefringence.[1] The sensitivity of the laser frequency and polarization characteristics to the nature and magnitude of the intracavity birefringence makes possible a number of techniques for practical application of such devices. Some examples to be discussed below are: DP Frequency Modulation, which results when the birefringent phase shift is varied; DP Polarization Modulation, which utilizes a variation in the direction of the birefringent axes, and DP Frequency Stabilization.

A typical DP laser is shown schematically in Figure 1. For the sake of generality we have included both circular and linear birefringence. These are indicated in the form of Faraday Rotation and the electro-optical effect respectively. It can in fact be shown that any arbitrary combination of birefringent elements is equivalent to a combination of one Faraday rotator, one linear birefringent element, and one optically active element.[2] Optical activity, however, does not affect the resonant structure of the Fabry-Perot cavity and thus can be excluded from further consideration.

The laser discharge tube indicated in Figure 1 utilizes windows oriented normal to the direction of light propagation rather than at Brewster's angle as is more common. The Brewster windows minimize the reflection losses for one state of linear polarization but at the same time restrict oscillation to that state. In the DP laser the reflection losses are

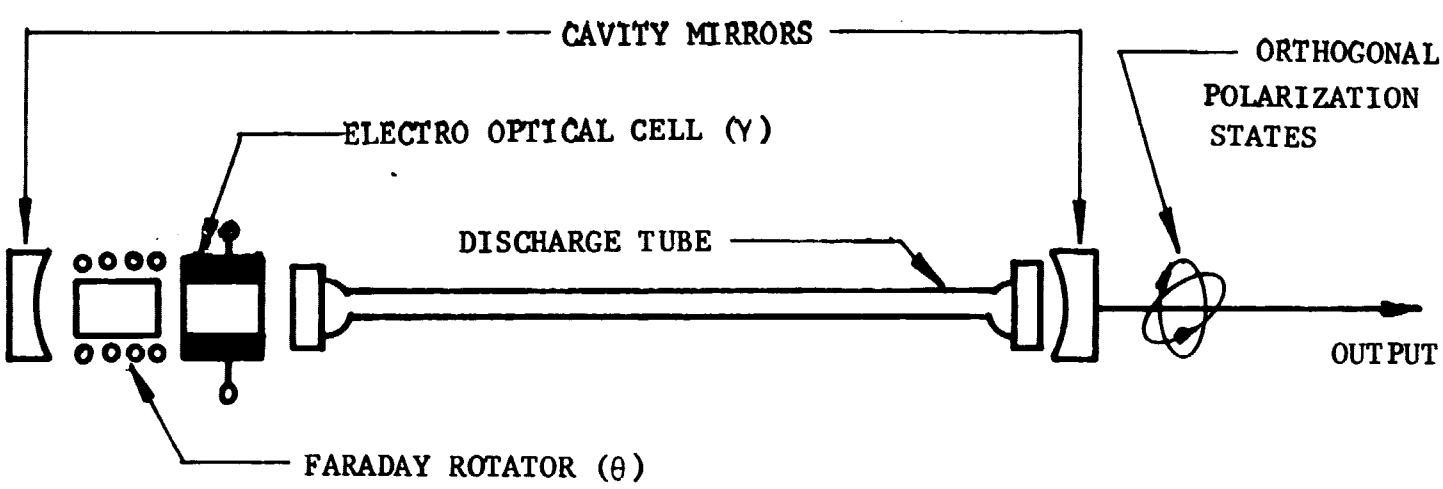

FIGURE 1. DUAL POLARIZATION LASER.

minimized either by utilizing antireflection coatings or by orienting the windows in such a way as to allow the reflections from the two surfaces of each window to cancel.

The output characteristics of any laser are determined jointly by the gain profile of the lasing atomic transition, the spectrum of cavity resonances, and nonlinear interactions between the optical modes. In Figure 2 we see a possible sequence of DP cavity modes superimposed on a Doppler gain curve. The width of the gain curve may be anywhere from 30 to 1500 MHz depending upon the transition involved. The separation between successive longitudinal modes is determined by the cavity length, L:

$$\nu_n - \nu_{n-1} = c/2L, \qquad (1)$$

where c is the speed of light. In our experiments this "intermode spacing" is typically 250 MHz.

For the general DP laser under discussion the frequency splitting between a given pair of orthogonal cavity modes is given by the expression

$$\Delta\nu = (c/2\pi L)\cos^{-1}(\cos 2\theta \cos 2\gamma) \qquad (2)$$

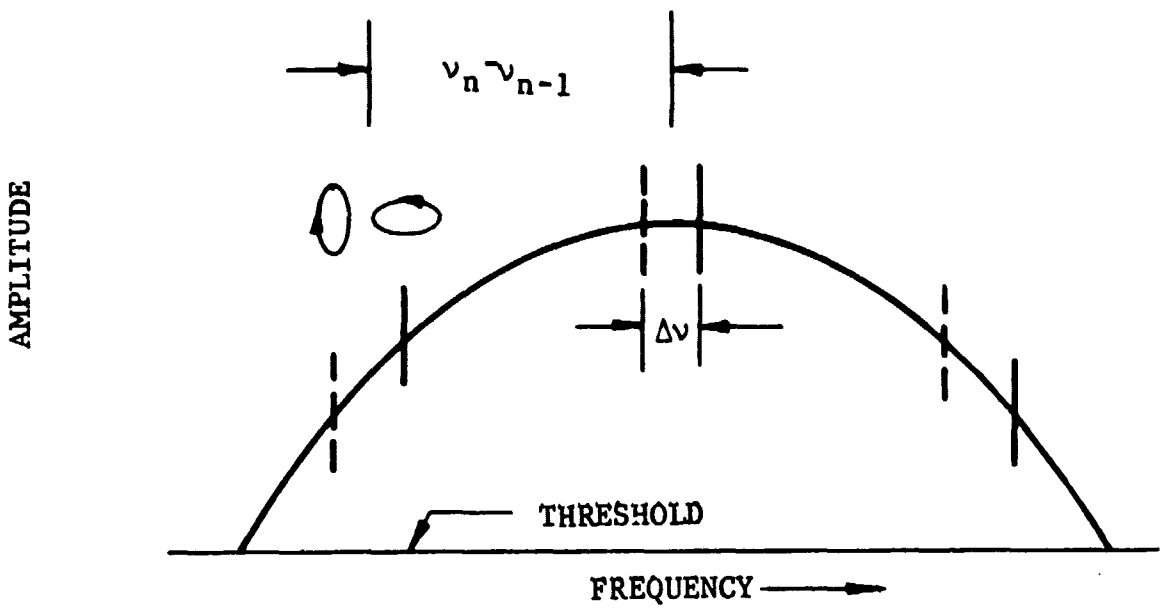

FIGURE 2. TYPICAL DUAL POLARIZATION MODE SPECTRUM.

where 2θ and 2γ are the single pass circular and linear birefringent phase shifts respectively. The ellipticity of the polarization states is given by the expression

$$r = \sin 2\theta / [(1-\cos^2 2\theta \cos^2 2\gamma)^{\frac{1}{2}} + \cos 2\theta \cos 2\gamma], \qquad (3)$$

where r, the ratio of minor to major axis of either state, varies from zero (plane polarization) for pure linear birefringence to one (circular polarization) for pure Faraday rotation. Finally, the axes of the polarization ellipses are always parallel and perpendicular to the optic axis of the net linear birefringence.(3)

In addition to the above cavity resonance conditions, a knowledge of the nonlinear interactions between the optical modes is necessary in order to predict the behavior of a DP laser. These interactions give rise to small departures from the predictions of Equations (2) and (3) and determine the intensities of the various oscillations. Most significantly they determine the conditions under which both members of a given pair of modes can oscillate simultaneously. A comprehensive theoretical treatment of a Dual-Polarization Laser has been given previously.(4) Below

we will summarize those results which are pertinent to the present program. We will assume a DP laser having a sufficiently short cavity length to restrict oscillation to a single pair of modes. We will also assume that the anisotropic effects are passive and independent of frequency and that the laser polarization states do not deviate significantly from the predictions outlined above.

To third order the optical field amplitudes of a two mode laser are determined by the equations

$$\dot{E}_1 = \alpha_1 E_1 - \beta_1 E_1^3 - \theta_{12} E_1 E_2^2 \tag{4}$$

and

$$\dot{E}_2 = \alpha_2 E_2 - \beta_2 E_2^3 - \theta_{21} E_2 E_1^2 \tag{5}$$

where the parameters α_i, and β_i, and θ_{ij} $(i, j = 1,2/2,1)$ depend on the mode frequencies and polarization states, on the nature of the particular atomic transition involved, and on the population inversion and cavity loss. In steady state these equations have the solution

$$E_i^2 = (\alpha_i \beta_j - \alpha_j \theta_{ij})/(\beta_i \beta_j - \theta_{ij} \theta_{ji}) \tag{6}$$

as long as the indicated values of both E_1^2 and E_2^2 are positive, and the solution

$$E_i^2 = \alpha_i/\beta_i, \; E_j^2 = 0 \tag{7}$$

if either vanishes. The condition for simultaneous oscillation of both modes (weak coupling) is clearly

$$\beta_1/\theta_{21} \geq \alpha_1/\alpha_2 \geq \theta_{12}/\beta_2. \tag{8}$$

In the case of orthogonal polarization of $\underline{E}_1$ and $\underline{E}_2$ (the Dual-Polarization case) the parameters appearing in the above equations are given approximately by

$$\alpha_i = c_g \; \mathrm{Im} \; Z \; (\nu_i - \omega) - c_\ell, \tag{9}$$

$$\beta_i = k\, Q_i(\nu_i - \omega)\left[B + C + D\,(1-r_i^2)^2/(1+r_i^2)^2\right] \tag{10}$$

and

$$\theta_{ij} = k\left[BM_{ij} + CM'_{ij} + D(M_{ij} + M'_{ij})\,(4r_i^2/(1 + r_i^2)^2)\right] \tag{11}$$

where c_g, c_ν, and k are constants; Z is the plasma dispersion function, r_i is the ratio of minor to major axis of the elliptical polarization state; B, C, and D depend upon the angular momentum eigen-values of the atomic states involved; and Q_i, M_{ij}, and M'_{ij} depend upon the atomic line widths, the mode frequencies and the mean transition frequency, ω.

If we specialize to the limiting case of zero frequency splitting it can be shown that $\alpha_1 = \alpha_2$, $\beta_1 = \beta_2$, and

$$\theta_{12} = \theta_{21} = F\,\beta_1 \tag{12}$$

where

$$F = \left[B + C + 8\,Dr^2/(1 + r^2)^2\right] \Big/ \left[B + C + D(1 - r^2)/(1 + r^2)^2\right] \tag{13}$$

The weak coupling condition thus becomes

$$F \leq 1, \tag{14}$$

which is dependent only on the ellipticity parameter, r, and the atomic angular momenta. In this limit the coupling is either weak or strong for all cavity tunings depending on the value of F.

Since the frequency splitting is not identically zero, the coupling strength will in practice depend on tuning, generally being weaker than that indicated by Equation 11 at central tuning and stronger far from central tuning. Thus is F = 1, for example, we would expect both E_1 and E_2 to exist in the vicinity of central tuning, whereas on either side of this tuning only the mode closest to the center would oscillate.

The experimental studies described below used only linear birefringence. Thus $\theta = 0$, $r = 0$, and Equation (2) becomes

$$\Delta\nu = \frac{c\gamma}{2\pi L} \, . \tag{15}$$

In addition the atomic transitions involved in both of the He-Ne lines and the CO_2 line are characterized by positive values of B and C and negative values of D so that at zero frequency splitting $F > 1$ and strong coupling would be expected to occur. Weak coupling would of course occur for splittings large compared to the atomic linewidth, in which case $\theta_{ij} < \beta_{ij}$. The splitting at which the transition from strong to weak coupling takes place will depend on the actual values of B, C, and D as well as on the collision broadened linewidths.

The general behavior outlined above is consistent with the operation of He-Ne DP lasers which we have studied. In contrast, however, the results of the CO_2 experiments to be described in Section 5 of this report appear to conflict with the theoretical predictions in that weak coupling was observed for all of the frequencies studied. This suggests the desirability of a detailed theoretical study of the CO_2 laser.

SECTION 3

DUAL POLARIZATION FREQUENCY MODULATION STUDIES

3.1 INTRODUCTION

The basic DPFM communication system is shown schematically in Figure 3. A single pair of perpendicular linearly polarized laser oscillations (frequencies ν_1 and ν_2) is established by the presence of an electro-optical birefringent modulator within the laser cavity. The frequency difference ($\nu_1 - \nu_2$) which serves as an rf subcarrier is adjusted by means of a dc bias on the crystal, and fm information is superimposed on the subcarrier by a conventional ac driver. After passing through a polarization analyzer located either at the transmitter or the receiver, the signal is demodulated by means of a photo detector and an fm radio receiver.

The attractiveness of the DPFM approach to laser modulation stems partly from the extreme modulation sensitivity resulting from the use of an intracavity birefringent modulator and partly from the transmitted reference fm nature of the output, which renders the system relatively insensitive to the effects of atmospheric turbulence. This turbulence insensitivity has been demonstrated previously.[5] However, prior to the present program our DPFM studies were restricted to relatively low modulation frequencies and bandwidths. The effort to be described below thus has been concerned primarily with determining the bandwidth capabilities of the system.

Clearly the first factor which must be considered in determining the system bandwidth is the range of subcarrier frequencies which can be established. For the lasers to be discussed in this section this range will be limited at the low end by the strong coupling phenomena discussed

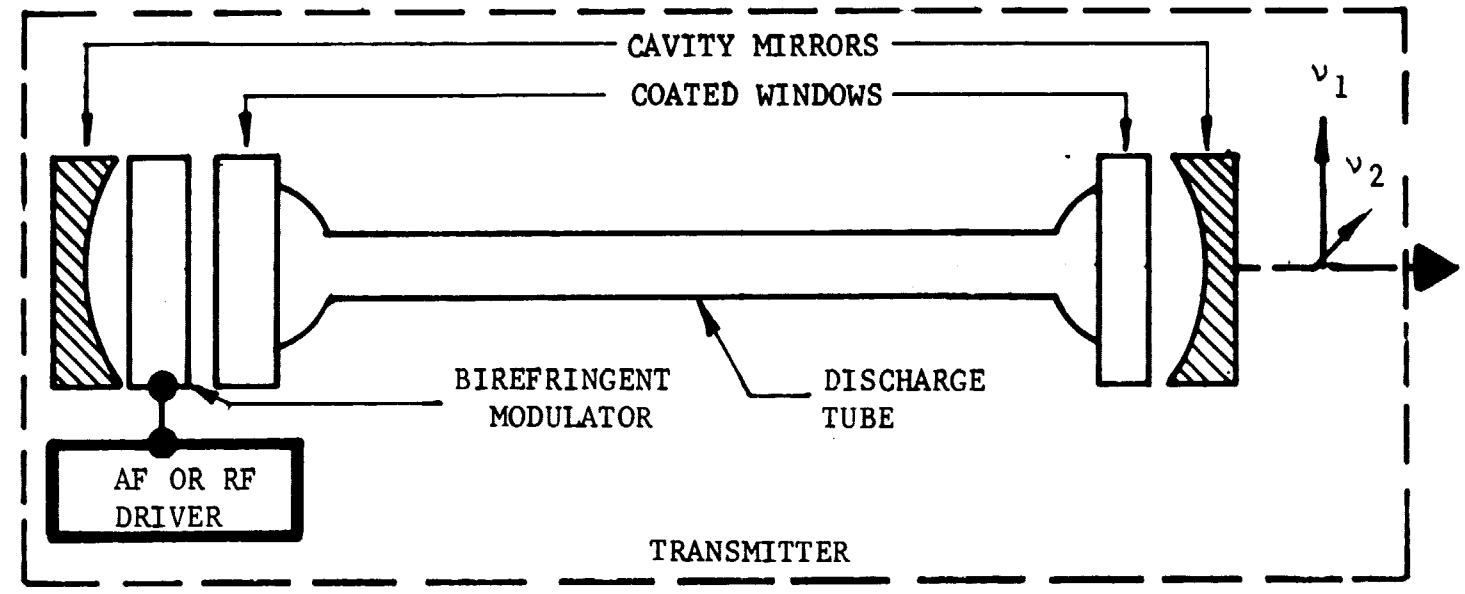

FIGURE 3. DPFM COMMUNICATION SYSTEM

in Section 2. At the high end the range will be limited ultimately by the width of the excess gain curve. However, in cases for which the excess gain width and the cavity length are such as to make possible the simultaneous establishment of two or more subcarriers, the range of subcarrier frequencies will be determined by the complex interplay of mode competition effects and the gain characteristics. Finally, the existence of any frequency dependent losses in the laser cavity will effect the subcarrier behavior.

The modulation response characteristics of the system at low driving frequencies can be determined adequately by studying the static dependence of the subcarrier intensity on frequency. At higher frequencies, however, the behavior is expected to become quite different, and a number of limiting factors must be considered individually. These are:

1. Strong coupling phenomena at low subcarrier frequencies.
2. Subcarrier switching phenomena.
3. Frequency dependent gain or loss.
4. Cavity mode width limitations.

The first three of these factors are expected to become less severe as the modulation frequency increases. The last factor should be important only at quite high frequencies and bandwidths.

The expected decrease in the importance of factors 1 and 2 results from the fact that a finite time is required for mode buildup and decay. Thus, if the time dependent frequency splitting excurts into a region where the static behavior suggests that one mode should be surpressed (1) or where a different subcarrier is favored (2) the signal will be sustained for some time. Since the oscillations will be in a state of unstable equilibrium, this time will depend quite critically upon their initial balance and may under some conditions be much longer than either the cavity ringing time or the time usually required for an isolated mode to build up from zero intensity.

The effects of frequency dependent loss or gain at high frequencies will depend upon the ringing time associated with the active resonant cavity. As the effective cavity length is changed, the optical signals in the cavity will be parametrically shifted in frequency and will tend to follow the change in resonant frequency. If the cavity resonant frequency excurts to a point where the atomic gain is exceeded by the cavity losses, the parametrically shifted optical signal will start to decay. The decay time, however, will depend upon the gain deficiency and may in some cases be quite long compared to the modulation period.

The bandwidth limitation imposed by the cavity mode width is not as severe as might at first be expected. This is a result of the parametric frequency shift mentioned above. In fact, it can be shown that

to first order in the ratio of the modulation frequency to the intermode frequency (c/2L) the laser oscillation will exactly follow the cavity resonance frequency.[6]

Since the theoretical study of the bandwidth limitations discussed above would involve a number of uncertainties, the work reported below has been concerned primarily with the experimental evaluation under realistic operating conditions. These conditions are sufficiently typical, however, to give the results a fairly general validity.

3.2 EXPERIMENTAL APPARATUS AND PROCEDURES

The equipment used for the purpose of studying response characteristics and modulation techniques is shown in Figure 4. The basic configuration indicated was applicable to both the rare-gas and CO_2 studies. A typical crystal mount is illustrated in Figure 5. Figures 6 and 7 are a photograph of the He-Ne system and the modulator mount used in both cases. Figure 8 shows a typical dual-polarization laser tube. The ensuing description of equipment involved pertains to both systems and is followed, where applicable, by specific references to modifications required in each case.

The laser was adjusted to operate in a dual-polarization mode with the modulator crystal present in the cavity. A ceramic transducer driven at 60 Hz by a Variac/transformer combination permitted the cavity length to be swept a distance of approximately 12 microns. The resulting output of the laser was displayed through the use of a Hewlett Packard 450A low-frequency amplifier and an oscilloscope. Optimum adjustment of the cavity was determined by observing the balance between the mode structure of the two polarization states. The equipment thus utilized is shown in dotted lines on Figure 4. In the course of these initial adjustments a cavity length was chosen which resulted in the desired intermode frequency; mirror transmissivities were selected to give the proper cavity "Q"; the aperture size was adjusted to eliminate off-axis modes; and the laser drive was optimized to give the greatest output. The modulator crystal orientation was temporarily established at this time by optimizing the trade-off between maximum cancellation of reflections through interference and the minimum residual birefringence. This position was further optimized later by maximizing the electro-optical response. Further description of these adjustments is given in later sections.

A quartz lens focused the laser output through a polarizer and onto a detector. The detectors used were an RCA 7102 photomultiplier, a Philco L4530 Indium Arsenide diode, and either a gold doped (Philco GPC 215) or copper doped (Santa Barbara Research) Germanium diode for 1.15 micron, 3.39 micron, and 10.6 micron studies respectively. The detected signal corresponding to the cross-beat between the orthogonally polarized modes was amplified by a Keithy Model 110 unity-gain stage followed by either a Keithy Model 108 or a Hewlett-Packard Model 462A amplifier, resulting in an

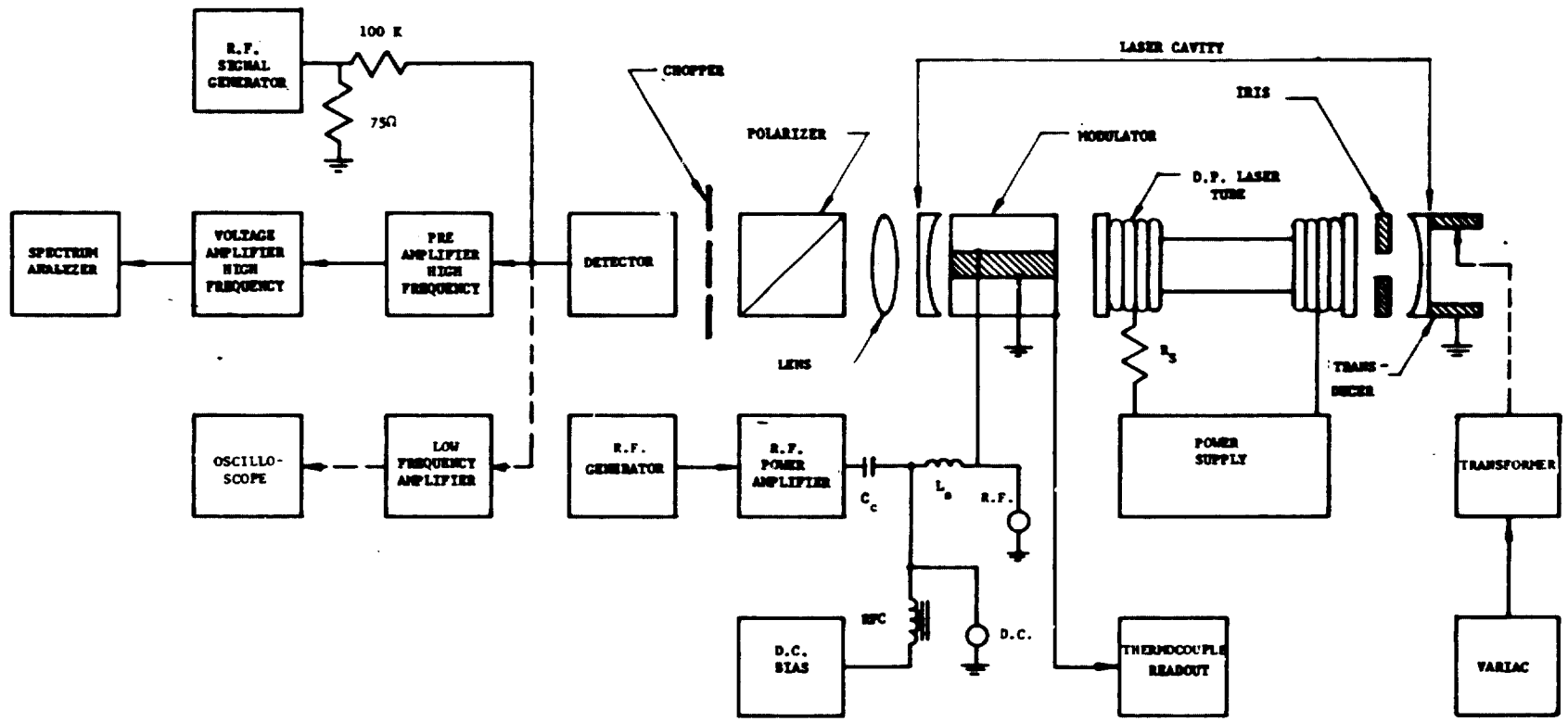

FIGURE 4. APPARATUS USED FOR MODULATION STUDIES

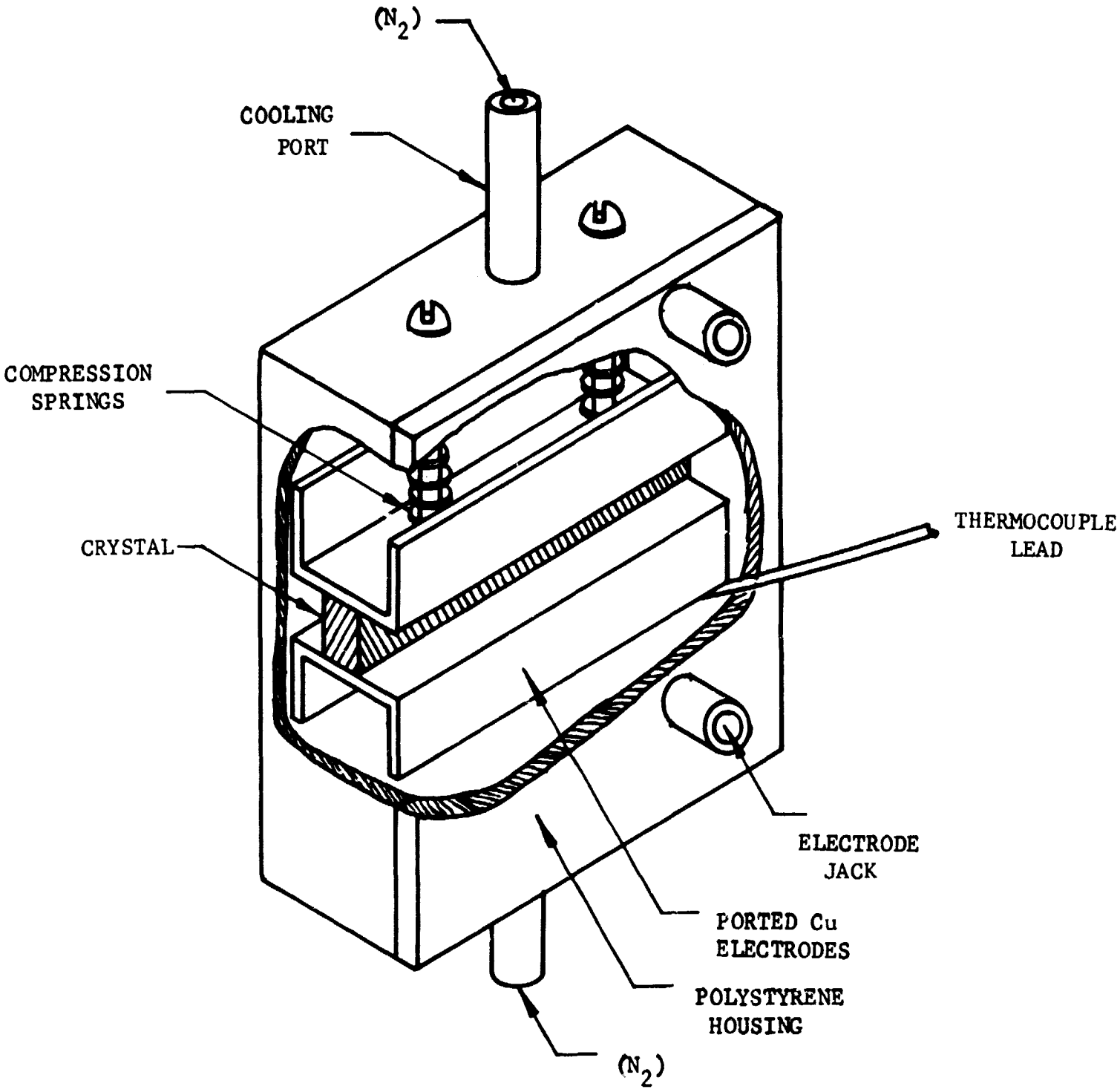

FIGURE 5. MODULATOR MOUNT.

FIGURE 6. He-Ne EXPERIMENTAL EQUIPMENT

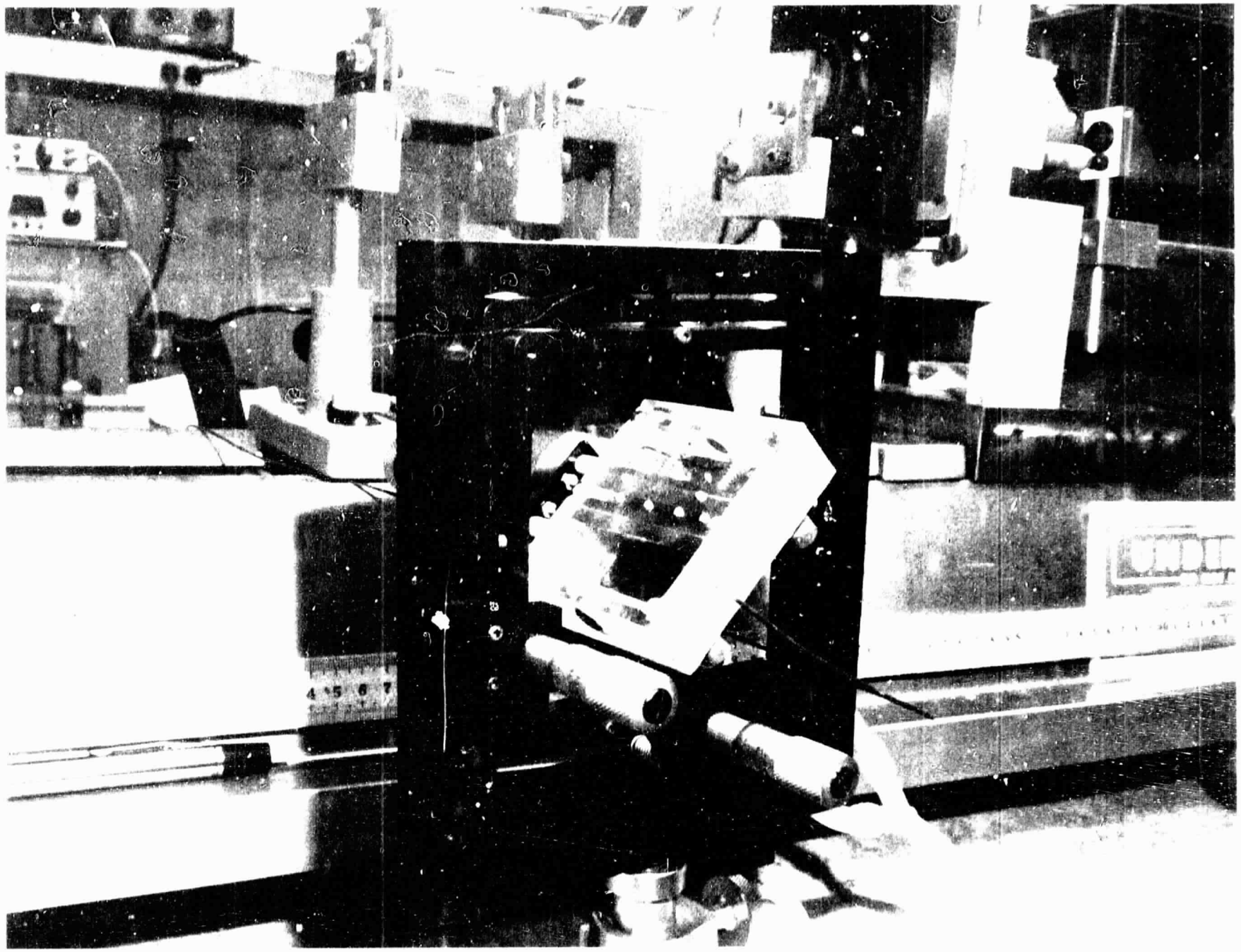

FIGURE 7. MODULATOR MOUNT

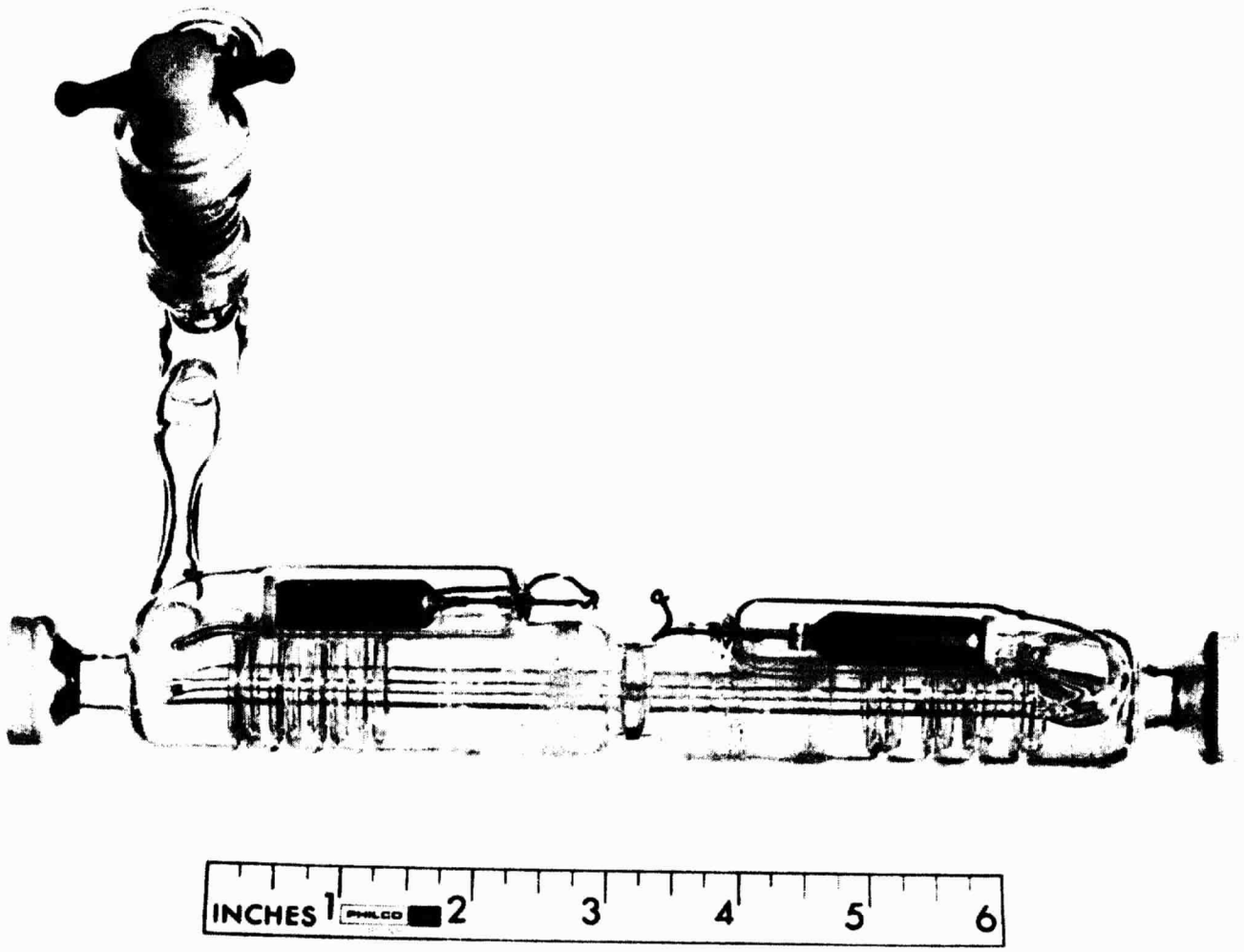

FIGURE 8. DUAL POLARIZATION LASER TUBE

overall gain of 20 to 40 db. When using the photomultiplier, the first of these stages was omitted. The amplified signal was processed by an appropriate spectrum analyzer to permit study of the modulation characteristics. Analyzers used were either a Polarad Model TSA-W or a Tektronix 1L20 and 1L10 pair, depending upon the frequencies in question. For purposes of studying the dc level, a chopper was inserted into the optical path, and the resulting signal was again processed by the low frequency amplifier and oscilloscope shown in dotted lines.

The modulator crystal to be evaluated was held between two copper electrodes in a mount offering six degrees of motion, thereby permitting translation along and rotation around each of the three axis. The electrodes were contained in a Lucite housing with one fixed and the other under a slight spring tension. Input ports were provided at the top and bottom of the housing for the introduction of flowing dry nitrogen to assist in cooling the crystal during runs involving high power dissipation or the absorption of 10.6 microns radiation. The electrodes contained side ports for expulsion of this flow. The crystal itself was sufficiently enclosed to eliminate any turbulence in the optical path. A Chromel-Alumel thermocouple was attached to the grounded electrode to permit monitoring of the crystal temperature by an appropriate bridge. Contacts were made between the electrodes and a pair of bananna jacks on the housings for connection to the driving source.

Uniform contact was made to the crystals by one of two methods. In the majority of the $LiNbO_3$ experiments, the electrodes were treated so as to provide a mercury-copper amalgum surface. This surface is highly conductive while remaining semi-liquid. Conformity to the crystal surface was made nearly perfect with this technique. The second process, used on later $LiNbO_3$ runs as well as in all GaAs experiments, involved the evaporation of silver or gold electrodes on the appropriate surfaces of the crystals in order to accomplish the uniform contact. Both techniques worked equally well.

A general Radio 1330-A signal generator was used to drive the crystal at frequencies from 5KHz to 50 MHz. In order to deliver the voltage required to accomplish meaningful modulation, a Hewlett-Packard Model 230A power amplifier was utilized above 10 MHz to drive a series resonant circuit composed of a coil appropriately selected to resonate with the crystal, thereby achieving a value of "Q" times the voltage applied to the resonant circuit. "Q" values of about (10^2) were achieved, thus permitting the application of better than 300 V_{RMS} for all but the highest frequencies studied.

In addition, a 1500V regulated power supply was used to furnish a dc bias voltage to the crystal, and isolation between the rf power amplifier and the dc supply was accomplished as indicated. This supply permitted the study of the dc response characteristics of the crystal, and

provided a means of biasing the crystal's birefringence so as to establish the cross-beat (carrier) frequency desired during the rf modulation studies.

A concurrent in-house program involved the construction of a small, fixed cavity He-Ne laser for the purpose of demonstrating various techniques of stabilization, modulation, etc., which have been developed at Philco-Ford. Advantage was taken of this unit to conduct some of the more basic studies of the modulator crystals and the stabilization techniques, thus permitting the more detailed and complex studies to proceed simultaneously and uninterrupted. The details of this cavity are very similar to those already described. A photo of this unit is presented in Figure 9.

Great amounts of care were taken to obviate any discrepancies in data due to detection equipment nonlinearities. Although all components were specified as wide-band flat-gain units, the precaution of making individual and system response calibrations was taken.

Response of the amplifier system was found to be relatively flat over the frequency range of prime interest (10 MHz- 150 MHz), and usable to 300 MHz with reference to the calibration curves obtained. However, while the photomultiplier added no apparent problems, the InAs detector and its bias network resulted in input circuit resonances. Attempts were made to reduce these effects to as large an extent as possible while still maintaining adequate signal strength. Although not all resonance was eliminated, the response was made flat enough to be useful, and the resulting overall system response incorporated into the final data reduction process.

The equipment discussed thus far imposed a fixed response curve that could easily be taken into consideration when reducing the data. The spectrum analyzer, however, presented a varying response that depended not only upon the frequency of the input, but also upon the position it occupied on the display. Thus, the further data reduction problems imposed by the analyzer were functions of the frequency, the frequency dial setting, the display center frequency, the display dispersion, the gain control, the bandwidth control, the sweep speed, and the display position controls.

It was decided, therefore, to calibrate the analyzer response with a constant amplitude signal generator before every data run, with the analyzer controls set as required by that run. This resulted in a loss of flexibility in the use of the analyzer during any one run, but also resulted in the most accurate data reduction possible.

In the final version, the signal generator was permanently installed in shunt with the detector through an isolating network as shown in Figure 1. This procedure not only permitted calibration of the analyzer under constant circuit conditions, but also served to further reduce the resonance problems mentioned with respect to the Indium Arsenide detector.

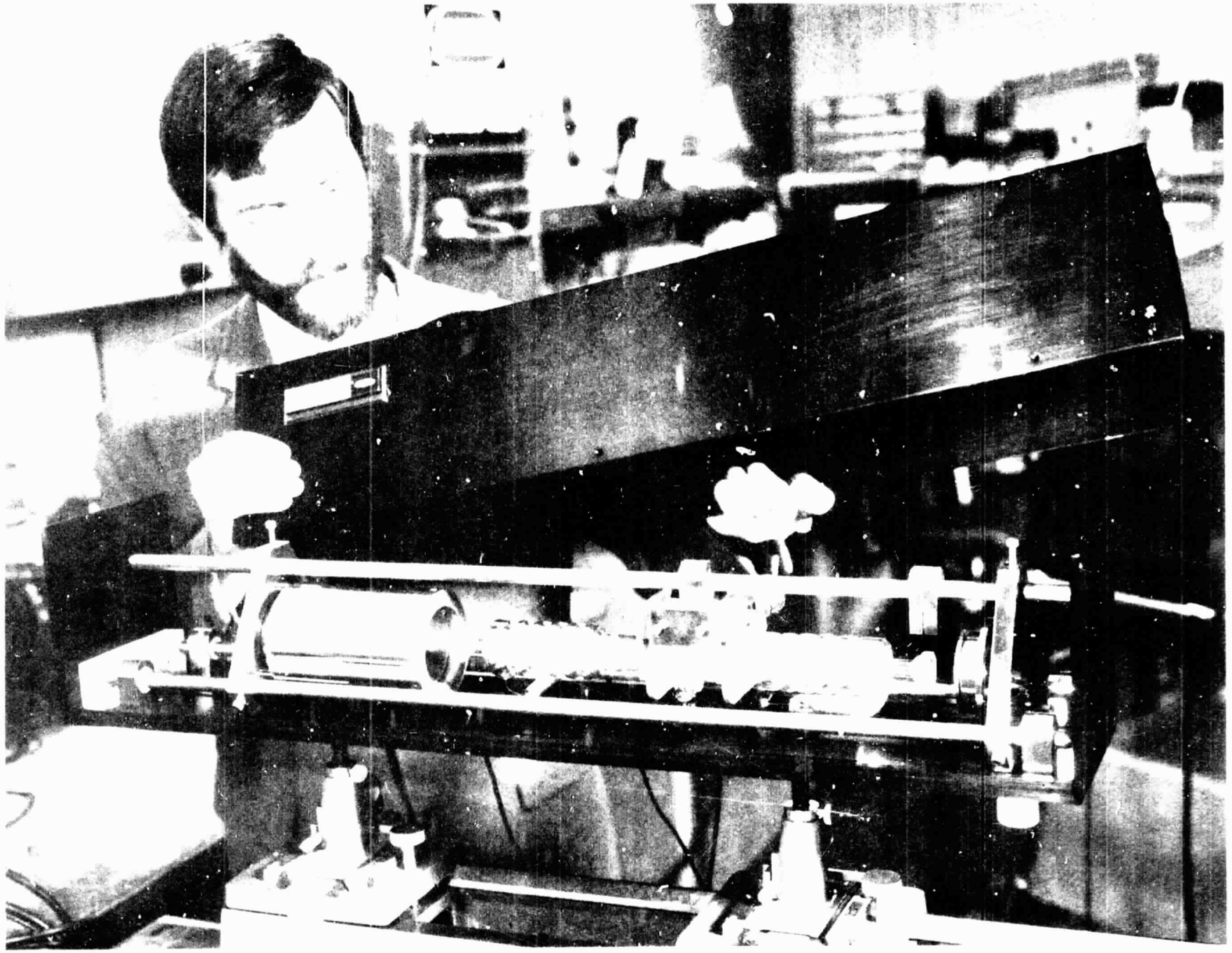

FIGURE 9. He-Ne DEMONSTRATION LASER

Photographs were taken of the analyzer response to the calibration procedure, and of the experimental data subsequently displayed. Reduction of the data was then accomplished by the utilization of the previously mentioned "fixed" response curves in conjunction with the analyzer calibration photo.

3.3 MODULATOR RESPONSE

In this section we discuss the characteristics of the two $LiNbO_3$ and two GaAs modulators used in the experiments to be reported and illustrate the fm sensitivity characteristic of our apparatus.

Crystal (I) is a 3 mm x 5 mm x 30 mm $LiNbO_3$ transverse modulator oriented with the a-axis normal to the 5 mm x 30 mm plane and the c-axis parallel to the 30 mm length. The field was applied along the a-axis with the c-axis defining the optical path, thus providing an aspect ratio of (10:1).

Crystal (II) is a 3 mm x 3 mm x 17 mm sample of the same material, oriented so that the a-axis and the c-axis direction were the reverse of those of the first crystal. The field in this case is along the c-axis, normal to the 3 mm x 17 mm plane, and the optical path is parallel to the 17 mm a-axis. The aspect ratio is therefore (5.7:1).

The first of the GaAs samples (III) was a 5 mm x 10 mm x 20 mm longitudinal modulator. The sample faces in this case were not oriented normal to the crystallographic axes. Precise orientation of the crystal was not determined, and no attempt was made to compare the results obtained with other crystals.

The final GaAs crystal (IV) was again oriented for transverse modulation. Dimensions were 3 mm x 3 mm x 50 mm, with the field applied perpendicular to the 3 mm x 50 mm faces (110) and the optical path normal to the 3 mm x 3 mm (110) planes, both along the crystallographic axis of the cubic structure. The aspect ratio was, in this case, (16.7:1).

To minimize losses, the transverse GaAs crystal was anti-reflection coated for the 10.6 studies. However, because of the desire to study the modulation characteristics at several wavelengths, the other crystals were not coated. In all cases, attempts were made to minimize the reflection losses by cancellation techniques, as described in Section 3.2.

The two materials involved show similar electro-optical properties. Lithium Niobate is of the trigonal R3C space group, while Gallium Arsenide has cubic structure. When functioning as transverse modulators, such as our samples (I) and (IV), both materials become biaxial, providing an index ellipsoid whose axes make angles of 45^{o} with the a-c plane of the crystal and are normal to the c-axis.[7], [8], [9]

In the case of $LiNbO_3$, a relationship relating the change of the index of refraction to the applied field may be extracted from the general equation of the ellipsoid.[7] For sample (I) the birefringence may then be expressed as

$$\Delta n = n_o^3 \, r_{22} E \tag{16}$$

where Δn is the birefringence, n_o is the ordinary index of refraction, r_{22} the electro-optic coefficient, and E is the electric field in volts/meter.

Our experimental data provides a value of $(d\nu/dV)$ characteristic of the crystal/cavity combination. When related to the appropriate cavity parameters, this yields the effective change in length of the cavity for a given voltage applied to the crystal $(d\ell_c/dV)$, which is, in turn, directly related to the induced birefringence,

$$\Delta n_x = \left(\frac{\Delta \ell_c}{\ell_x}\right), \tag{17}$$

where ℓ_x is the length of the crystal. Equating the two expressions involving Δn_x, defining R as the aspect ratio, and substituting $E = (V/d_x)$, where V is the peak voltage applied and d_x is the crystal dimension in the direction of the field, we obtain

$$r_{22} = \left(\frac{\Delta \ell_c}{V}\right)\left(n_o^3 \, R\right)^{-1} \tag{18}$$

Using this relationship, comparison may be made with previously published values of the electro-optic coefficient.

A similar analysis for $LiNbO_3$ in the orientation of crystal (II) results in the following relationship,

$$\left[\left(\frac{n_e}{n_o}\right)^3 r_{33} - r_{13}\right] = \left(\frac{\Delta \ell_c}{V}\right)(R)^{-1} \tag{19}$$

The Gallium Arsenide transverse crystal, sample IV, involves somewhat different parameters, but the result is similar.[8], [9] In this case the resulting equation again becomes

$$r_{41} = \left(\frac{\Delta \ell_c}{V}\right)(n^3 R)^{-1} \tag{20}$$

Alternatively, the result may be written in terms of phase retardation for purposes of comparison. In this case the pertinent equation becomes

$$2\gamma = \left(\frac{2\pi \ell_x}{\lambda}\right) (n^3) (r_{41}) \left(\frac{V}{d_x}\right) \qquad (21)$$

where 2γ is the linear birefringent phase shift defined in Section 2.

In the final case, modulator (III), the orientation of the crystal was sufficiently unclear to preclude analysis in the above manner. As a result, determination of the basic parameters was not accomplished with this unit.

In addition to the electro-optical coefficients discussed above other parameters of the crystals were ascertained by using straightforward techniques. Capacitance was measured using bridge techniques, as were loss tangents. Temperature dependent effects were observed and noted, but in the case of both of these measurements, the goal was one of determining practical limitations upon its use as a modulator as opposed to a definitive study of the material. Results of this phase of the study are summarized below for each modulator.

CRYSTAL (I)

Material: $LiNbO_3$
Size: 3 x 5 x 30 mm
Orientation: Field parallel to a-axis; optical path parallel to c-axis.
Tan δ: $5(10^{-2})$ @ 1 MHz @ room temperature[10]
Aspect ratio: (10:1)

Electro-optic coefficient:

		Experimental Results	Reference Value	Source
3.4μ	$(r_{22})_{DC}$ =	$2.94(10^{-12})$M/V	$3.1(10^{-12})$M/V	Turner[11]
1.15μ	$(r_{22})_{DC}$ =	$5.18(10^{-12})$M/V	$5.4(10^{-12})$M/V	Smakula[12]
1.15μ	$(r_{22})_{RF}$ =	$4.98(10^{-12})$M/V	$2.74(10^{-12})$M/V	Turner[11] (See Text)

CRYSTAL (II)

Material: $LiNbO_3$
Size: 3 x 3 x 17 mm
Orientation: Field parallel to c-axis; optical path parallel to a-axis
Capacitance: 5 pf
Tan δ: $<(10^{-3})$ @ .1 MHz, @ room temperature[10]
Aspect ratio: (5.67:1)

Electro-optic coefficient:

	Experimental Results	Reference Value	Source
$3.4\mu \left[\left(\frac{n_e}{n_o}\right)^3 r_{33} - r_{13}\right]_{DC} =$	$7.05(10^{-11})$M/V	$1.8(10^{-11})$M/V	Lenzo[7]
$\left[\left(\frac{n_e}{n_o}\right)^3 r_{33} - r_{13}\right]_{RF} =$	$9.7(10^{-11})$M/V	----	------

---

CRYSTAL (III)

Material: GaAs
Size: 5 x 10 x 30 mm
Orientation: (?)
Capacitance: <1 pf
Tan δ: $<10^{-3}$(2.5 to 10 $(10^9)H_z$)[13]
Aspect: (1:1) (Longitudinal)

Electro-optic coefficient: (See text)

CRYSTAL (IV)

Material: GaAs
Size: 3 x 3 x 50 mm
Orientation: Axes perpendicular to faces
Capacitance: 5 pf (14 pf mounted)
Tan δ: 10^{-3}(2.5 to 10 (10^9) Hz)[13]
Aspect: (16.7:1)

Electro-optical coefficient:

		Experimental Results	Reference Value	Source
3.4μ $(r_{41})_{DC}$	=	$1.12(10^{-12})$M/V	$1.2(10^{-12})$M/V	Walsh[13]
3.4μ $(r_{41})_{RF}$	=	$1.12(10^{-12})$M/V	----	(Note: Done at 2, 4, 10, & 20 MHz)
10.6μ $(r_{41})_{DC}$	=	$0.9(10^{-12})$M/V	$1.3(10^{-12})$M/V	Monsanto[14]

As indicated by Equation (15) the modulation sensitivity of the DPFM system is inversely proportional to the cavity length. Thus no fixed values of sensitivity can be given. For a cavity length of 60 cm, crystals I, II, and IV yielded dc sensitivities of 54.4 kHz/Volt, 37.0 kHz/Volt, and 99.0 kHz/Volt respectively at 3.39 microns. Crystal (I) yielded a dc sensitivity of 268.8 kHz/Volt at 1.15 microns. The sensitivity of Crystal (IV) at 10.6 microns was 28.1 kHz/V. These figures can clearly be improved significantly by shortening the cavity length. For a given modulation index, the drive amplitudes and, therefore, modulator heating would be largely reduced by this measure.

Representative curves of beat-frequency as a function of modulator dc voltage are shown in Figures 10 and 11 for crystal (I) and crystal (IV), respectively. In these figures the two lines indicated correspond to the voltage dependence of the two possible beats, at $\Delta\nu$ and $\Omega - \Delta\nu$, where Ω $(= \nu_n - \nu_{n-1})$ is the intermode spacing discussed in Section 2. These lines necessarily cross at $\Delta\nu = \Omega/2$. In each figure the circles and triangles correspond to the same run but different cavity length adjustments. The squares and x's are different runs. Similar curves were obtained for rf drives by first determining the rms voltage required to cause the "zeroing" of various fm sidebands. Reference to a table of Bessel functions then provided the modulation index and thus the deviation. Finally, the $(d\nu/dV)$ characteristic was determined from the plot of deviation versus peak voltage.

The dc and rf values of $(d\nu/dV)$ obtained from our data were used to calculate the experimental electro-optic coefficients given above. In general, the response of our crystals is comparable with the published values. Two apparent discrepancies occur, however, in the $LiNbO_3$ data.

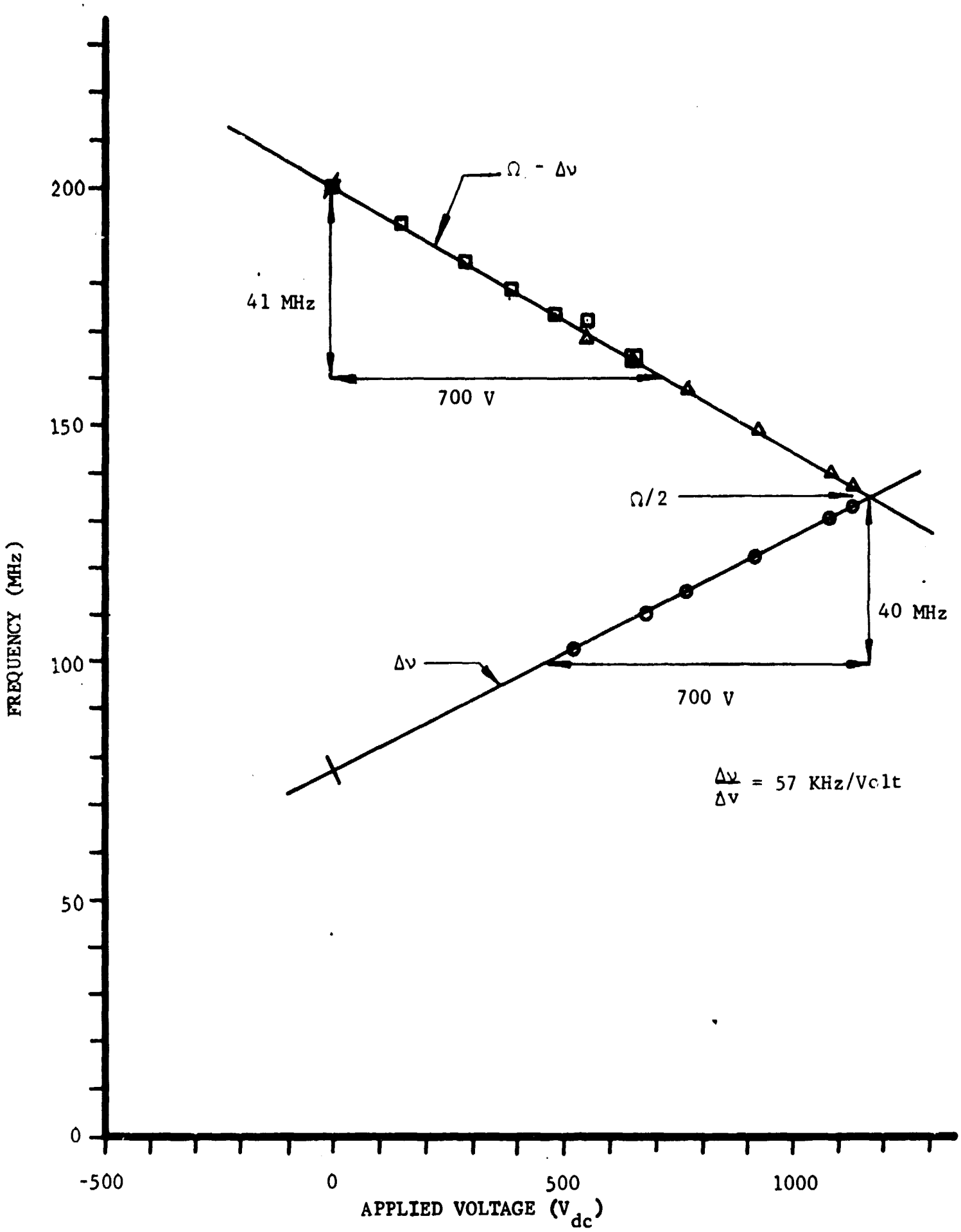

FIGURE 10. TYPICAL CURVE OF BEAT FREQUENCY -VS - APPLIED VOLTAGE FOR $LiNbO_3$ CRYSTAL (I)

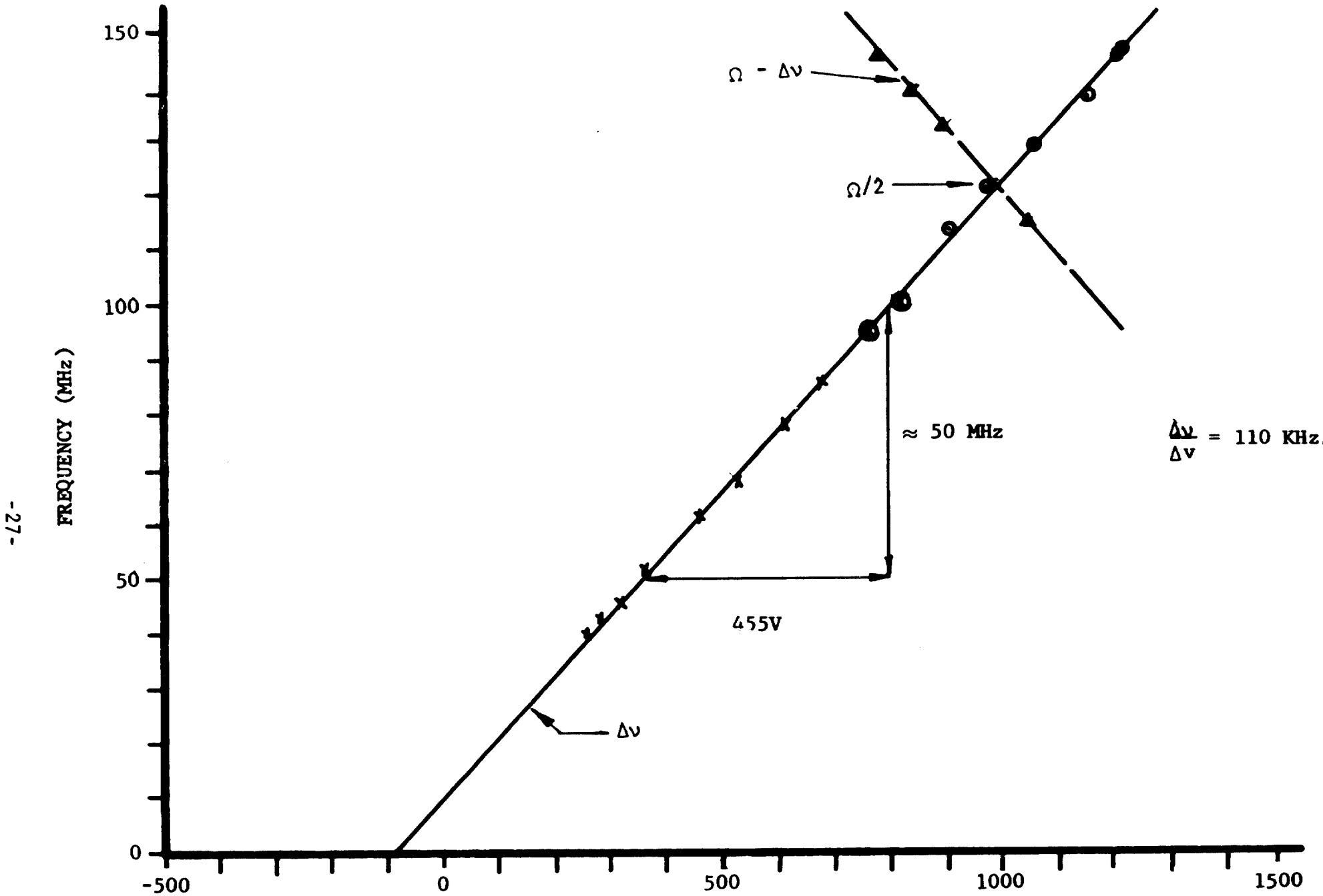

FIGURE 11. TYPICAL CURVE OF BEAT FREQUENCY - VS - APPLIED VOLTAGE FOR GaAs CRYSTAL (IV)

In the case of crystal (I), the (r_{22}) value used for comparison was extrapolated from Turner's results.[12] While our data indicates that the dc and rf values are similar, he found that at 632.8 nm the coefficient dropped to ≈ 57% of its dc value at radio frequencies. Using this ratio with Smakula's[12] quoted dc coefficient at 3.4 micron, the reference value was obtained. As our experimental results indicate, this assumed behavior may be in error.

The electrooptical coefficient values obtained experimentally for crystal (II) appear higher than the reference values. Again, the comparison is made with data obtained at a different wavelength. In particular, the $(n_e/n_o)^3$ factor in equation (19) would be different for 3.4 microns than the value (0.9) value applicable at 632.8 nm.

During our He-Ne modulation experiments it became apparent that the $LiNbO_3$ modulators being used were experiencing much greater dielectric heating than we had anticipated. This heating was sufficient to make modulation at frequencies above about 12 MHz quite difficult. Subsequently, we learned that $LiNbO_3$ had been observed to exhibit an anomalous dielectric loss, with a peak at about 10 mHz.[10] This loss apparently is peculiar to $LiNbO_3$. Other similar electrooptical crystals such as $LiTaO_3$ appear to have very low losses.[15] Thus dielectric heating, while a nuisance in our experiments, is not a fundamental limitation.

We studied dielectric heating in our crystals by measuring the temperature increase over a given period of time as a function of applied voltage and frequency. Results for $LiNbO_3$ crystal (I) and GaAs crystal (IV) are shown in Figures 12a and 12b respectively. In order to compare these results with the theoretically expected dependence the data of Figure 12a has been replotted in Figure 13 as a set of constant temperature change (or power) curves. The power dissipated in the crystal is expected to obey the relationship

$$P = V_{RMS}^2 \, 2\pi \, \nu_m \, C \tan\delta \qquad (22)$$

The dashed line of Figure 13 is a representative constant power curve generated from this expression by using the tan δ data of reference 10. It has the same general shape of the solid curves.

As we saw above, crystal (II) exhibits the greatest modulation sensitivity of our samples. However, the orientation of this crystal is such that the direction of light propagation is perpendicular to the optic (c) axis. As a result the modulator exhibits a large residual birefringence which, naturally, changes with temperature, making its use quite difficult. In the experiments to be described in Sections 3.4 and 3.5 crystal (II) was used at 3.39 microns, while the more stable crystal (I) was used at 1.15 microns.

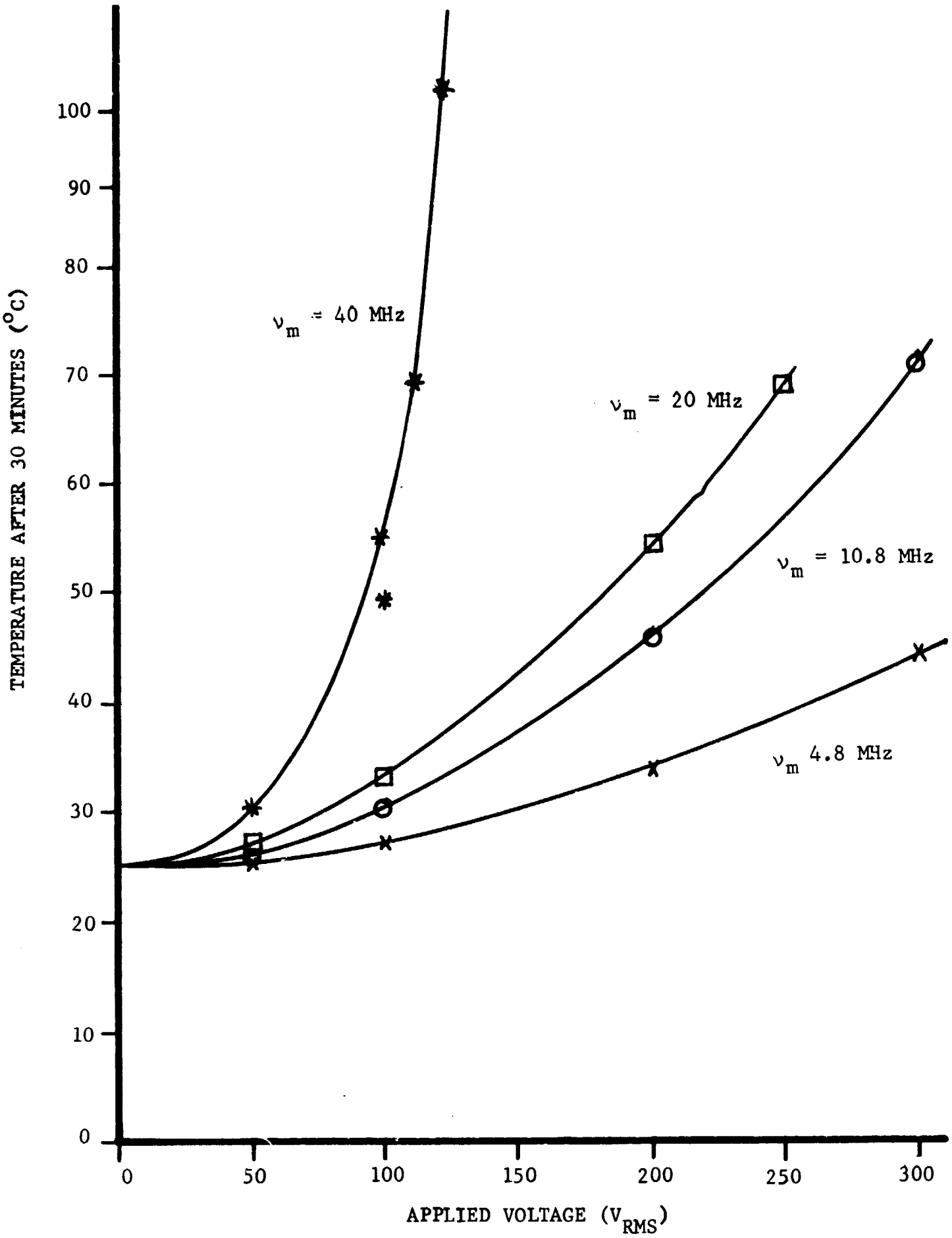

FIGURE 12a. TEMPERATURE VS APPLIED VOLTAGE AT VARIOUS MODULATION FREQUENCIES, $LiNbO_3$ CRYSTAL (I)

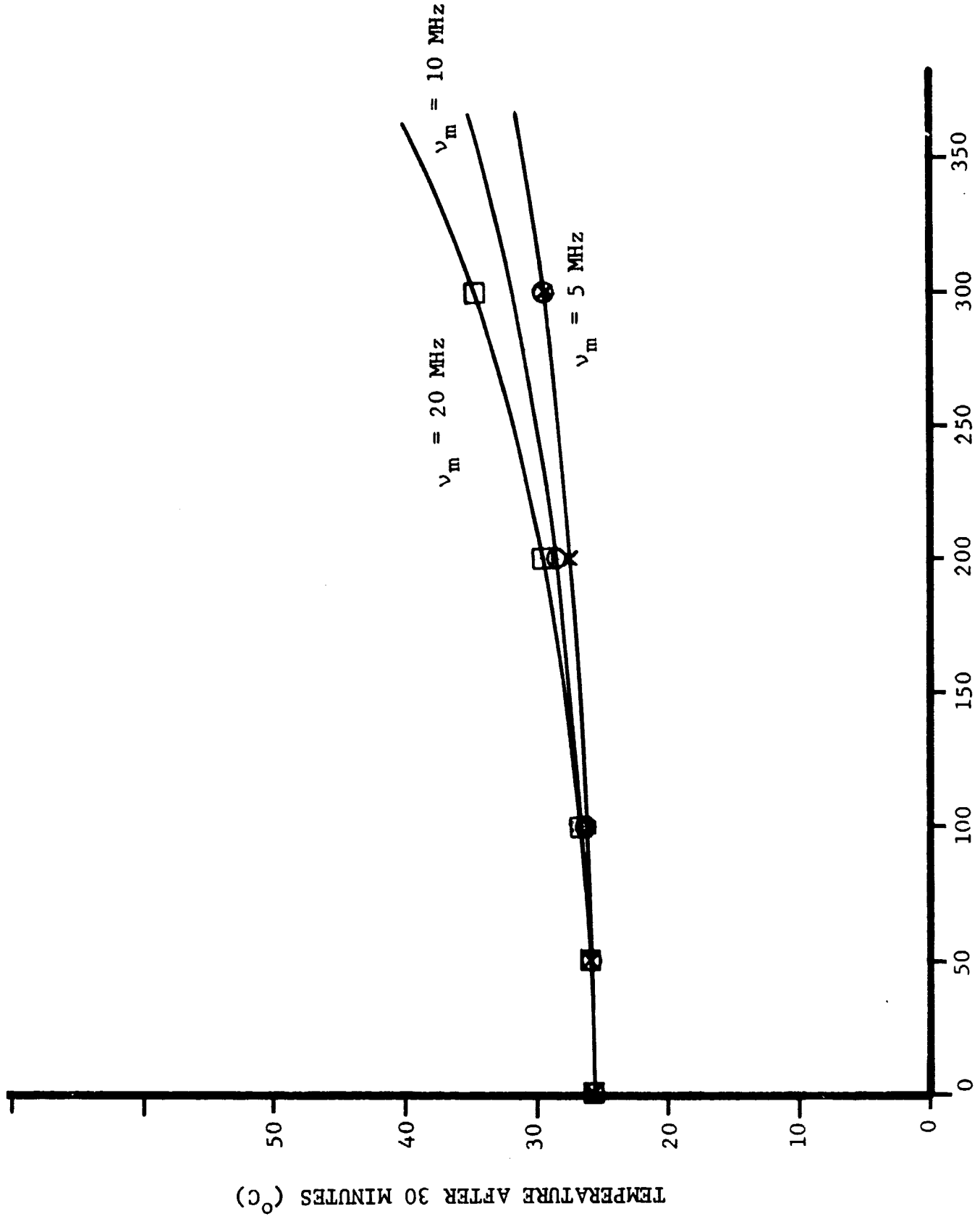

FIGURE 12b. TEMPERATURE VS APPLIED VOLTAGE AT VARIOUS MODULATION FREQUENCIES, GaAs CRYSTAL (IV)

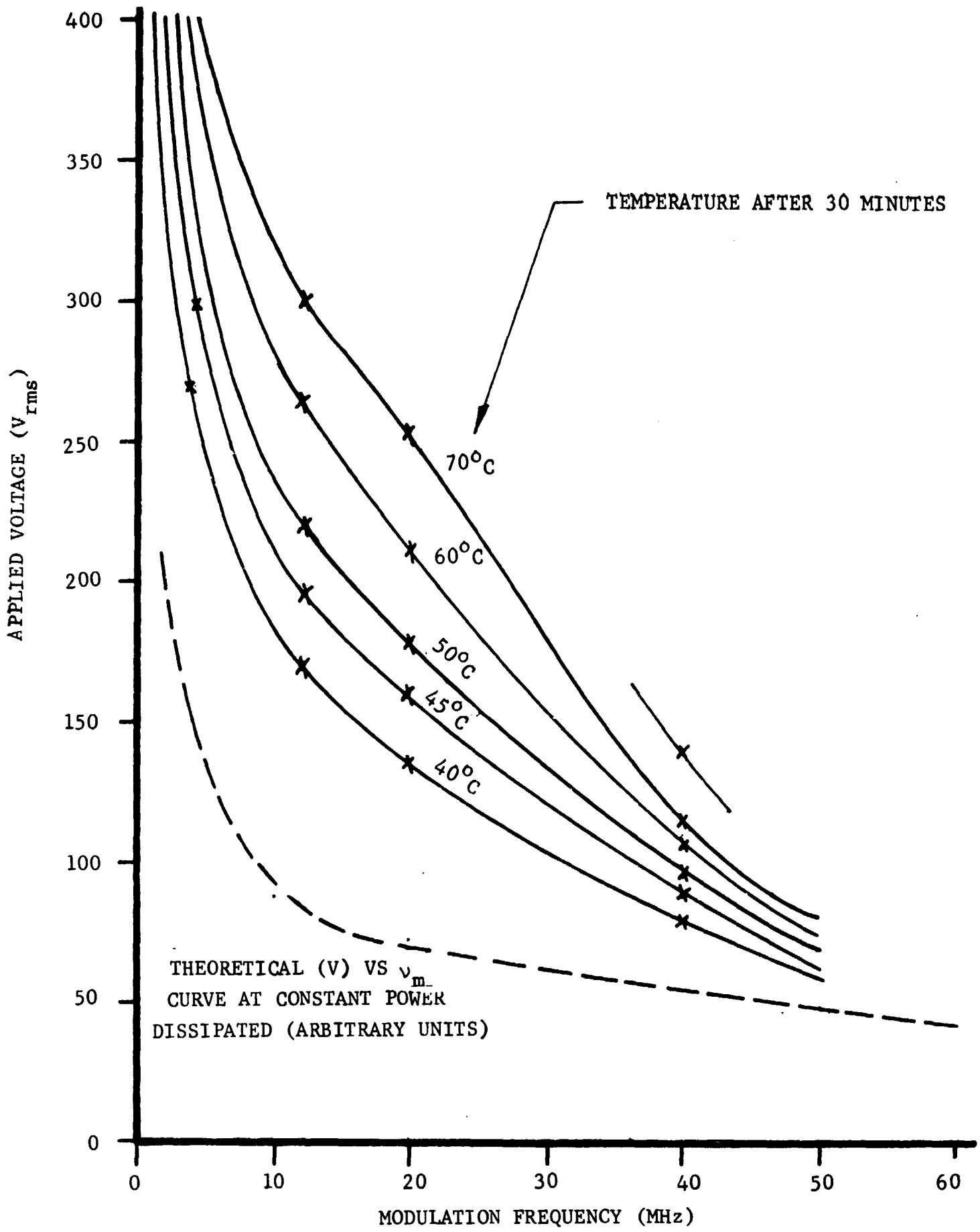

FIGURE 13. VOLTAGE VS MODULATION FREQUENCY FOR CONSTANT TEMPERATURES $LiNbO_3$ CRYSTAL (I)

3.4 STATIC LASER CHARACTERISTICS

The static subcarrier characteristics obtainable with both the 3.39μ and 1.15μ lasers were studied by monitoring the beat intensity observed on the spectrum analyzer while the modulator bias was varied. We will discuss the 3.39μ results first.

The range of subcarrier frequencies obtainable at 3.39μ was found to extend from approximately 40 MHz to the intermode frequency for all of the modulators tested and for the range of cavity lengths used (about 55 cm to 100 cm). For most bias voltages, subcarriers could be observed at either $\Delta\nu$ or Ω-$\Delta\nu$, where Ω is the intermode frequency ($\Omega = \nu_n - \nu_{n-1}$), depending on the cavity length tuning. This behavior can be understood with reference to Figure 2. When the cavity length is such that a given pair of modes, separated by $\Delta\nu$, is centered on the gain profile a subcarrier is observed at $\Delta\nu$. When two pairs are more or less symmetrically placed on either side of the profile, only the modes closest to the center oscillate and a subcarrier is observed at Ω-$\Delta\nu$. Under most conditions, only one of these subcarriers was observed at a given time, indicating that no more than two optical oscillations existed. In addition, no subcarrier beats were observed at frequencies above the intermode frequency.

The study of the subcarrier amplitude at 3.39μ was hampered somewhat by the limitations of the circuitry used with the In As detector. First, the amplifier response fell off rapidly above 200 MHz. Second, resonances in the detector circuit itself made normalization of the data quite difficult. The best results were obtained with the standard signal generator loosely coupled directly in parallel with the detector element as discussed in Section 3.2. Results obtained with the c-axis $LiNbO_3$ modulator crystal (II) and an effective cavity length of 60 cm (intermode frequency 250 MHz) are shown in Figure 14. The output peak observed at about 50 MHz is believed to be due to the normalization difficulty. To check this the dc level of the laser output was measured under the same experimental conditions. Since only one subcarrier beat was observed, its intensity should be closely paralleled by the dc level. The results (Figure 15) show only a very slight decrease in dc level with increasing subcarrier frequency.

The subcarrier measurements at 1.15μ were not limited by the response problems discussed above since the use of a photomultiplier obviated the need for preamplification and eliminated the circuit resonances. Typical results obtained with crystal (II) are shown in Figure 16. The fluctuations in the data which occur between 220 MHz and 290 MHz were not repeatable and hence and attributed to laser intensity drift. The other features will be interpreted in terms of the hypothetical mode sequences shown in Figure 17. Here, the short vertical lines indicate cavity modes which are not in oscillation.

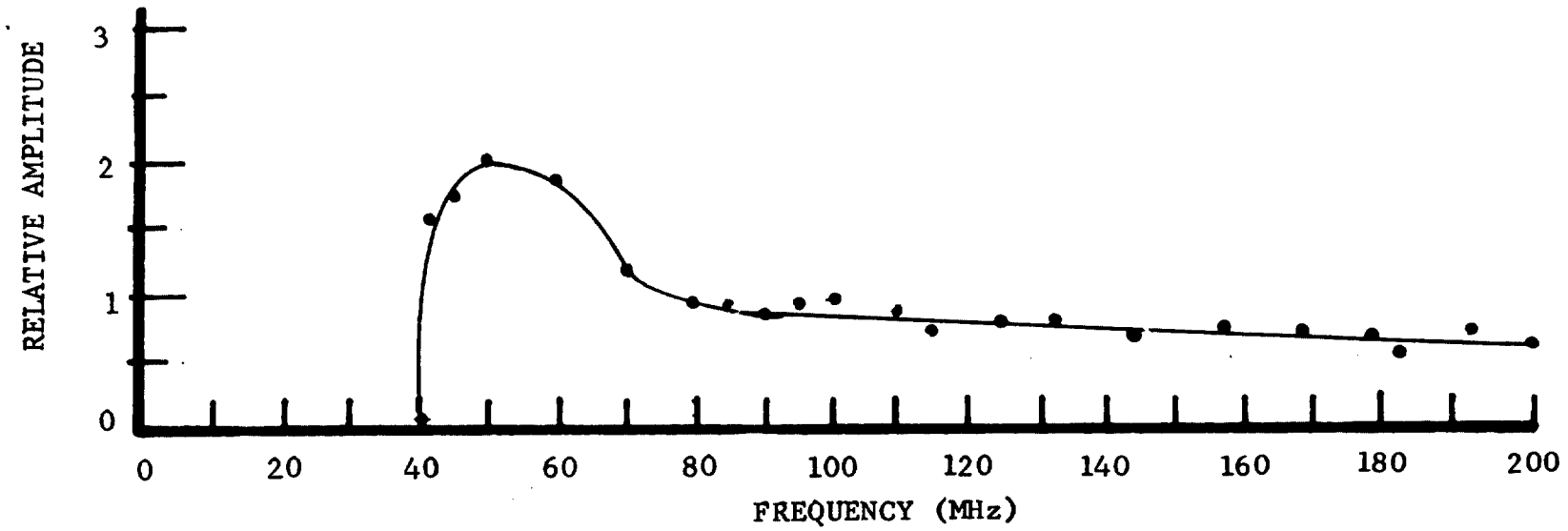

FIGURE 14. 3.39μ SUBCARRIER AMPLITUDE

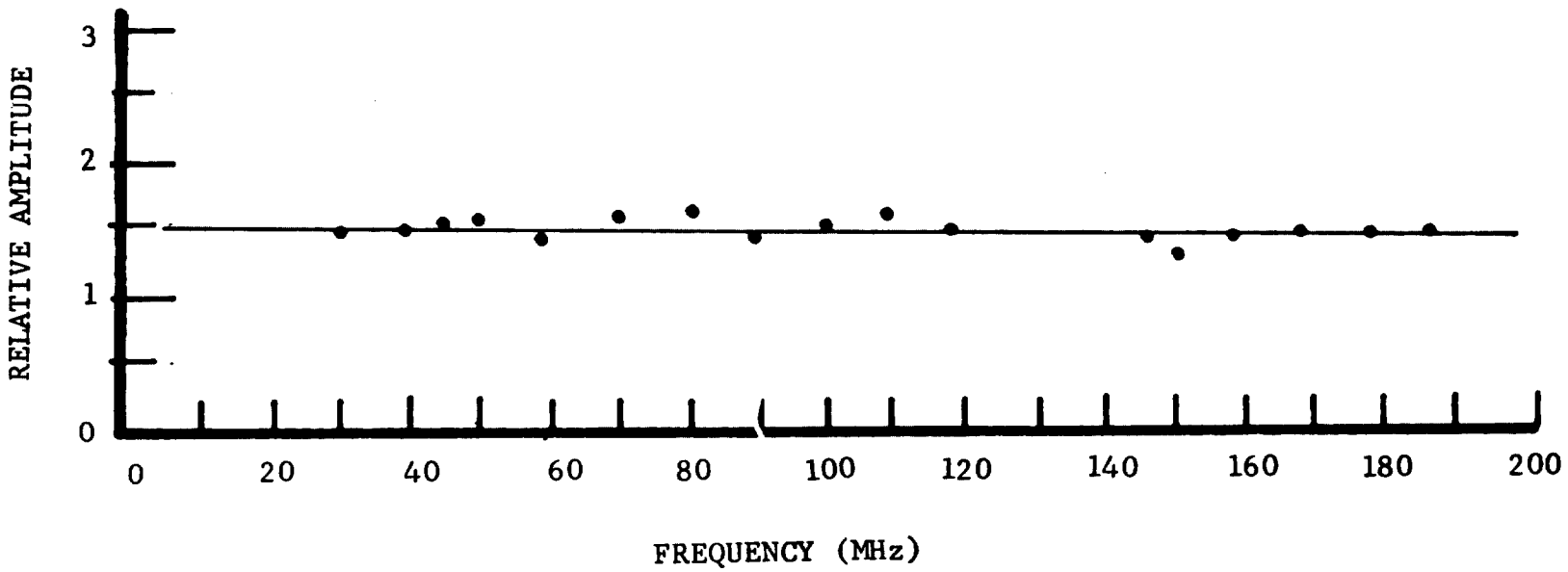

FIGURE 15. TOTAL LASER OUTPUT AS A FUNCTION OF SUBCARRIER FREQUENCY

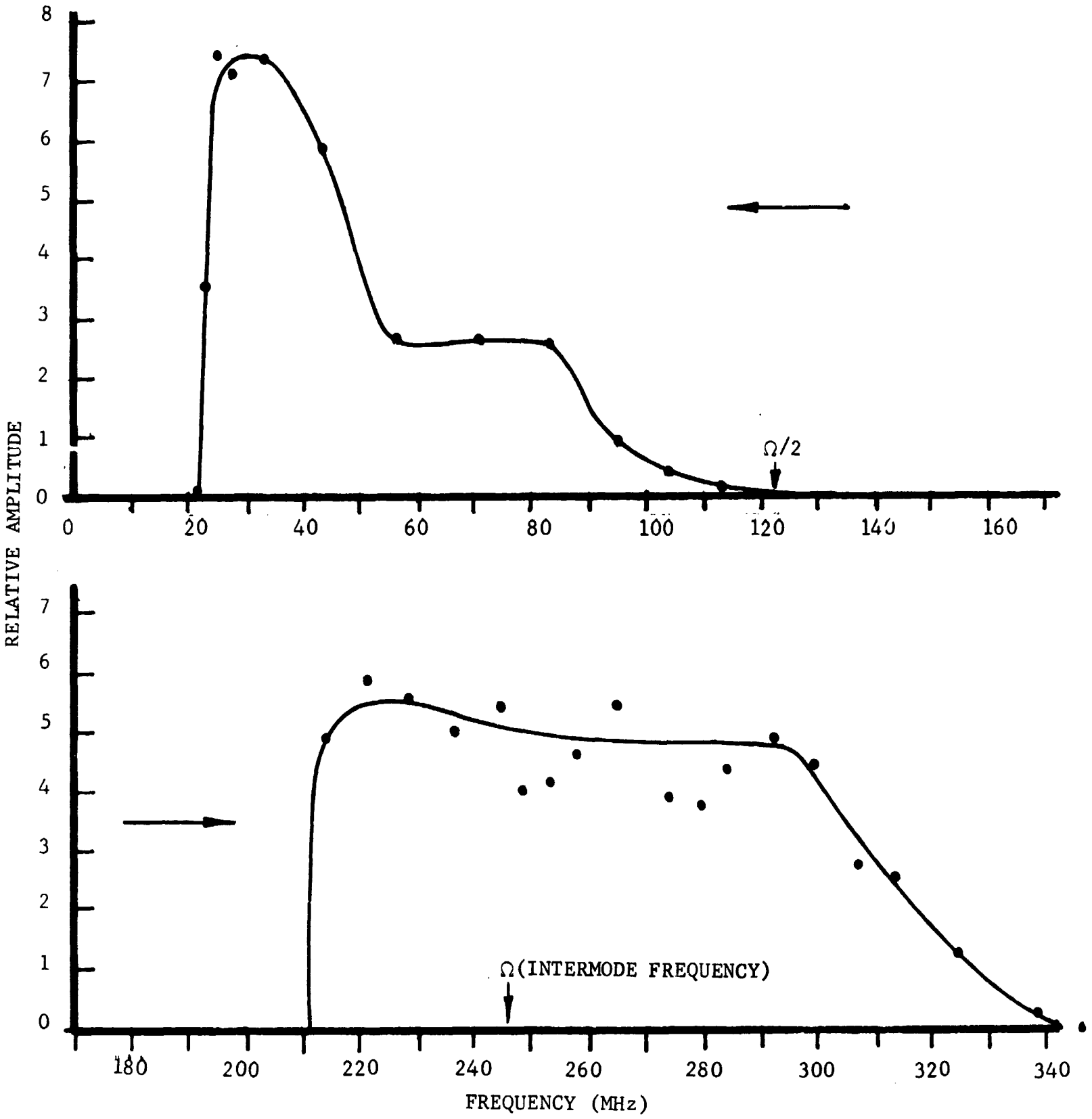

FIGURE 16. 1.15μ SUBCARRIER AMPLITUDE

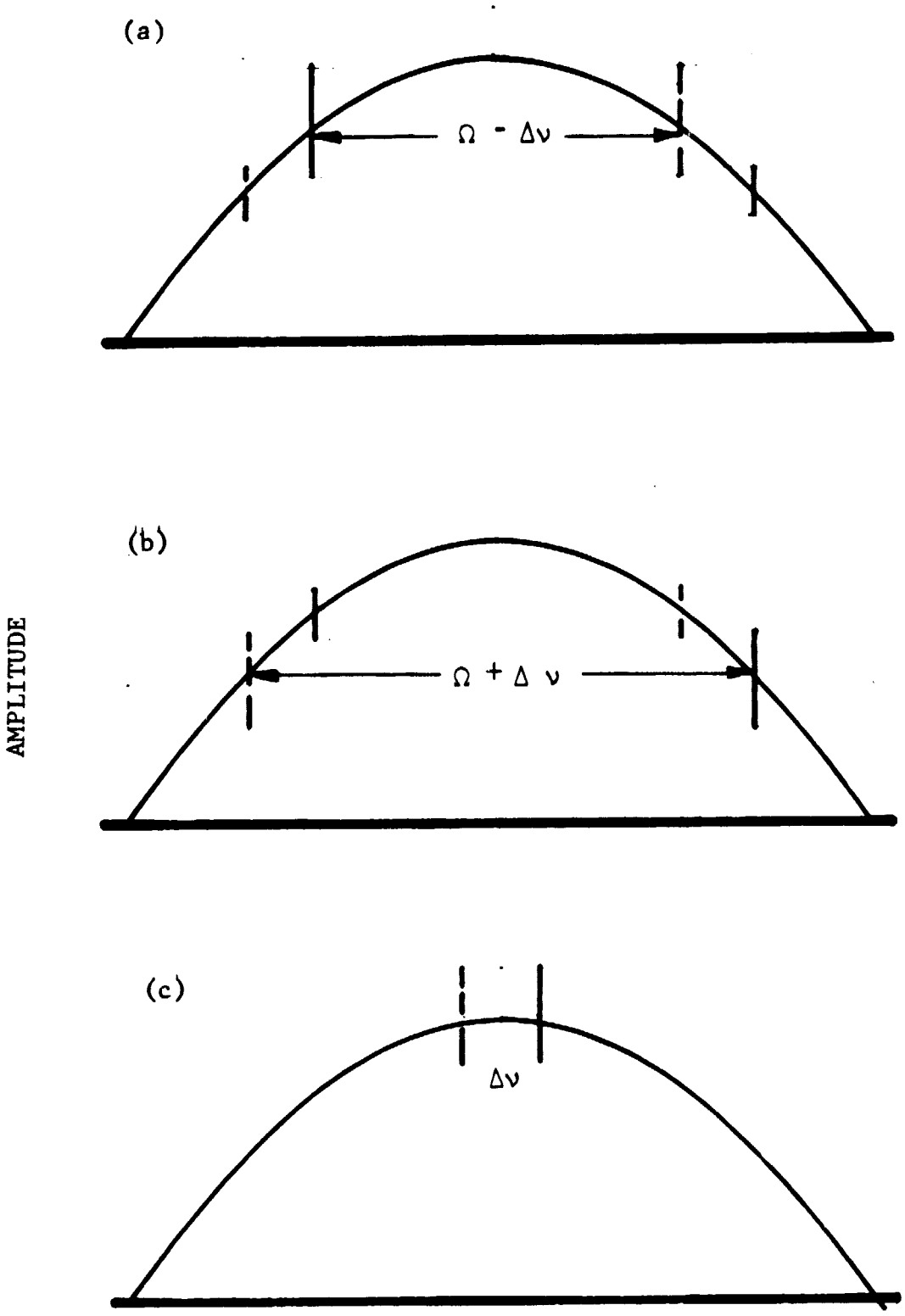

FIGURE 17. DUAL POLARIZATION MODE SEQUENCES FOR THREE POSSIBLE SUBCARRIERS (THE SHORT LINES INDICATE MODES NOT IN OSCILLATION)

At the narrowest birefringent splittings, strong coupling occurs between the two members of a given pair of modes, and thus only one oscillates at a given time. When two such pairs are placed symmetrically on the gain profile either sequence 'a' or 'b' will occur depending (for a presently unknown reason) on the polarity of the bias voltage. We thus obtain subcarriers at either $\Omega-\Delta\nu$ or $\Omega+\Delta\nu$. As the splitting is increased, a point is reached at about 22 MHz where weak coupling occurs for central tuning (sequence 'c'). Behavior 'a' or 'b' is still obtained for off-central tuning. If the splitting is further increased under the conditions for which behavior 'a' is obtained, a point is reached at $\Delta\nu \sim 30$ MHz where the behavior suddenly switches to sequence 'b'. This phenomena is probably due to the increasing coupling between the two oscillations of sequence 'a' as their separation ($\Omega-\Delta\nu$) decreases. At $\Delta\nu > 30$ MHz this coupling hypothetically is sufficiently strong to make sequence 'b' the favored mode of operation even though its oscillations occur at lower gain positions on the fluorescence profile.

As $\Delta\nu$ is increased beyond 30 MHz, behaviors 'b' and 'c' continue to occur at their appropriate cavity tunings. The subcarrier intensity and, in fact, the dc laser output decrease markedly, however, as the frequency $\Omega/2$ is approached. This decrease is believed to be due to the reflection losses of the modulating crystal, as will be explained below, and hence could be easily avoided by the use of anti-reflection coating. Such coating was not used in our experiments, however, for two reasons: first, 1.15μ coatings would degrade the operation of the crystals at other wavelengths such as 3.39μ; second the reflection phenomena gave us a good example of a frequency dependent loss for use in our modulation studies. Evaluation of the laser behavior in the presence of this loss should give an indication of the effects to be expected from a frequency dependent gain such as would be provided, for example, by the narrow Doppler line of the CO_2 laser.

In order to understand the nature of the frequency dependent reflection loss it should first be recalled that our general experimental procedure involves the orientation of all intracavity optical components in such a way as to allow cancellation of the reflections from the two surfaces. The transmittance of such a Fabry-Perot plate for infinite plane waves is[16]

$$T = 1/\left[1 + \frac{4r^2}{(1-r^2)^2} \sin^2 \frac{\delta}{2}\right] \tag{23}$$

where

$$r^2 = \left(\frac{n-1}{n+1}\right)^2 \tag{24}$$

and

$$\delta = \frac{4\pi}{\lambda} nd \cos \varphi. \tag{25}$$

Here r^2 is the reflectance, n is the index of refraction, d is the plate thickness, δ is the double pass phase shift, and φ is the angle of incidence. For $LiNbO_3$, $n \simeq 2.3$, so that the transmittance will vary between 0.53 and 1.0 as the angle is varied. In the absence of a subcarrier bias the condition for a transmission maximum can be readily satisfied. As the bias is increased, however, the indices of refraction for the two polarization states become different, so that the Fabry-Perot condition cannot be satisfied simultaneously for both states, and a compromise is necessary. This condition is most severe when the double pass birefringent phase difference is equal to π, at which point subcarriers should occur at $\Omega/2$ and $3\Omega/2$. At this point the best compromise is achieved when $\delta = \pm \pi/2$ for the two states, in which case T = 0.69. This transmittance is sufficiently low to extinguish oscillation in a 1.15μ laser. Although the Fabry-Perot condition was also utilized at 3.39μ, no definite observation was made of the frequency dependent loss. This is probably due to the much higher gain and mirror transmission of the 3.39μ laser and to the uncertainties involved in normalization.

3.5 HIGH FREQUENCY MODULATION EXPERIMENTS

Extensive modulation studies have been carried out at both 3.39μ and 1.15μ using the $LiNbO_3$ modulators described in Section 3.3, modulation frequencies from dc to 20 MHz, and bandwidths up to 130 MHz (at 1.15μ). As a standard for comparison with later results and as an illustration of the inherent capabilities of the DPFM approach we will first consider some modulation data obtained under conditions for which the bandwidth limiting factors are expected to be minimal. Inspection of the static subcarrier intensity curves of Section 3.4 indicates that the high subcarrier frequency region of the 3.39μ curve is the least frequency dependent and thus the most satisfactory for this purpose. In addition, the normalization uncertainty encountered in this region is not particularly great for moderate bandwidths.

Raw modulation data is collected in the form of spectrum analyzer photographs. Three examples, obtained with modulator crystal (I), a modulation frequency of 3 MHz, a subcarrier frequency of about 150 MHz and an intermode frequency of 186 MHz are shown in Figure 18. The spurious signals at the left side of each photograph are spectrum analyzer images. As one would expect, the sideband amplitudes conform to the well known Bessel function spectra.[17] The data shown were taken under conditions for which (a) the carrier, (b) the first pair of sidebands, and (c) the third pair of sidebands dipped approximately to zero. The figure illustrates the symmetry in the positions of the nulls which is usually observed in our experiments.

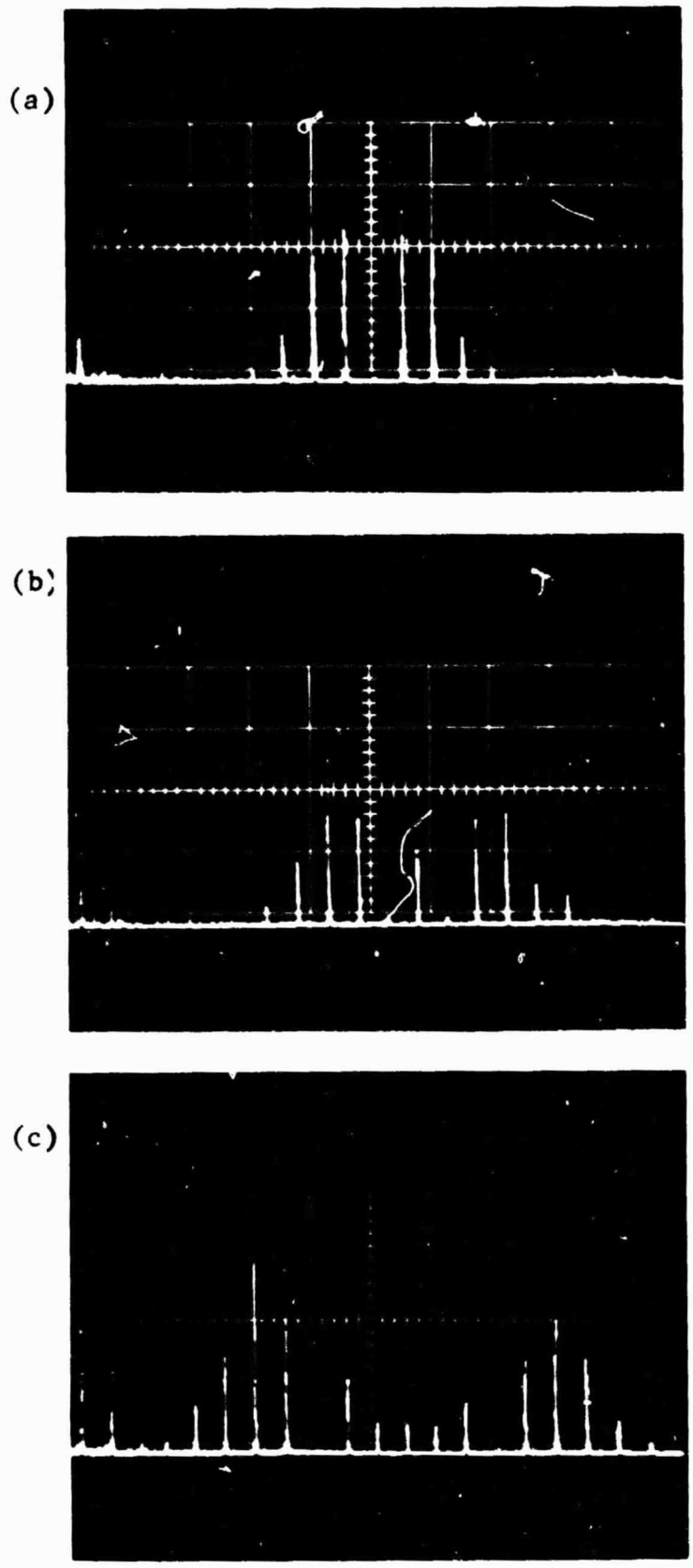

FIGURE 18. DPFM SIDEBAND SPECTRA AT 3.39 μ WITH A MODULATION FREQUENCY OF 3 MHz AND DRIVING VOLTAGES OF (a) 110 V_{rms}, (b) 170 V_{rms}, AND (c) 290 V_{rms}

In order to accurately determine the actual sideband amplitudes, the data must be normalized by the appropriate response curves for the detector circuitry and the spectrum analyzer. A set of normalized data obtained from a series of five photos taken under conditions similar to those of Figure 18 is shown in Figure 19 fitted to theoretical Bessel function curves. Here $J_n(x)$ is the n'th order Bessel function and x is the deviation ratio, i.e. the ratio of the maximum deviation to the modulation frequency. For clarity only the odd order sidebands are shown. The scaling of the experimental points was established by varying x and an overall normalization parameter so as to obtain the best fit for the complete set of odd and even ordered sidebands corresponding to each drive voltage. The channel bandwidth characteristic of an fm signal is usually taken to be $(2x + 2)\,\omega_m$ where ω_m is the modulating frequency.[18] Thus, point (e) of Figure 19 corresponds to a bandwidth of 51 MHz.

We will now proceed to a study of the potential bandwidth limitations discussed in Section 3.1. We first consider frequency dependent loss. Inspection of the static subcarrier curves indicates that this factor is quite signficant in the 40 MHz to 100 MHz region of the 1.15μ curve. Figure 20 consists of three normalized sideband spectra obtained with a subcarrier frequency of about 80 MHz (Figures 20a-c), and the corresponding segment of the dc curve (Figure 20d). The three spectra represent roughly the same maximum deviation (20 MHz) and modulating frequencies of 2.6 MHz, 4.5 MHz and 10 MHz. The circles indicate theoretical sideband amplitudes obtained by fitting Bessel function spectra to the date. Crystal (II) was used for this and all subsequent 1.15μ data.

The sideband spectra of Figure 20 are seen to deviate from the theoretical amplitudes in two ways. First, there is general asymmetry of the sidebands which is most pronounced at the lowest modulating frequency. Second, at the higher modulating frequencies the higher order sidebands tend to be suppressed in favor of the lower ones. For now we will concern ourselves with the first factor, sideband asymmetry, reserving the second factor for later discussion.

The action of our bandwidth limiting factors can be most easily understood if we adopt the reasonable, simplified view that their operation is linear in signal intensity, in other words, that they act like conventional band pass filters. In this case they would be expected to simply suppress the various sidebands in proportion to their response at the sideband frequencies.[17] This picture appears to fairly well represent the action of the frequency dependent loss at 2.6 MHz. However, at the higher frequencies the action is clearly much less pronounced than expected on the basis of the static response. The behavior is seen quite clearly in Figure 21. Here we have plotted the normalized sideband asymmetry, i.e.: $(A_\ell - A_u)/(A_\ell + A_u)$ where A_ℓ and A_u are the lower and upper sideband amplitudes respectively, as a function of distance from the carrier

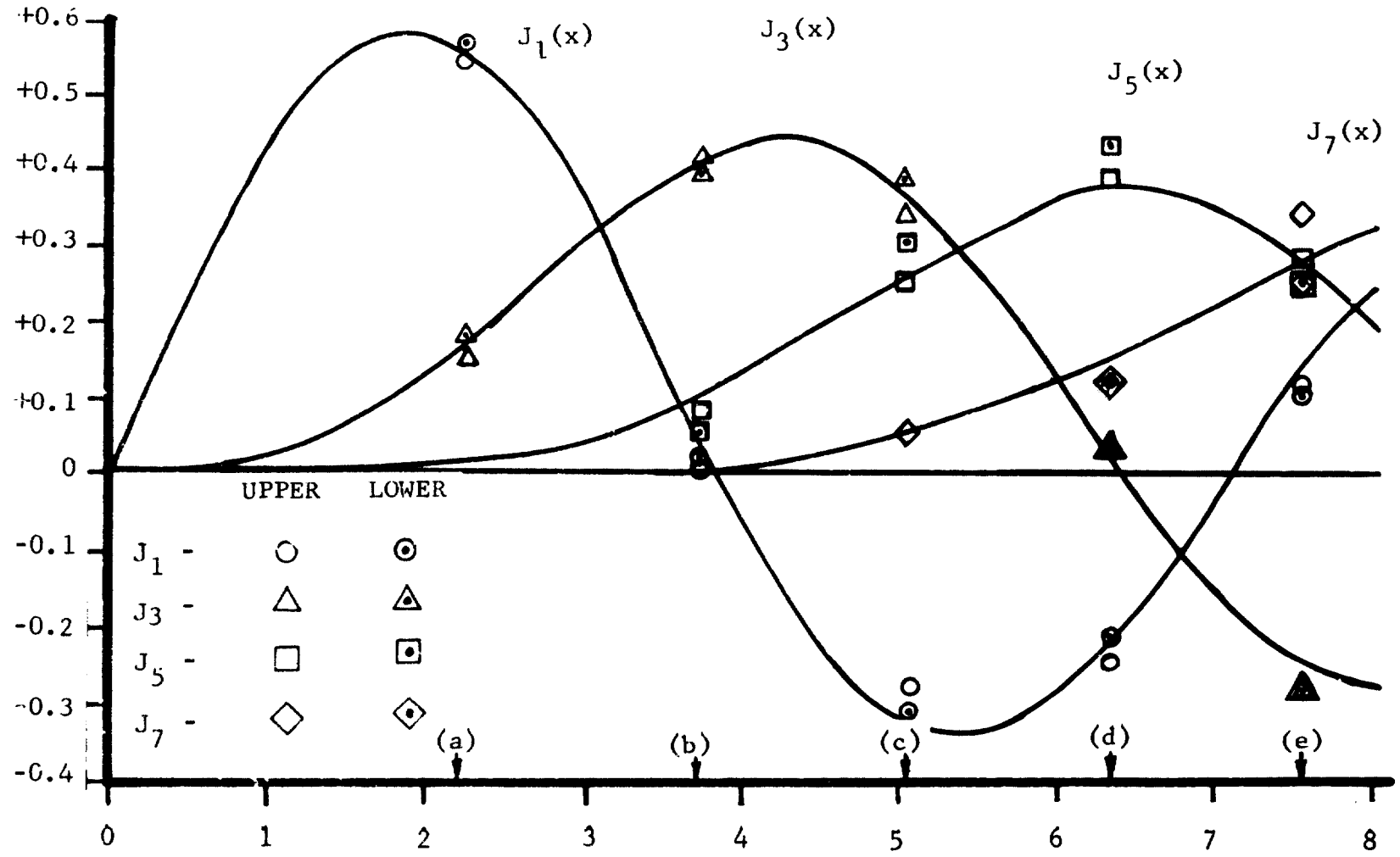

FIGURE 19. EXPERIMENTAL SIDEBAND AMPLITUDES FITTED TO ODD ORDER BESSEL FUNCTION AMPLITUDES.

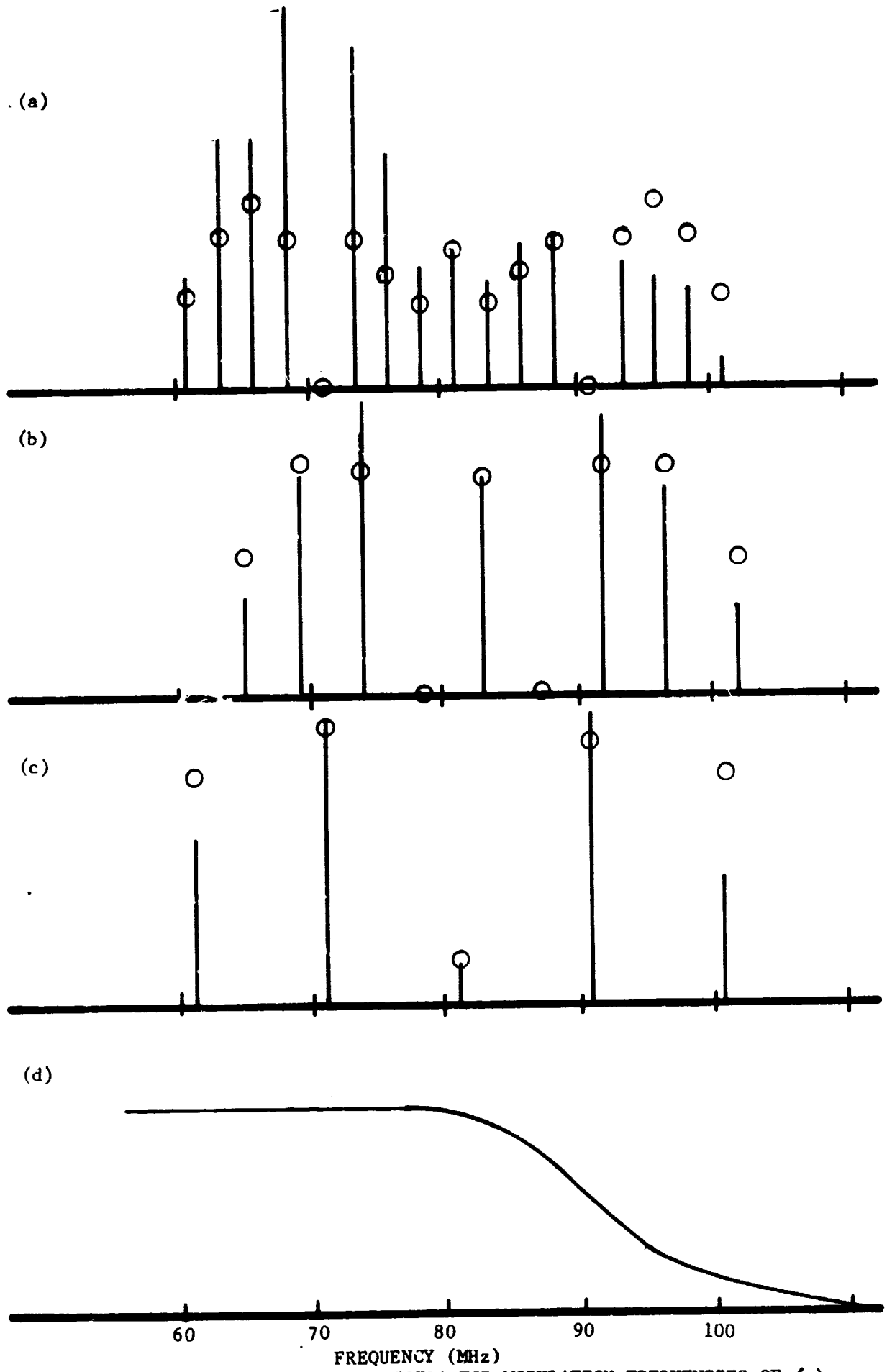

FIGURE 20. NORMALIZED SIDEBAND SPECTRA FOR MODULATION FREQUENCIES OF (a) 2.6 MHz, (b) 4.5 MHz, (c) 10 MHz, and (d) THE CORRESPONDING DC RESPONSE.

frequency. The dc curve is taken directly from the static response shown in Figure 20d. A similar set of curves showing the asymmetry observed at 4.5 MHz as a function of deviation ratio is shown in Figure 22. As indicated by these two figures, sideband asymmetry is less severe at higher frequencies for a given maximum deviation but more severe at higher maximum deviations for a given modulation frequency.

As we increase the fm deviation beyond that used for the above figures we soon reach a point where both frequency dependent loss and strong coupling must be considered. Such a situation is illustrated by Figures 23 and 24 which were obtained with a modulation frequency of 12 MHz and a maximum deviation of 43 MHz (bandwidth 110 MHz). Not only is the frequency dependent loss still considerably reduced in effectiveness, but in addition there is little or no sideband suppression due to strong coupling.

Strong coupling effects can be most advantageously studied at 3.39μ where they are not complicated by frequency dependent loss. In addition we would expect them to be more severe at this wavelength since the cavity decay time and mode buildup time are much shorter than at 1.15μ. The one complication is the uncertainty in normalization imposed by the frequency dependence of the detector circuit discussed in Section 3.4. For the results reported here we used a detector circuit which appeared to yield a flat response below about 60 MHz; this allowed extrapolation of the response into the strong coupling region.

Sideband asymmetry plots obtained with modulation frequencies of 5 MHz and 10 MHz are shown in Figure 25. Hence we have plotted the asymmetry of the individual sidebands as a function of subcarrier frequency. Strong coupling was obtained at frequencies below about 42 MHz. The vertical bars indicate the points at which each sideband would be expected to fall to zero on the basis of the dc response. The results indicate that the effect of strong coupling on a given sideband tends to become less severe as the deviation is increased and that the effect at a given deviation is less severe at higher modulating frequencies. The positive bias toward the right side of the figures is probably due to the normalization uncertainty.

A phenomenon closely related to the strong coupling behavior discussed above is the subcarrier switching observed at 1.15μ with subcarrier frequencies of about 210 MHz (see Section 3.4). Such switching was not found to occur at the modulation frequencies used (2 MHz to 12 MHz). A typical spectrum overlapping the switching point is shown in Figure 26 with the corresponding dc curve. The symmetry evident in this figure is typical of the results obtained in the flat region of the subcarrier response curve.

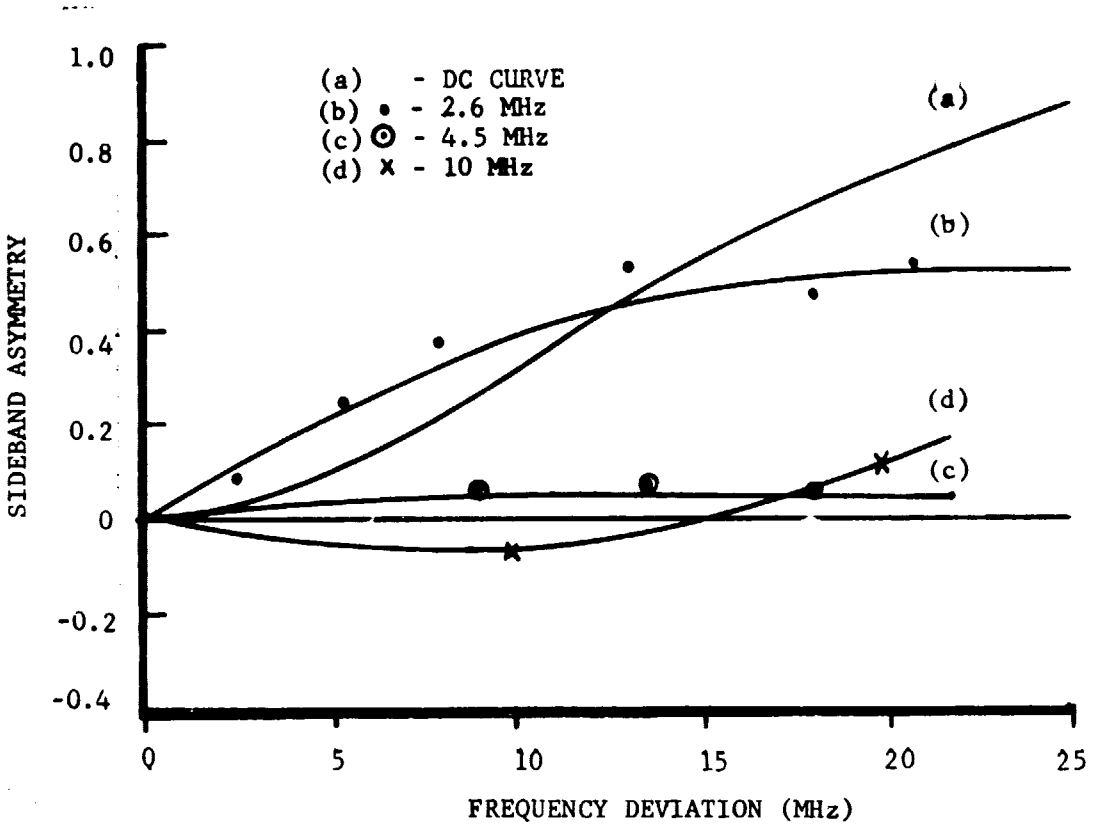

FIGURE 21. SIDEBAND ASYMMETRY FOR THREE MODULATION FREQUENCIES.

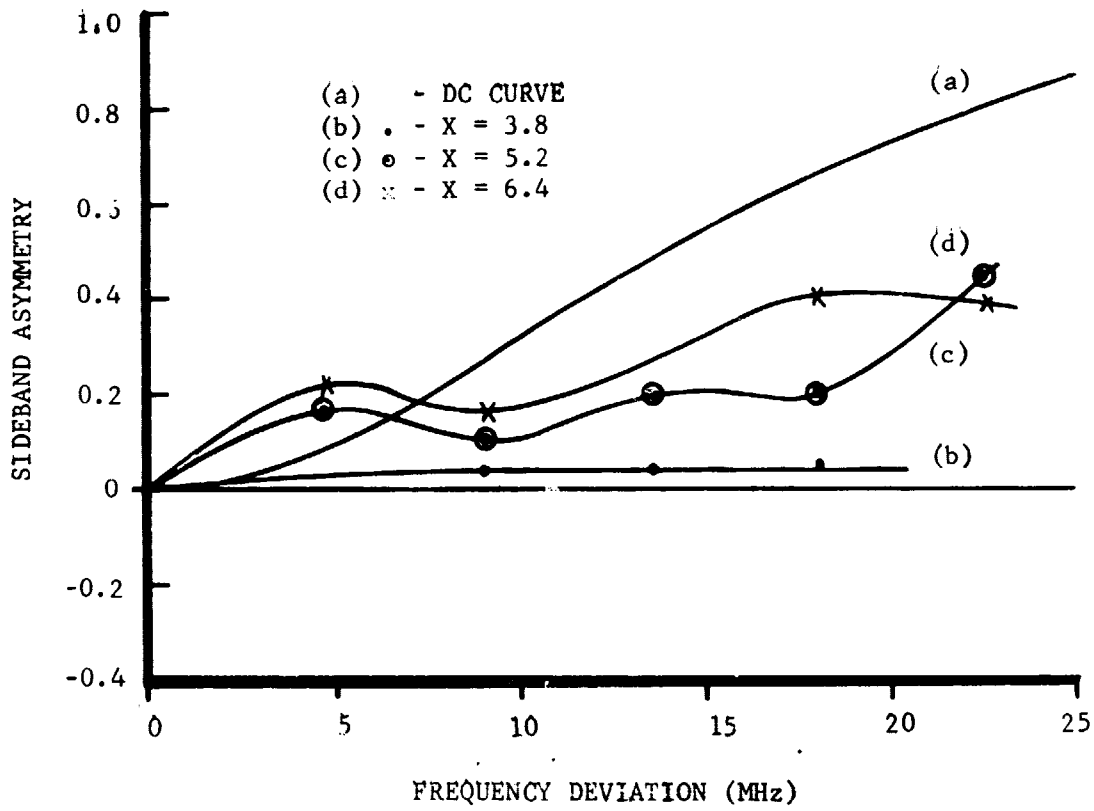

FIGURE 22. SIDEBAND ASYMMETRY FOR A MODULATION FREQUENCY OF 4.5 MHz AND THREE DEVIATION RATIOS.

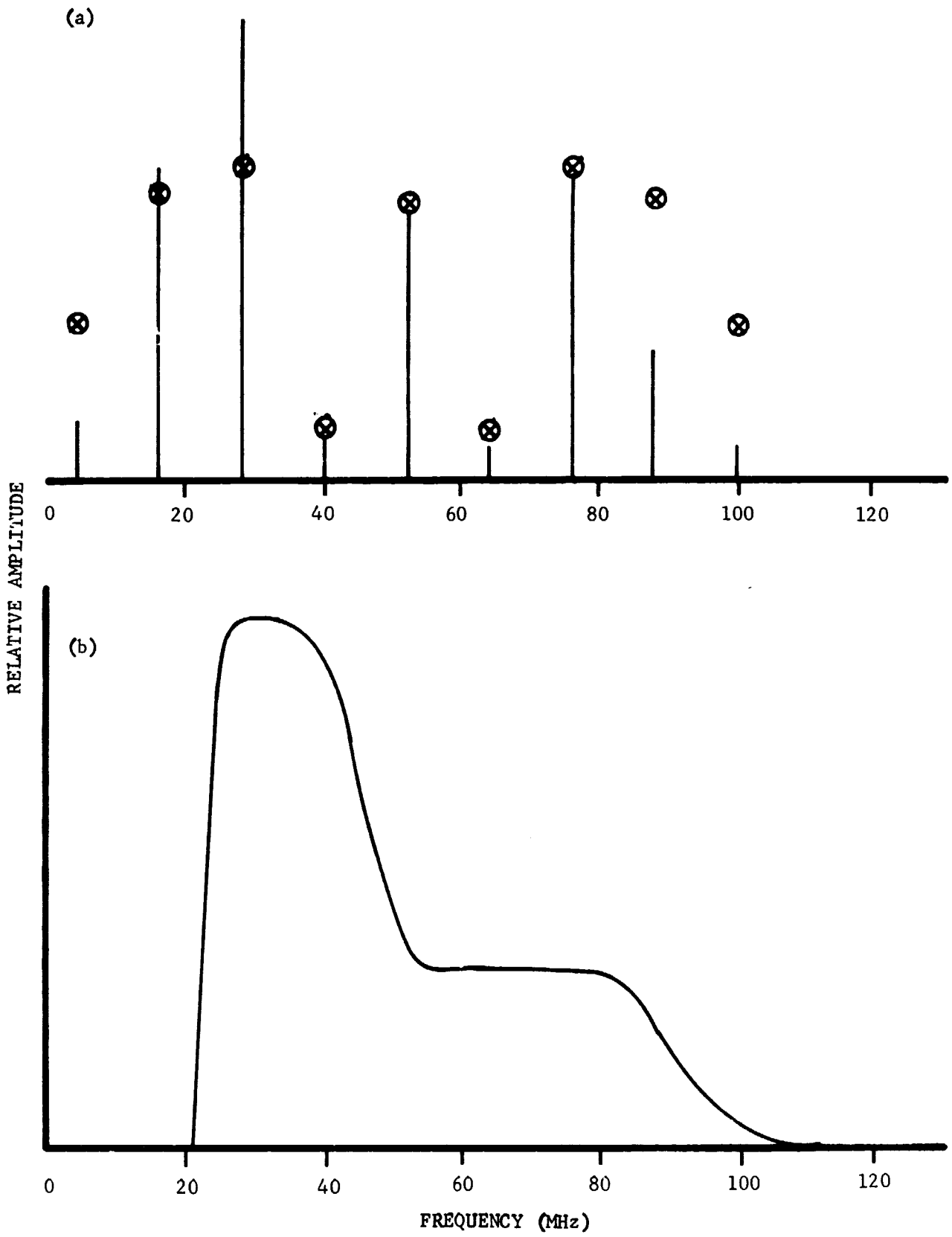

FIGURE 23. (a) NORMALIZED SIDEBAND SPECTRA FOR A MODULATION FREQUENCY OF 12 MHz AND AN FM BANDWIDTH OF 110 MHz. (b) THE CORRESPONDING DC RESPONSE.

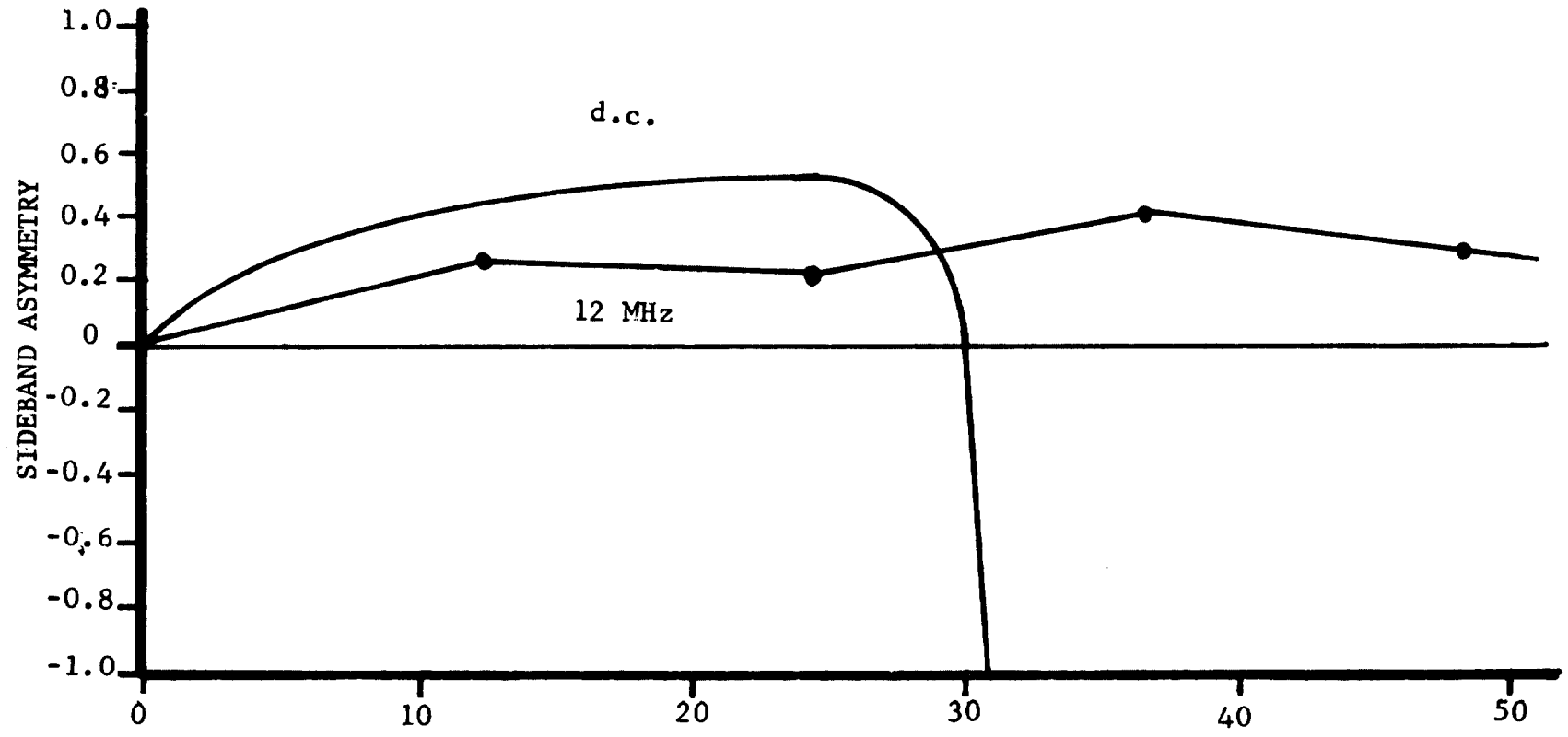

FIGURE 24. SIDEBAND ASYMMETRY PLOT CORRESPONDING TO FIGURE 23.

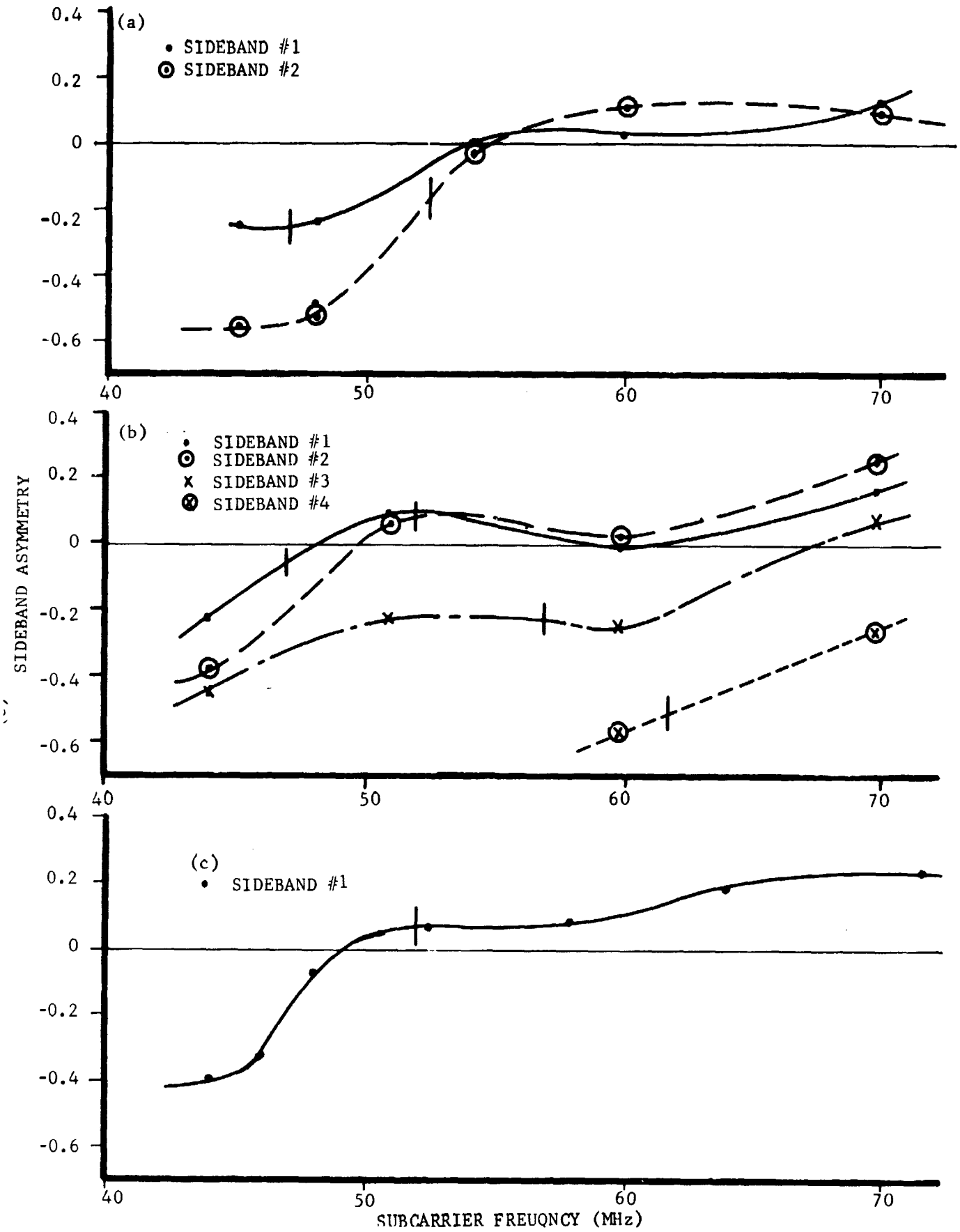

FIGURE 25. SIDEBAND ASYMMETRY AT 3.39μ AS A FUNCTION OF SUBCARRIER FREQUENCY. (a) ν_{mod} = 5 MHz, x = 1.5; (b) ν_{mod} = 5 MHz, x = 2.7; (c) ν_{mod} = 10 MHz, x = 0.75.

We now return to the high order sideband suppression mentioned earlier. As is evident in Figure 20, the phenomenon tends to be more severe at higher modulating frequencies. Data taken with a fixed modulating frequency also indicates that it is more severe at greater deviation ratios. However, the phenomenon was found to vary considerably with experimental laser conditions and was generally unpredictable from day to day. For example, the high order sideband suppression evident in Figure 26 is only slightly more severe than that of Figure 20b even though the former corresponds to both a modulation frequency and a maximum deviation nearly three times that of the latter. This phenomenon is probably due primarily to the cavity width limitation mentioned in Section 3.1 and thus should depend quite strongly on both cavity loss and excess laser gain. It was not observed at 3.39μ where the excess gain is quite high and where the estimated cavity transmission and loss total of 40% would lead to a cavity width of 25 MHz.[19] At 1.15μ the transmission and loss probably total between 15% and 20% for a cavity width of the order of 15 MHz. It should be noted that the bandwidths achieved in this program (over 100 MHz) are considerably greater than this cavity width and certainly much greater than the width above oscillation threshold.

In addition to the work reported above, some tests were made at higher modulating frequencies. These tests were hampered, however, by dielectric heating of the modulator crystal which was discussed in Section 3.3. This factor resulted in a rapid degradation of the laser output above 12 MHz. The greatest bandwidths at high frequencies were observed when the 'a' axis crystal was used at 1.15μ. The resulting subcarrier drift, on the other hand, prevented detailed measurements from being made. The highest modulating frequency used was 20 MHz at which point an fm spectrum having a bandwidth of approximately 120 MHz was observed.

3.6 DISCUSSION

In the preceding sections we have considered the nature and severity of the bandwidth limiting factors characteristics of a He-Ne DPFM laser and have illustrated the distortions of the fm sideband spectrum caused by these factors. Two questions remain to be answered: (1) What effect will the spectrum distortion have on the operation of a practical communication system? and (2) What are the dependences of the various limitations on laser characteristics?

In order to answer the first of the questions above we must determine the types of distortion represented by our sideband spectra. First of all, it is quite clear that the distortions are of a harmonic nature since all of the sidebands observed in our experiments were harmonically related to the modulation frequency. In addition, as we will demonstrate below, no evidence of fm distortion was found. This statement is based on the fact that at all of the modulation frequencies used the upper and

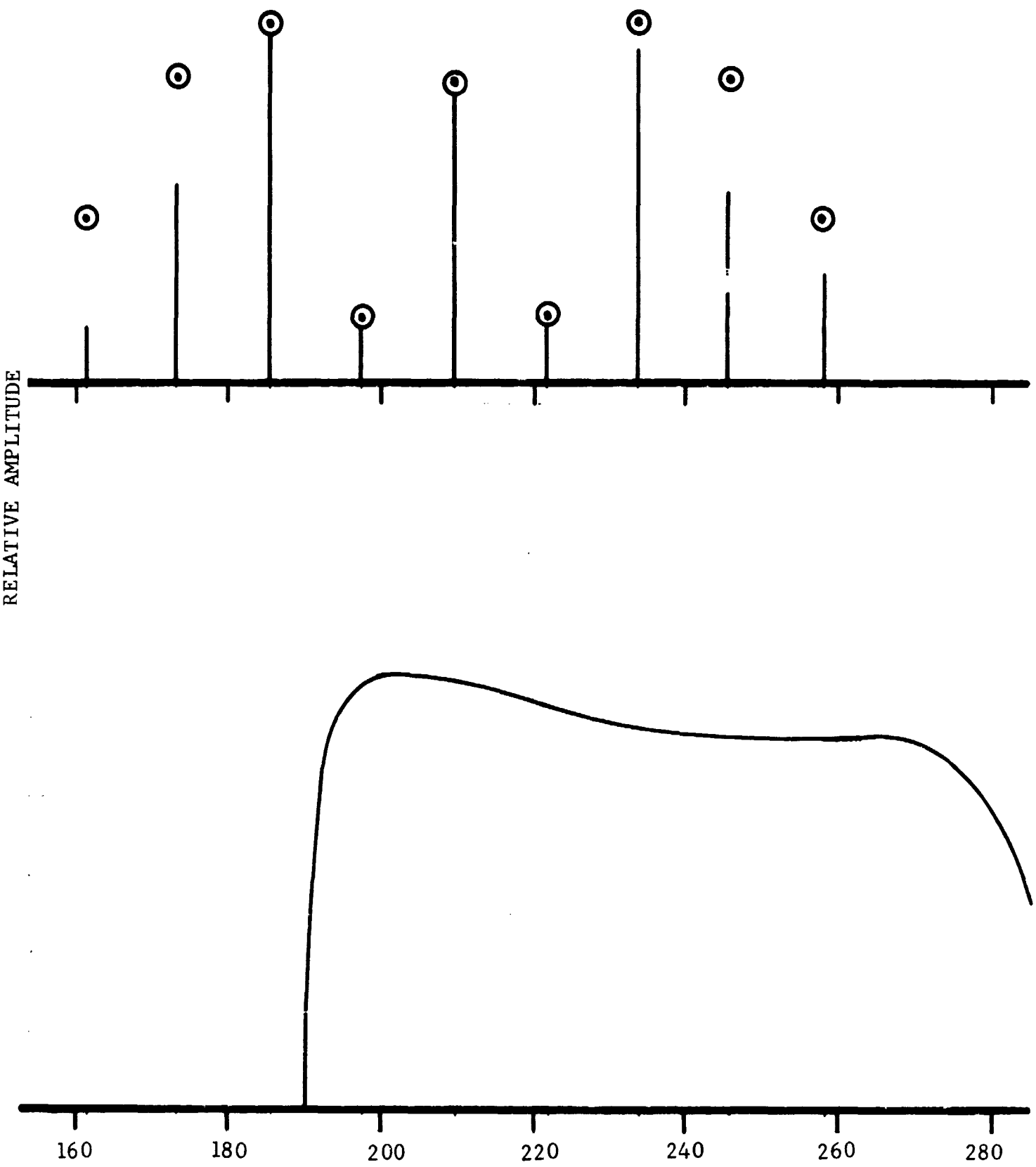

FIGURE 26. (a) SIDEBAND SPECTRA OVERLAPPING THE SUBCARRIER SWITCHING POINTS, ν_{mod} = 12 MHz, Bandwidth = 110 MHz. (b) CORRESPONDING DC RESPONSE.

lower sidebands of a given order were observed to be nulled at the same deviation ratio.

If we assume the presence of a spurious (perhaps harmonically related) modulation frequency in our fm output, the signal amplitude will have the form

$$f(t) = A_c \cos [\omega_c t + x_1 \sin \omega_1 t + x_2 \sin \omega_2 t] \tag{26}$$

where ω_c, ω_1, and ω_2 are the frequencies of the carrier, the desired modulation and the spurious modulation respectively and x_1 and x_2 are the corresponding deviation ratios. Expanded in a Fourier series, this has the form[17]

$$f(t) = A_c[\sum_{n=-\infty}^{\infty} \sum_{m=-\infty}^{\infty} J_n(x_1)J_m(x_2) \cos (\omega_c + n\omega_1 + m\omega_2)t] \tag{27}$$

where $J_n(x_1)$ is the n'th order Bessel function. If we next assume that ω_2 is a multiple of ω_1 we can take

$$\omega_2 = h\omega_1, \qquad (h = 2, 3, 4, ---) \tag{28}$$

$$n\omega_1 + m\omega_2 = (n + hm)\omega_1 = k\omega_1, \qquad (k = 0, 1, 2, ---) \tag{29}$$

and

$$f(t) = A_c[\sum_{k=-\infty}^{\infty} \sum_{m=-\infty}^{\infty} J_{k-hm}(x_1)J_m(x_2) \cos (\omega_c + k\omega_1)t]. \tag{30}$$

The amplitude of the k'th sideband is simply

$$A_k = A_c[\sum_{m=-\infty}^{\infty} J_{k-hm}(x_1)J_m(x_2)] \tag{31}$$

In order to most easily demonstrate that a balance between the null positions at upper and lower sidebands implies the absence of fm distortion we will take a specific example; weak second harmonic distortion. In this case we have h = 2 and we need consider only m = 0 and m = $\pm$ 1. The condition for a null of the first upper sideband (k = 1) is

$$A_1 = 0 = J_1(x_1)J_o(x_2) + J_3(x_1)J_{-1}(x_2) + J_{-1}(x_1)J_1(x_2)$$

$$= J_1(x_1)J_o(x_2) - J_3(x_1)J_1(x_2) - J_1(x_1)J_1(x_2) \tag{32}$$

where we have used the identity $J_{-k} = (-1)^k J_k$. Similarly a null of the first lower sideband is given by

$$A_{-1} = 0 = -J_1(x_1)J_1(x_2) - J_3(x_1)J_1(x_2) - J_1(x_1)J_1(x_2) \tag{33}$$

Subtracting the second expression from the first, we have

$$2J_1(x_1)J_o(x_2) = 0. \tag{34}$$

This equation cannot be satisfied for arbitrary values of x_2. Thus the simultaneity of the sideband nulls implies that $x_2 = 0$ and hence that the assumed fm distortion does not exist.

The above discussion implies not only that fm distortion is negligible but also that nonlinear amplitude distortion is negligible. Nonlinear distortion might arise, for example, from the interaction between the time varying optical field and the atomic medium and would be characterized by the appearance of spurious, harmonically related, sidebands (combination tones).[20] The mathematical treatment would be similar to the treatment of the second harmonic sidebands above and would again imply an imbalance of the sideband nulls.

If fm and nonlinear amplitude distortions are not present, the deviations of our sideband spectra from pure Bessel function distributions must be due to linear amplitude distortions. This justifies our earlier assumption that the action of the bandwidth limiting factors was similar to that of simple bandpass filters. The above results have considerable significance from the practical standpoint since both fm and nonlinear distortions can lead to degradation of the information content of an fm communication channel and to crosstalk between channels. The effects of linear amplitude distortion, on the other hand, can be effectively minimized by conventional fm receiver circuitry.

We will now discuss, qualitatively, the expected relationships between the various bandwidth limitations and general laser characteristics.

(1) Strong coupling phenomena: The width of the strong coupling region (lower subcarrier limit) is dependent upon the atomic angular momentum and the collision broadened atomic linewidth. It ranges from zero to about 50 MHz for various gas lasers. The experiments to be reported in Section 5 below indicate that it is close to zero for the CO_2 laser. The effect of strong coupling on the fm sideband spectrum is expected to decrease with increasing cavity lifetime and mode buildup time, and as a result, should be least severe for low gain, high cavity Q systems. Our 3.39μ results should thus serve as an upper limit of the severity to be expected with other lasers.

(2) Subcarrier switching: This phenomena only occurs in rather special situations and can probably be avoided in most system designs by proper choice of cavity length and subcarrier frequency. In addition, at rf modulation frequencies our experiments indicate that it has little effect on system operation.

(3) Frequency dependent gain or loss: Frequency dependent loss can usually be eliminated by proper design of intracavity components. Frequency dependent gain, on the other hand, will occur in the form of the restricted Doppler width of some lasers, most notably the CO_2 laser. The effect of this factor on high frequency modulation is expected to depend upon the cavity ringing time, as discussed in Section 3.1. With a sufficiently high Q cavity our experimental results suggest that it should be possible to establish fm sidebands at frequencies considerably above the range of subcarrier frequencies allowed by the width of the gain profile above threshold.

(4) Cavity mode width limitation: The passive cavity width is proportional to the cavity length and inversely proportional to the Q. The limitation should thus be least severe with a short, high Q, system. In some situations it may be necessary to select a Q which optimizes the tradeoff between the cavity limitation and frequency dependent gain. Our experiments however indicate a considerable degree of flexibility since we were able to obtain fm spectra with bandwidths of the order of eight times the passive cavity width. It seems probable, for example, that operation of a CO_2 laser can be achieved with modulation frequencies of several megahertz and bandwidths approaching twice the maximum allowable subcarrier frequency.

SECTION 4

STABILIZATION OF A DPFM LASER

4.1 INTRODUCTION

In order to effectively utilize the DPFM system in a practical application it is necessary to stabilize the cavity length sufficiently to maintain the proper sequence of oscillating modes. This requires the derivation of a suitable error signal from the laser output and the use of a compensating feedback system. Fortunately this is much easier to do with the DP laser than with the ordinary Brewster window laser for which a dithering technique is generally required. With the DP laser an error signal can be obtained quite simply by separating the two polarization states in the laser output and comparing their intensities. A null in the intensity differences will occur whenever the orthogonally polarized modes are symmetrically placed on the Doppler line. In addition, the sign of the error signal will indicate the direction of the required correction.

Earlier studies of the DP Stabilization System have concentrated on the behavior obtained for small birefringent frequency splittings.[21] It was found that extremely steep discriminant slopes could be obtained by appropriately adjusting the relative amounts of linear birefringence and Faraday rotation. If the stabilization system is to be used with DPFM, on the other hand, we need to determine its behavior for relative large frequency splittings (subcarriers) which are brought about by linear birefringence alone. In addition we must determine whether the modulating process itself has any effect upon the stabilization behavior. Some experiments devoted to the answer of these questions and to the demonstration of simultaneous stabilization and frequency modulation are described below.

4.2 STABILIZATION APPARATUS AND PROCEDURES

The dual-polarization stabilization technique used involves a closed-loop linear feedback system.[22] The open loop gain of this type of system determines the residual error

$$\epsilon = \left(\frac{R}{1 + GH}\right) \tag{35}$$

where R is the input, open loop, or attempted error; G is the open loop gain; and H is the feedback function. Relating this to our particular application, GH (=G') may be considered to be the product of the discriminant slope ($dv/d\ell_c$), the transducer response ($d\ell_c/dv$), and the amplifier gain (G). A stability factor may now be defined as

$$S = \left(\frac{\epsilon}{R}\right)(100) = \left(\frac{1}{1 + G'}\right)(100) \tag{36}$$

which indicates the effectiveness of the stabilization process in terms of percentage of attempted drift remaining.

It is obvious that the highest possible gains will result in the minimum residual error. However, consideration of the overall operating capabilities desired of our system resulted in practical limitations of this parameter. The range needed could be determined from the free-running laser drift, and was found to be rather large (> 5 microns). To accomodate this, a large transducer and a driver with a high-voltage capability were required. Due to the large capacitance associated with such a transducer, and the finite impedance of the driver, response times become important. A reasonable compromise was felt to have been reached by limiting the system response to 40 Hz, below which most of the instabilities occurred.

Overall system gain was now limited by the amplifier used plus the ratio of discriminant slope to transducer response. In all cases, available amplifier gain was in excess of that usable because of the instability factors involved in the second order effects of the transfer functions. Excess gain simply resulted in either hunting or lock-up, characteristic of such under-damped systems.

It may be mentioned that the higher frequency instabilities (> 40 Hz) may also be discriminated against using the same techniques. Either a straightforward extrapolation of the present system involving wide-band components could be used, or a secondary high-frequency channel, composed of a driver and transducer, could be added. This second channel would not require the large dynamic range and thus could provide full

stabilization with only slight additional equipment. In our experiments, the instabilities in this region were not sufficient to warrant concern.

The actual system components used are described below. Satisfactory results were obtained with both the rare gas and the CO_2 lasers. At times when the laser drift exceeded the dynamic range of the system, the loop was simply opened momentarily, causing the transducer to delay, and permitting the acquisition of a different pair of modes on the dopper profile.

The stabilization apparatus used in this program is shown schematically in Figure 27. The laser cavity includes the modulator crystal, which, while providing modulation, also establishes the birefringence necessary for dual polarization behavior. The output obtained at the rear of the laser through a low transmission mirror was split by a Wollaston prism into the two orthogonally polarized components, each of which was detected by a separate photo multiplier (or copper-doped Germanium detector) in the case of CO_2. The detected signals were displayed directly on an oscilloscope and were also supplied to the two inputs of a Tektronix Type G differential amplifier. The resulting amplified difference signal was used to drive a 1500 V Kepco Model 1500-M dc supply operated in a servo mode, thus providing a high output driver stage for the transducer. One mirror of the cavity was mounted on this transducer, which was a 3" x 6" cylinder of PZT ceramic supplied by Clevite.

To obtain stabilized operation, the cavity was swept by the Variac/transformer combination while the output of the two detectors (signals (a) and (b)) was observed on the oscilloscope. The detector gains were balanced and the Wollaston orientation adjusted to properly separate the two polarization states. Proper adjustment of the cavity and birefringent parameters resulted in the desired balance and discriminant slopes of the two signals, as indicated in Section 4.3. A calibration of the discriminant slope $(dv/d\ell)$ could then be made using signal (c).

For stabilized operation of the system the transducer sweep source was removed, and the driver amplifier inserted. Lock-on was indicated by a meter built into the driver unit. Driver output was also displayed on the oscilloscope (Signal d), and, using the previously obtained $(d\ell/dv)$ characteristics of the transducer, the total correction applied could be ascertained. A comparison of the input (C) and output (D) levels of the driver permitted determination of the effective stabilization factor. Examination of the discriminant data alone, with knowledge of other cavity parameters, yielded the actual stabilization accomplished.

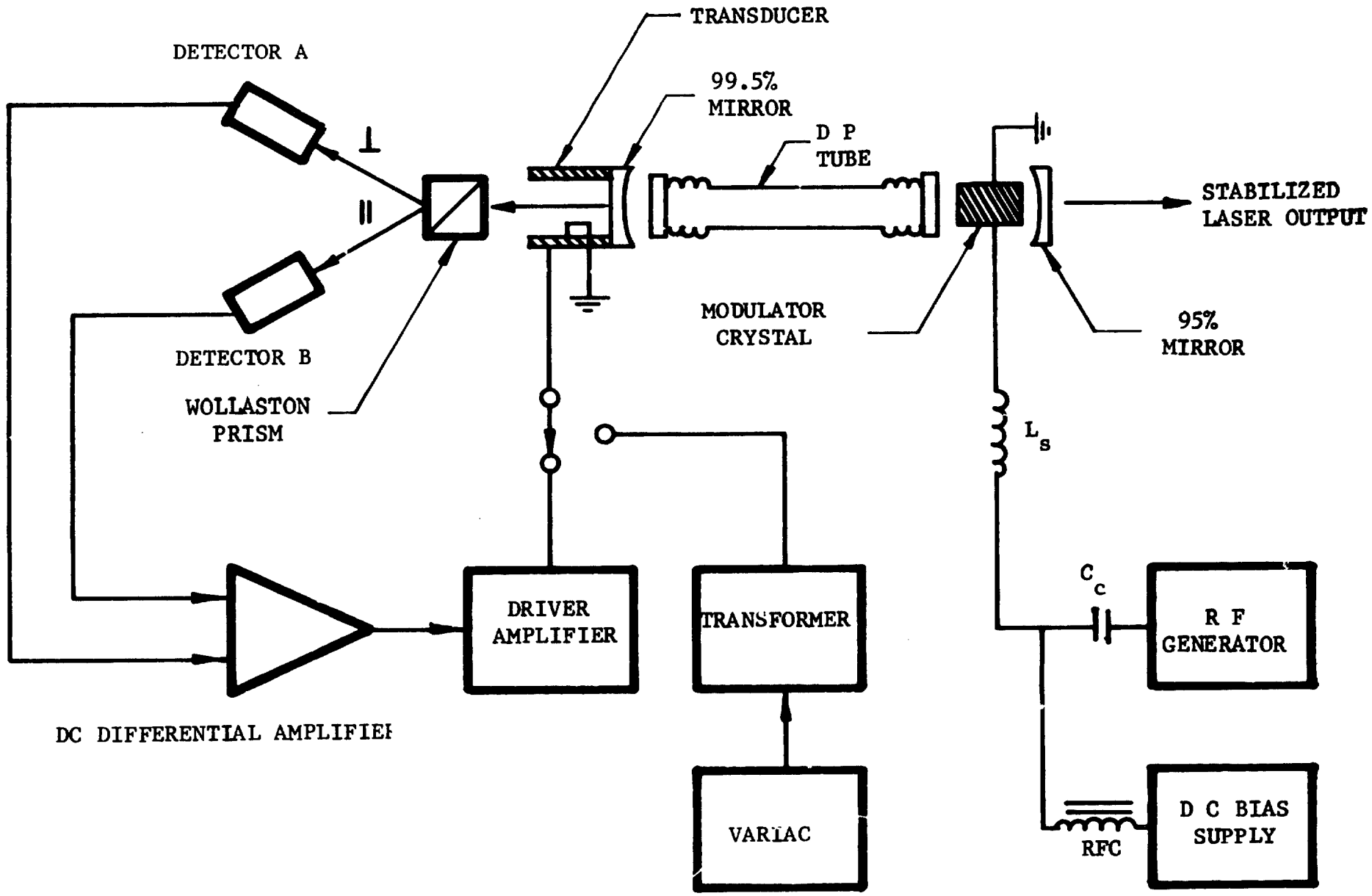

FIGURE 27. STABILIZATION APPARATUS

4.3 EXPERIMENTAL STABILIZATION RESULTS

In studying the discriminant characteristics obtained with the DP Stabilization System we will be interested in two regions of operation: first, operation with cavity lengths appropriate to place the two members of a single, weakly coupled, pair of modes symmetrically on the Doppler line, and second, operation with two pairs of cavity modes symmetrically placed on the line. In the first case we will obtain a relatively low frequency subcarrier (at $\Delta\nu$). In the second place we will obtain a high frequency subcarrier at either $\Omega-\Delta\nu$ or $\Omega+\Delta\nu$ depending on the experimental conditions.

Typical discriminants obtained with an unmodulated laser and four values of dc bias are shown in Figure 28. The low subcarrier region occurs roughly at the center of each photograph. The fairly complicated behavior indicated can be explained on the basis of the hypothetical mode sequences shown in Figure 29. The discriminant curves are reproduced on the left. The arrows indicate (I) central tuning of one pair of modes, (III) symmetrical tuning of two pairs, and (II) an intermediate tuning. The diagrams on the right represent the mode sequences occuring at each of these tunings. As in Section 3.5, the short vertical lines indicate cavity modes which are not in oscillation.

In Figure 29a strong coupling occurs for all tunings. Except for a region of hysteresis near central tuning the member of each pair of modes nearest the center of the Doppler line oscillates. In Figure 29b the birefringent splitting is sufficient to allow weak coupling near the center of the line. In Figure 29c the splitting is large enough so that apparently the coupling between successive mode pairs is an important factor. As a result oscillation switches to the modes farthest from the center whenever two successive pairs are able to oscillate simultaneously. Of course, once the mode sequence has switched it will remain fixed until weak coupling again occurs. As a result, no intensity crossover is observed. In Figure 29d, the region of weak coupling has broadened sufficiently to allow the laser to pass directly from weak coupling to the two pair behavior. At this point the discriminant curve is the reverse of that shown in Figure 29b.

The discriminant slopes obtained at both low subcarrier and high subcarrier crossover points are plotted in Figure 30. Except for the region from 44 MHz to 58 MHz where behavior (c) of Figure 29 occurs, the discriminant is adequate for the requirements of the DPFM system. The frequency and width of the region of weak discriminant appear to depend on laser gain, cavity length and mirror transmission. Thus, with appropriate adjustment a usable discriminant can probably be obtained with any subcarrier frequency.

(a)

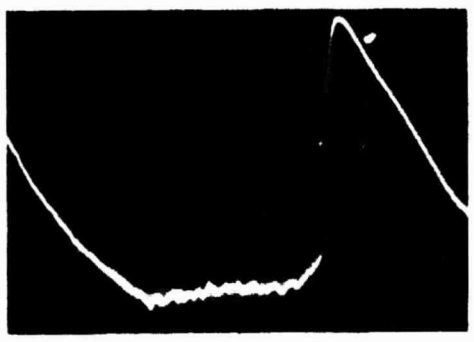

(b)

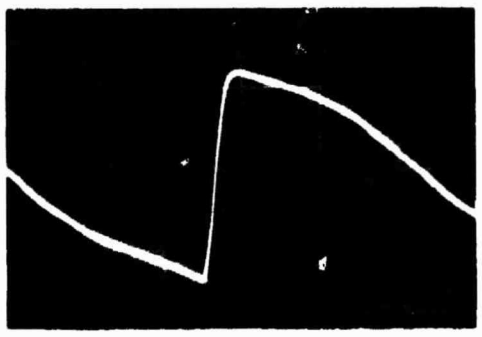

(c)

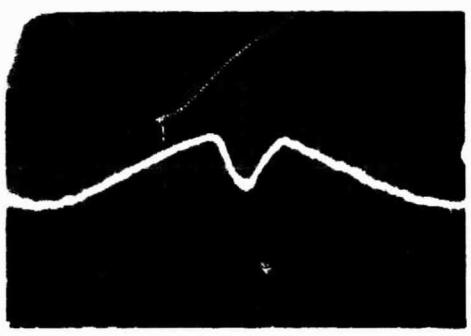

(d)

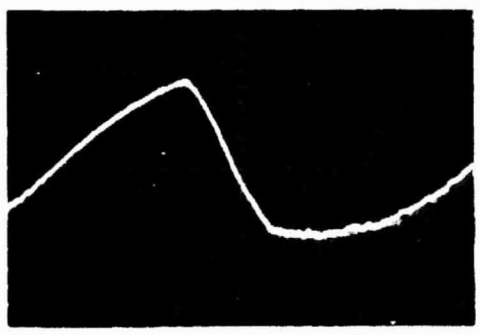

FIGURE 28. STABILIZATION DISCRIMINANTS FOR FOUR VALUES OF BIREFRINGENT SPLITTING; (a) $\Delta\nu \sim 0$ MHz, (b) $\Delta\nu = 24$ MHz, (c) $\Delta\nu = 44$ MHz, and (d) $\Delta\nu = 69$ MHz.

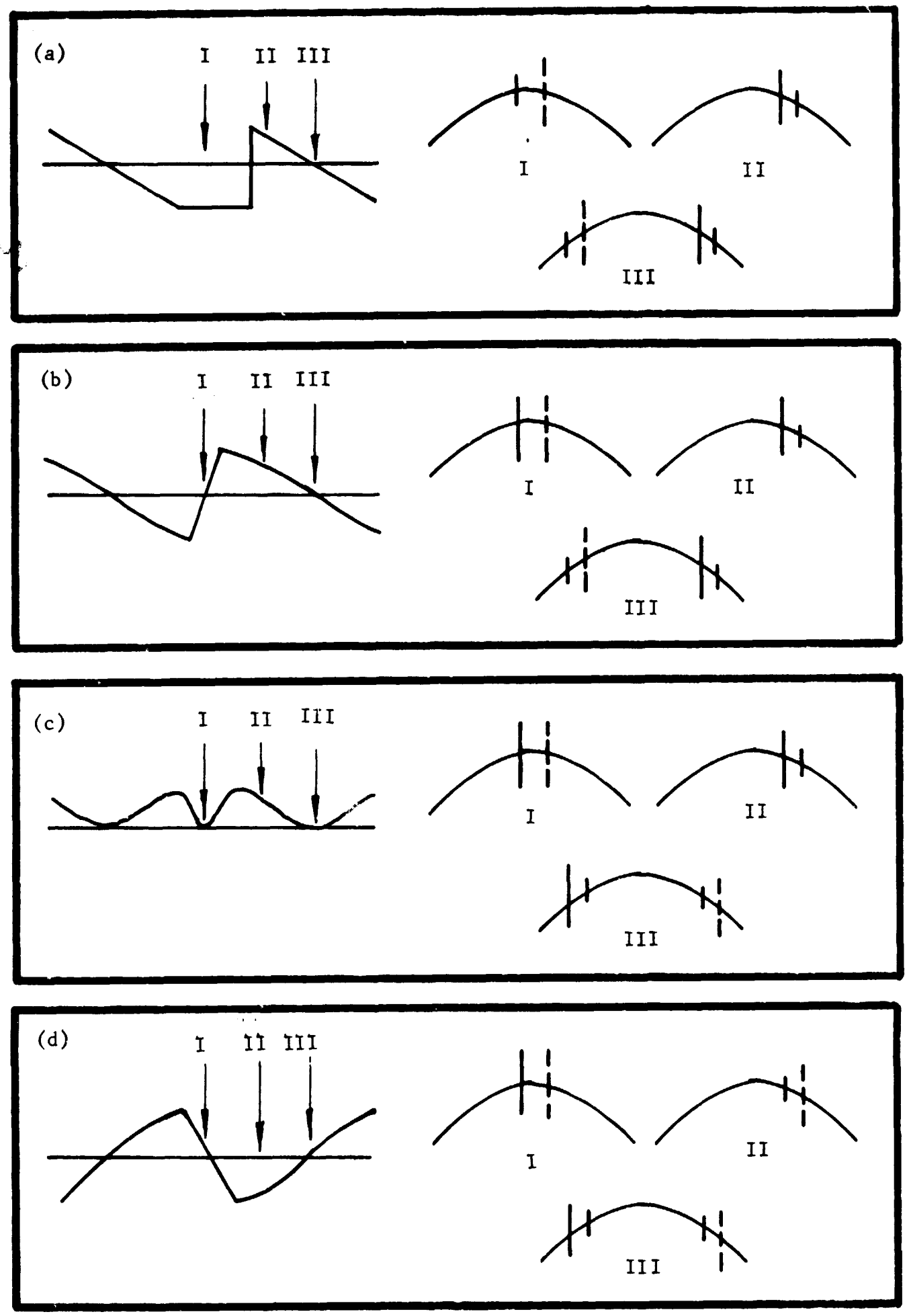

FIGURE 29. MODE SEQUENCES CORRESPONDING TO THE DISCRIMINANTS OF FIGURE 28. THE SHORT LINES REPRESENT CAVITY MODES NOT IN OSCILLATION.

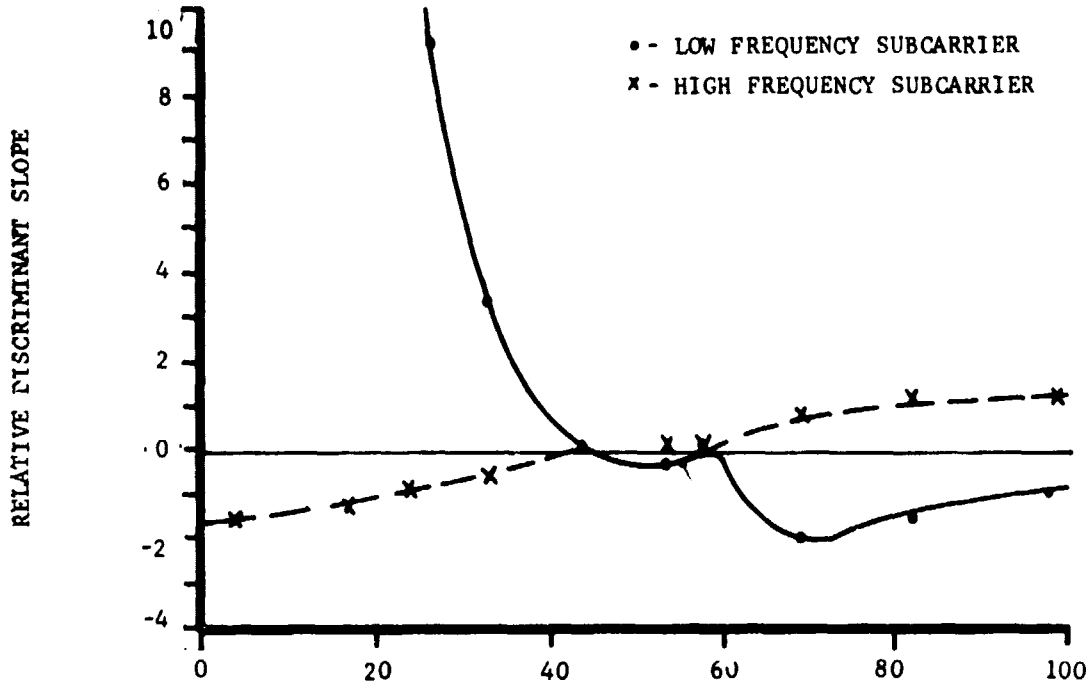

FIGURE 30. DISCRIMINANT SLOPE FOR AN UNMODULATED DP LASER.

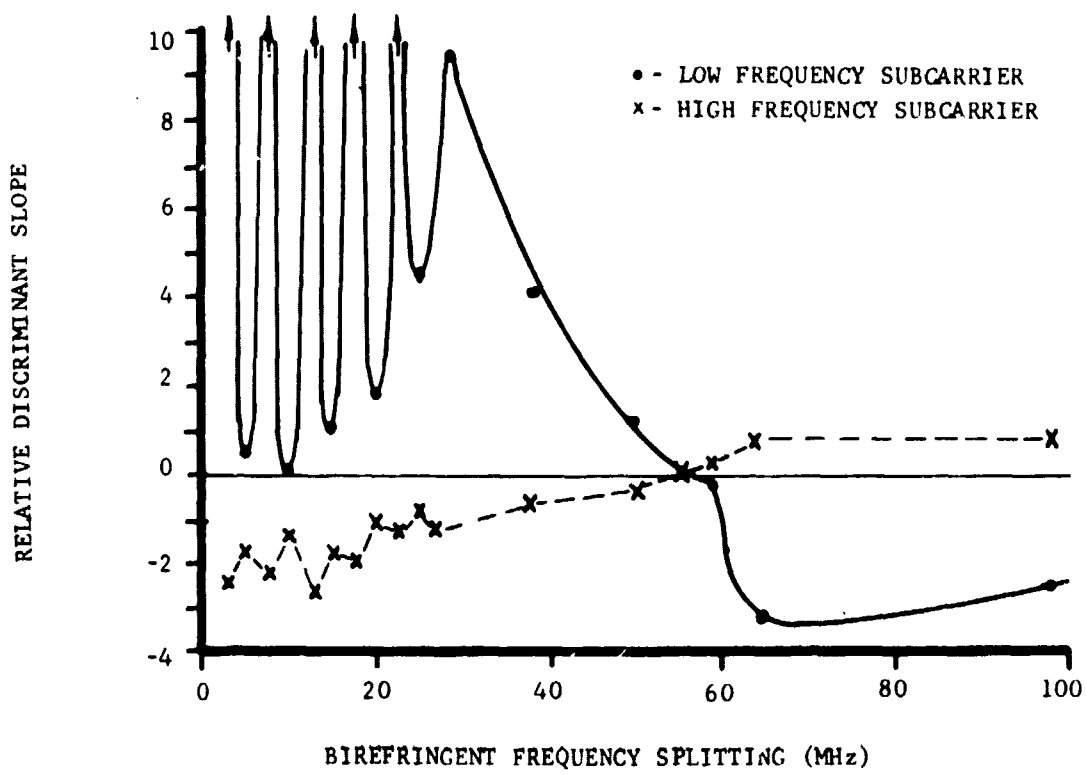

FIGURE 31. DISCRIMINANT SLOPE DURING MODULATION; ν_{mod} = 5 MHz, x = 2.5.

The slopes plotted in Figure 31 are typical of those obtained during DP frequency modulation. In this case the modulation frequency and deviation ratio were 5 MHz and 2.5 respectively. At high values of birefringent splitting the results are not significantly different from those of Figure 30. However, when the splitting was low enough so that the low frequency fm spectrum overlapped zero frequency, the behavior was drastically altered. This effect was most pronounced whenever a sideband of the spectrum coincided with zero, in which case the slope was greatly reduced. Although the effect is quite interesting and not at all easy to understand, it is probably not important from a practical standpoint since one would not use a low frequency subcarrier under conditions for for which the fm spectrum overlapped zero, and since the high frequency subcarrier appears to be only modestly affected.

In addition to the experiments described above, the discriminant slope was studied as a function of fm deviation for a number of subcarrier frequencies. Deviation ratios from zero to 10 were used with a 5 MHz modulation frequency. Very little effect could be observed at sufficiently high subcarrier frequencies aside from an apparent change in the effective dc bias which was reflected in a change in the slope for subcarriers around 50 MHz.

With the stabilization loop closed it was found that the system could be locked to almost any portion of either the low or high frequency discriminant curve of Figure 30 with or without simultaneous modulation. Although the tracking range naturally depended on discriminant slope, it was generally adequate for the requirements of the DPFM system. Typical results are those obtained with a subcarrier of 290 MHz ($\Delta\nu$ = 65 MHz). Here the system remained locked while the cavity mirror mount was translated a distance of about 1.4 microns (800 volts of correction signal).

SECTION 5

DP OPERATION OF A CO_2 LASER

5.1 INTRODUCTION

The output power capability of the CO_2 laser far exceeds that of any other gas laser. Furthermore, this laser's output wavelength at 10.6μ lies within an atmospheric transmission window. For these reasons the CO_2 laser is one of the most promising choices for optical communications, ranging and Doppler navigation. A major difficulty associated with practical applications of the CO_2 laser is that the electrooptic modulators that are available for 10.6μ radiation are not nearly as efficient as those available for visible and near IR radiation. For example, GaAs, which seems to be the best all-around material for CO_2 laser modulation, has a half-wave retardation voltage at 10.6μ of about 100 kV for a 1 cm cube. The corresponding figure for a $LiTaO_2$ 1 cm cube at .63μ is 2.7 kV.

In view of the lack of good electrooptic modulators for 10.6μ radiation, the application of techniques such as the DPFM which put a minimum requirement on modulator performance assume particularly great importance for the CO_2 laser. Furthermore, the narrow fluorescent line-width which characterizes the CO_2 laser necessitates some form of active frequency stabilization, if uninterrupted output is to be achieved during actual field use of any practical system employing this laser. In the paragraphs below some experimental studies are described which indicate that broadband DP frequency modulation of the CO_2 laser can probably be achieved using commercially available GaAs electrooptic modulators, without the use of excessive driving voltages. These studies furthermore imply that the DP frequency stabilization system, discussed above in Section 4 is a very promising approach to precise frequency stabilization of the CO_2 laser.

5.2 EXPERIMENTAL APPARATUS

The CO_2 lasers used for our DP experiments were all of the continuous flow variety and employed one opaque gold-coated mirror and one 95% transmitting dielectric-coated germanium mirror. In most cases the gold-coated mirror was mounted directly on the end of the laser discharge tube while the germanium mirror was remotely mounted on a gimballed suspension. The other end of the discharge tube was sealed with a NaCl window whose flat surfaces were normal to the tube's axis. An intra-cavity adjustable diaphram was inserted between the salt window and the germanium mirror so as to allow non-axial modes to be suppressed.

In the most successful discharge tubes used, the salt window and gold-coated mirror were gimbal mounted in the same way as the remote mirror. It was found that the O-ring seals at the ends of the discharge tube were sufficiently flexible to allow the gold-coated mirror to be aligned for maximum laser output and the salt window to be aligned so as to equalize the reflection losses for the mutually orthogonal states of laser output polarization. All of the discharge tubes used employed internal nickel electrodes and required approximately 20 milliamps of DC current for optimum operation. It was found that a gas mixture of 1 torr of CO_2, 1.5 torr of N_2 and 10 torr of He yielded maximum laser output. This gas mixture was used in all cases except when the dependence of laser output characteristics on pressure was being checked. Discharge tubes with lengths ranging from 1.5 meters to .5 meters and with bore diameters ranging from .4 cm to 1 cm were tested. As might be expected, it was found that the smaller bore tubes possessed higher gains than those with larger bores. However, the smaller bore tubes were very unstable, presumably because of oblique wall reflections by the internal laser beam. Our later, more successful work was done with a one centimeter bore tube.

The output of the CO_2 laser was passed through a germanium Brewster angle polarizer and allowed to strike the active element of a Philco-Ford model 6PC215 Ge:Au detector. The output of the detector was fed through appropriate audio rf amplifiers and directly monitored using an oscilloscope. During most of our work the length of the laser cavity was sinusoidally swept over about a 5μ range at a 60 cycle rate. This was achieved by mounting the remote germanium mirror on a piezo-electric transducer which was driven by a line power transformer. Laser output power ranged from a fraction of a Watt to about 5 Watts, depending on the length of the discharge tube and the size of the intracavity aperture. The laser used for many of the more recent studies is seen in Figure 32.

5.3 EXPERIMENTAL RESULTS

During the early phases of our CO_2 laser DP studies considerable difficulty was encountered in obtaining dual-polarization behavior. It subsequently found, however, that DP behavior could be obtained on a routine

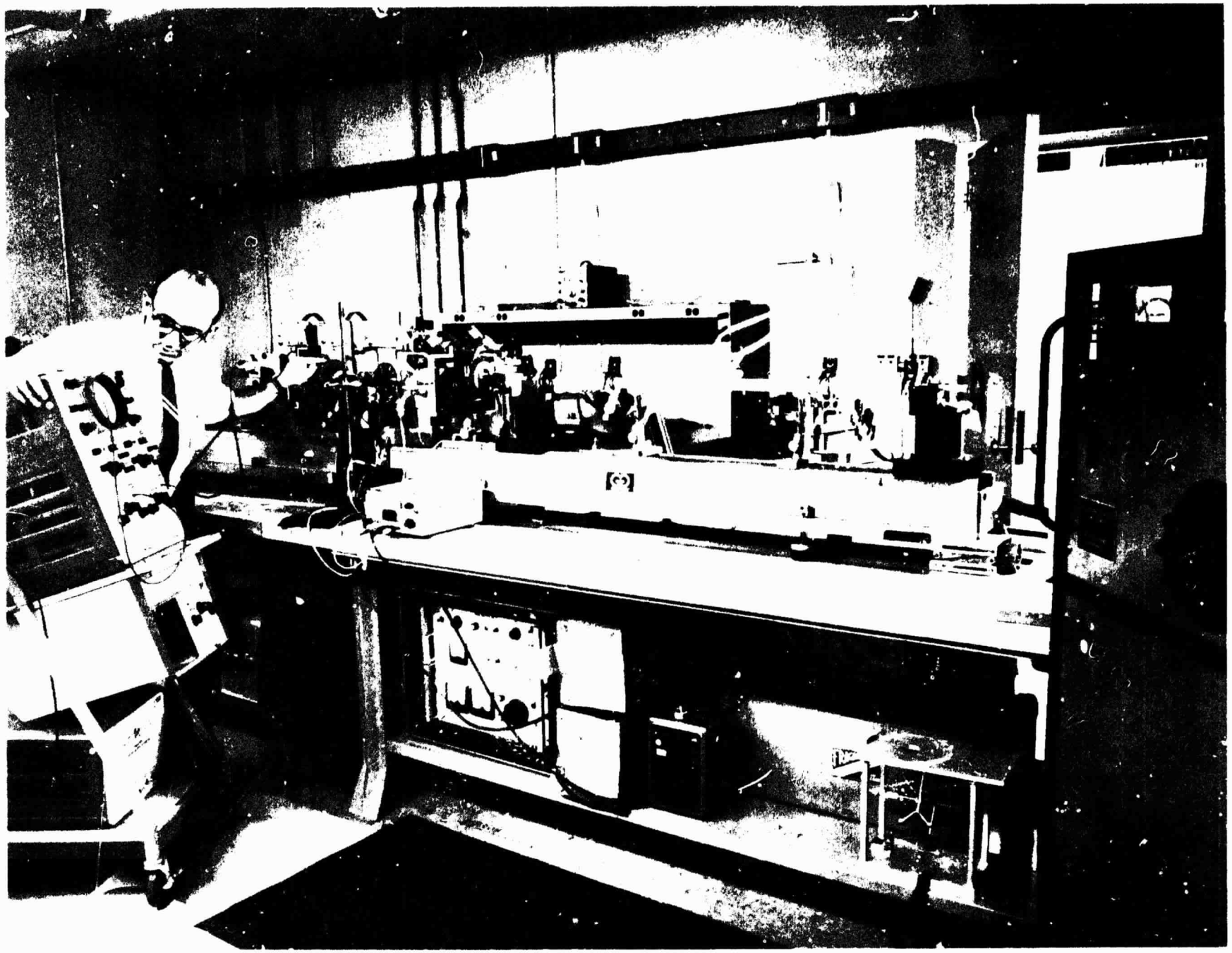

FIGURE 32. DUAL POLARIZATION CO_2 LASER AND ASSOCIATED EQUIPMENT

basis if the salt window of the discharge tube was tipped in such a way as to equalize reflection losses from mutually orthogonal states of polarization, and if, in addition, the mirror geometry of the laser cavity was arranged to yield a small laser mode size at the salt window. In retrospect, the latter requirement seems reasonable, since the smaller the spot size at the window, the less requirement is made on the window's optical quality. With no optical components inside the laser cavity other than the salt window, axial mode DP behavior has since been obtained with frequency splittings ranging from 1.5 MHz to less than .25 MHz, depending on the particular salt window used. In all cases in which DP behavior was observed, it was found to occur only when the laser oscillation frequency was very near the center of the laser's fluorescent line i.e., at near central tuning.

Our earliest attempts to control the DP splitting revealed that about a one MHz change could be produced by inserting a one-half inch thick NaCl flat into the cavity and compressing it to near its fracturing point. Additional preliminary attempts to vary the splitting involved applying voltage to a 2 cm long intracavity, longitudinal GaAs modulator and changing the orientation of a naturally birefringent CdS cube that was placed inside the laser cavity. It was found that splittings ranging from .5 MHz to 6 MHz could be achieved through use of the modulator and that splittings up to 10 megacycles could be obtained by properly tipping the CdS cube. However, since neither of these optical elements were anti-reflection coated, the laser output was very unstable during their use so that reproducible measurements could not be made.

Our more quantitative studies of DP CO_2 laser behavior began when we received a 5 cm long x 3 mm x 3 mm transverse GaAs electrooptic modulator crystal from Monsanto. This crystal, whose electrical properties are described above in Section 3.3 is anti-reflection coated at 10.6μ. It was mounted within the CO_2 laser cavity using an air cooled version of the type crystal holder that was used for our rare gas work (see Section 3.3). Because of the modulator's small transverse dimensions, laser action could not be achieved with the crystal in the cavity, unless it was placed near the 20 m radius curvature germanium mirror with the cavity arranged in a nearly hemispherical geometry. In this arrangement the mode size at the crystal is minimized. It was found that with the crystal removed from the cavity and with the intracavity diaphram restricted to equal the size of the modulator aperture, the laser output was about equal to that obtained with the crystal in and the aperture removed. This indicates that the reflection plus absorption losses of the crystal are small compared to the diffraction losses due to beam constriction. With the crystal in the cavity and the forced-air cooling in operation, a thermocouple attached to the crystal registered a negligible change in temperature over an extended period of time. Furthermore, laser stability was not significantly worse with the crystal in than it was with it out. It thus appears that crystal heating and distortion was not a serious problem for the power

densities used during our experiments. It was found emperically that fairly reproducible, stable behavior could be obtained with the crystal placed near the nearly flat mirror of a 153 cm long near-hemispherical laser cavity, if a 1 m long 1 cm bore discharge tube was used. Therefore, this arrangement was employed for the studies discussed below.

The static frequency characteristics of the DP CO_2 laser system described in the last paragraph were tested by applying various DC voltage levels to the electrooptic crystal and monitoring the laser output after it had passed through a properly oriented polarizer. Since, as mentioned above, DP behavior could only be achieved over a very restricted range of cavity tunings, these measurements were the most conveniently carried out by repetitively sweeping the cavity length through the weak-coupling region using the piezo-electric transducer. (See Section 5.2). At each modulator voltage, dual beam oscilloscope traces were used to display, (1) the DC output of the laser versus cavity tuning, and (2) the detailed waveform of the DP beat note that was obtained during weak coupling. A typical pair of dual beam traces photographed during these measurements is shown in Figure 33.

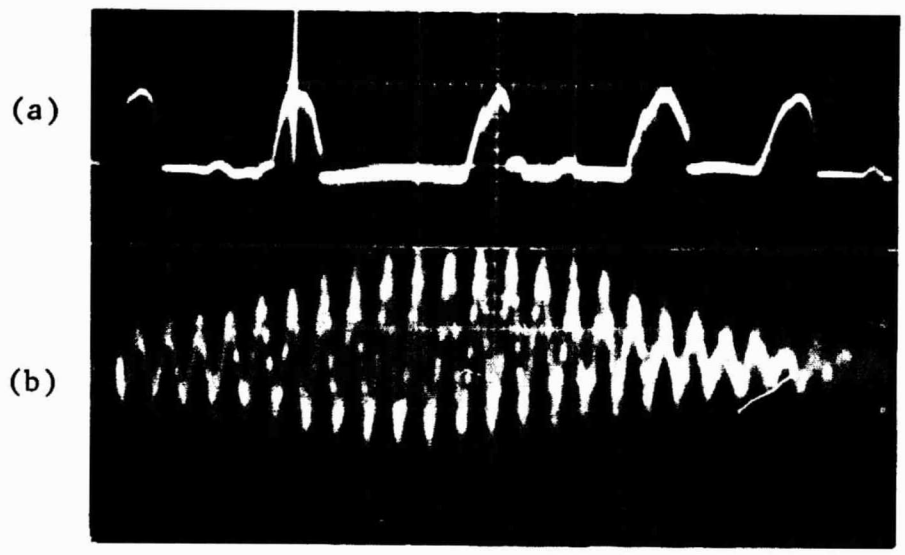

FIGURE 33. (a) LASER OUTPUT VS CAVITY LENGTH
THE POLARIZER IS 45° FROM THE PREFERRED DP POLARIZATION STATES. SWEEP SPEED = 2 msec/cm.
(b) SPIKED (WEAK COUPLING) REGION OF (a) DISPLAYED AT SWEEP SPEED = 2 μsec/cm.

In the upper trace (Figure 33a) the oscilloscope is line-triggered and the sweep rate is quite slow (2 msec/cm). The polarizer at the output of the laser is oriented at 45° with respect to the preferred DP polarization state so as to maximize the magnitude of the DP beat note. The fact that a number of bell shaped output profiles appear in Figure 1a indicates that under the experimental conditions that prevailed when the photographs were taken, several different rotational lines oscillated consecutively as the laser cavity length was swept. The narrow spike that appears near the center of the second profile from the left indicates that weak coupling occurred near central tuning for at least one of these rotational lines. The oscilloscope trace of Figure 33b displays the spiked region of Figure 33a at a much higher sweep speed (2μsec/cm). It is apparent that a fairly accurate value for the DP intermode splitting can be obtained by measuring the oscillation periods of the transient waveform shown in this trace. The splitting versus modulator voltage data plotted in Figure 34, were obtained in this way. Except for those points corresponding to the lowest modulator voltages, the measured frequency splittings of Figure 2 can be fitted quite well by a straight line having a slope 11 KHz/volt. For the 153 cm cavity length used, this slope corresponds to a half-wave modulator voltage of 8.9 kV. This value agrees satisfactorily with the value quoted by the crystal manufacturer, and with the results of our measurements at 3.4μ, (See Section 3.3). The deviation of the lower voltage points from a straight line is understandable since the natural birefringent axis of the salt window plus modulator crystal made an angle of 45° with the electrooptically induced birefringent axis. Several sets of data similar to that shown in Figure 34 were taken with different values of zero field birefringence. As would be expected, the frequency axis intercept of the resulting experimental curves varied from case to case, but the slopes at high voltages remained essentially the same.

It was observed that the DP beat note became steadily weaker as the frequency splitting was increased and that the highest frequency splittings at which DP behavior could be achieved was very dependent upon laser mirror adjustment, discharge tube current, and gas pressure. This behavior becomes readily understandable when it is realized that during our experiments the total optical frequency range over which oscillation on a single vibrational-rotational line could be sustained (hereafter referred to as $\Delta\nu_{osc}$) ranged from about 10 MHz to 34 MHz depending on the laser's excess gain. Hence, as the modulator voltage was increased the DP frequency splitting eventually exceeded $\Delta\nu_{osc}$ and it became impossible to observe a DP beat note. This situation is illustrated in Figure 35 where four oscilloscope traces, obtained at four different modulator voltages, are presented. At zero applied voltage a trace very similar to that shown in Figure 33a is obtained as the length of the laser cavity is swept (See Figure 35a). It should be noted that since the polarizer was set at 45° with respect to the birefringent axis the output profiles of Figure 35a appear smooth topped. Actually, there is an abrupt 90° change in the direction of laser output polarization as the central tuning region

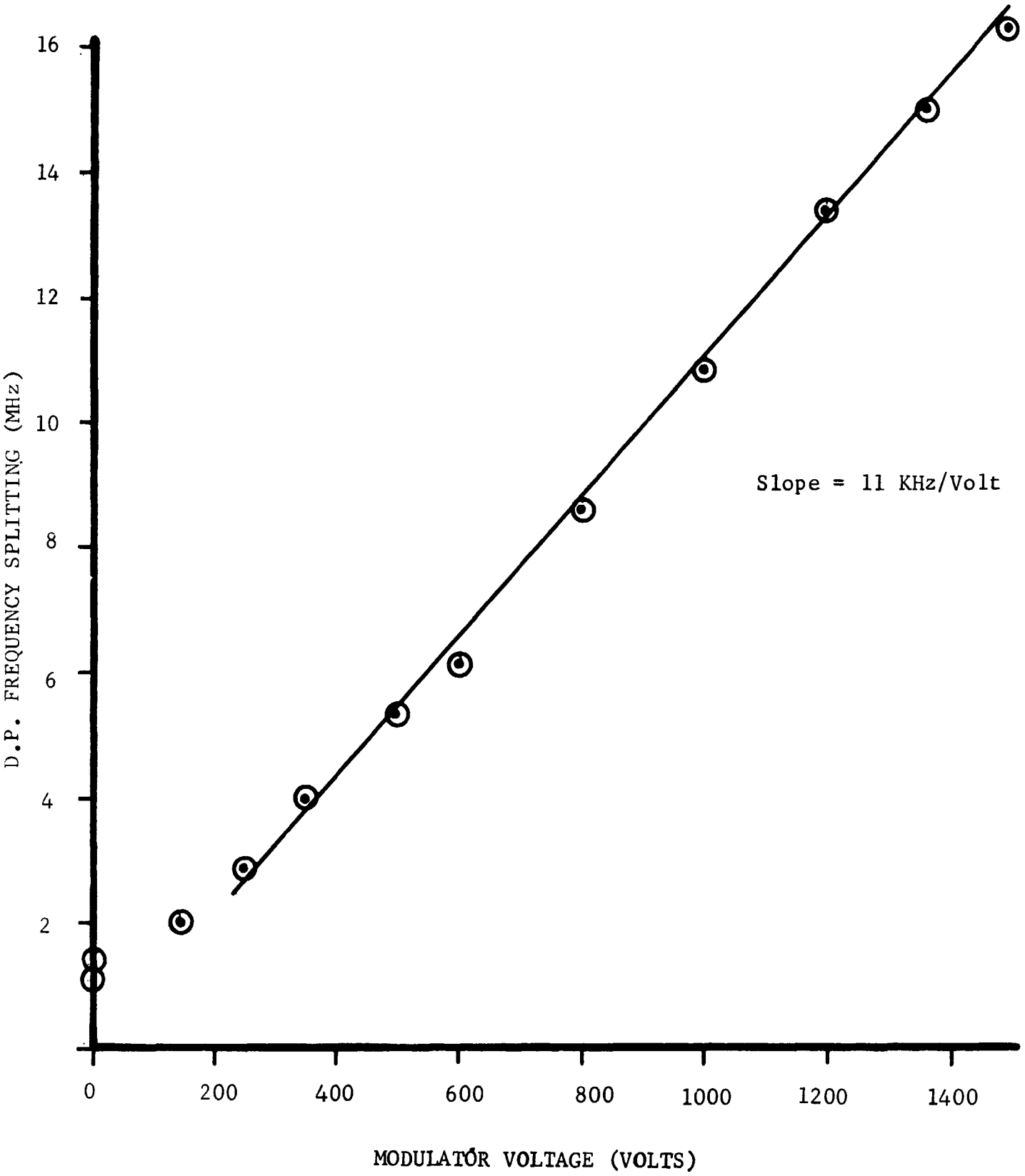

FIGURE 34. DUAL POLARIZATION FREQUENCY SPLITTING VS MODULATOR VOLTAGE.

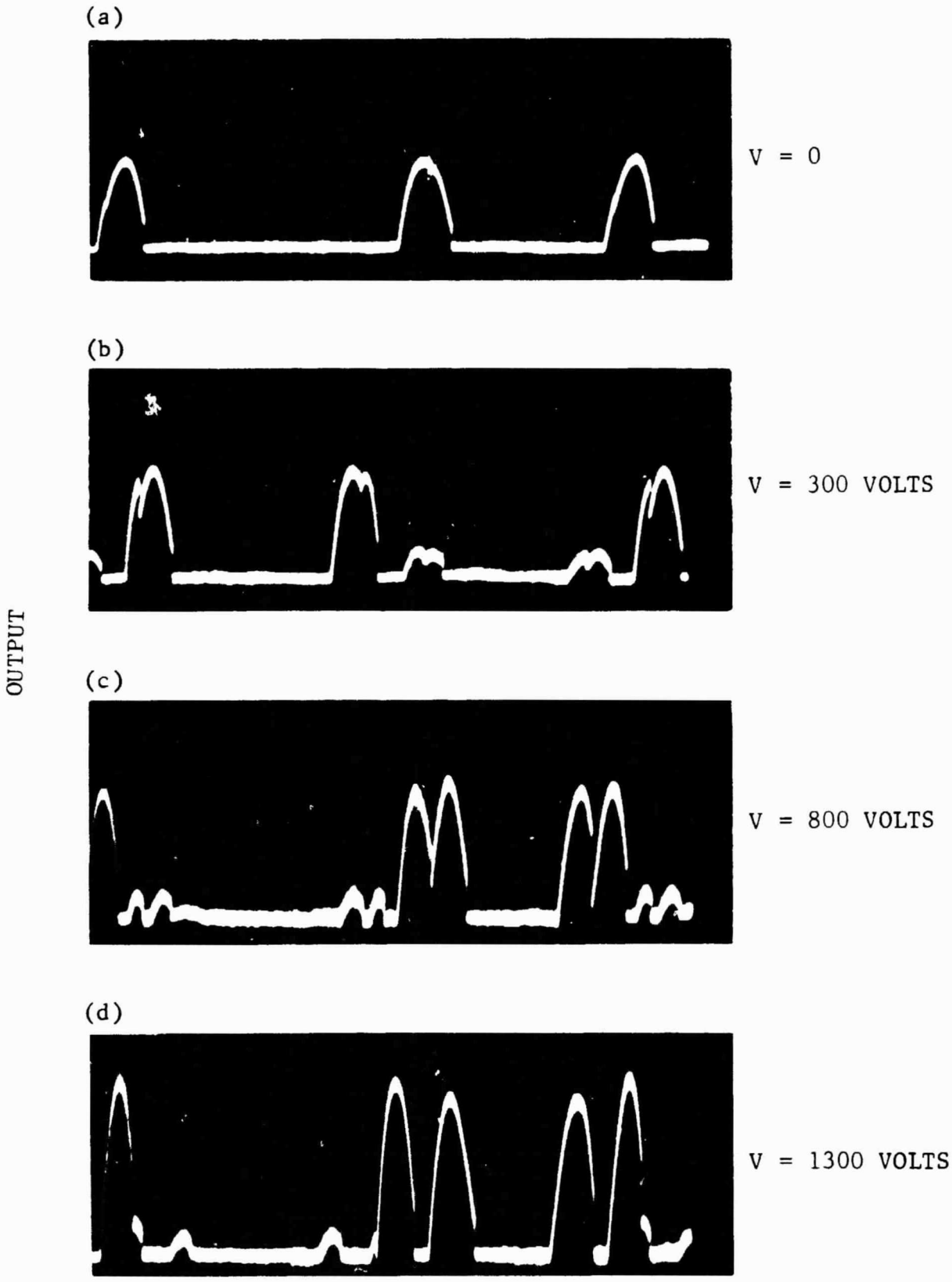

FIGURE 35. LASER OUTPUT VS CAVITY LENGTH FOR VARIOUS ELECTRO-OPTIC MODULATOR VOLTAGES. THE POLARIZER IS 45° FROM THE BIREFRINGENT AXIS OF THE TUBE CAVITY

is crossed. This fact is obvious in Figures 35b, through d, where an abrupt change in slope occurs at central tuning. Figures 35b and 35c indicate that as the modulator voltage is increased, the regions corresponding to oppositely polarized output draw away from each other, and finally in Figure 35d these regions are completely separated. Under the conditions of the last figure the DP frequency splitting (approximately 14 MHz) exceeds $\Delta\nu_{osc}$ and no DP beat can be observed.

In order to determine whether the strength of mode coupling varied significantly with frequency splitting, a systematic study was carried out in which pairs of oscilloscope traces similar to those shown in Figure 33 were taken at a variety of modulator voltages. In each case the ratio of the time during which weak coupling prevailed, Δt_{weak}, to the total oscillation time for a particular vibrational-rotational line, Δt_{osc}, was calculated. These ratios are plotted in Figure 36 as a function of DP frequency splitting. In reducing the data of this figure, Δt_{weak} was taken as twice the time necessary for the transient waveform to increase from one-half its maximum height to its maximum height.

Figure 36 indicates that $\Delta t_{weak}/\Delta t_{osc}$ decreases as the frequency splitting increases. This would seem to imply that the coupling becomes stronger as the DP modes move further apart. Behavior of this kind is completely contrary to the predictions of simple theory and is in marked contrast to what is generally observed using rare gas lasers. It should be noted that the ratio of Δt_{weak} to the time interval over which the excess gain of the laser would permit two modes spearated by the DP frequency splitting to oscillate simultaneously, is almost completely independent of DP frequency splitting.

In addition to the study of DP mode coupling versus frequency splitting at constant pressure described above, a study was conducted in which the frequency splitting was held fixed and the total gas pressure was varied. The results of this study are given in Figure 37. It is apparent from the figure that even at the lowest frequency splittings mode competition is substantially independent of gas pressure over a wide range of values. This behavior is quite surprising, since it seems to imply that the competition effects do not depend upon the collision broadened linewidth of the laser transition. Existing gas laser theories predict a marked dependence of this kind.

As a final experiment in this portion of the program, a preliminary demonstration of rf DPFM was made. Since the laser stability was not sufficient to allow steady-state two mode operation, observations were made while the cavity length was being swept. Photographs similar to Figure 33b revealed frequency excursions consistent with the dc response (Figure 34). A typical result was a peak excursion of 5 MHz with a drive of 300 Volts at 2.5 MHz and a subcarrier frequency of 13 MHz.

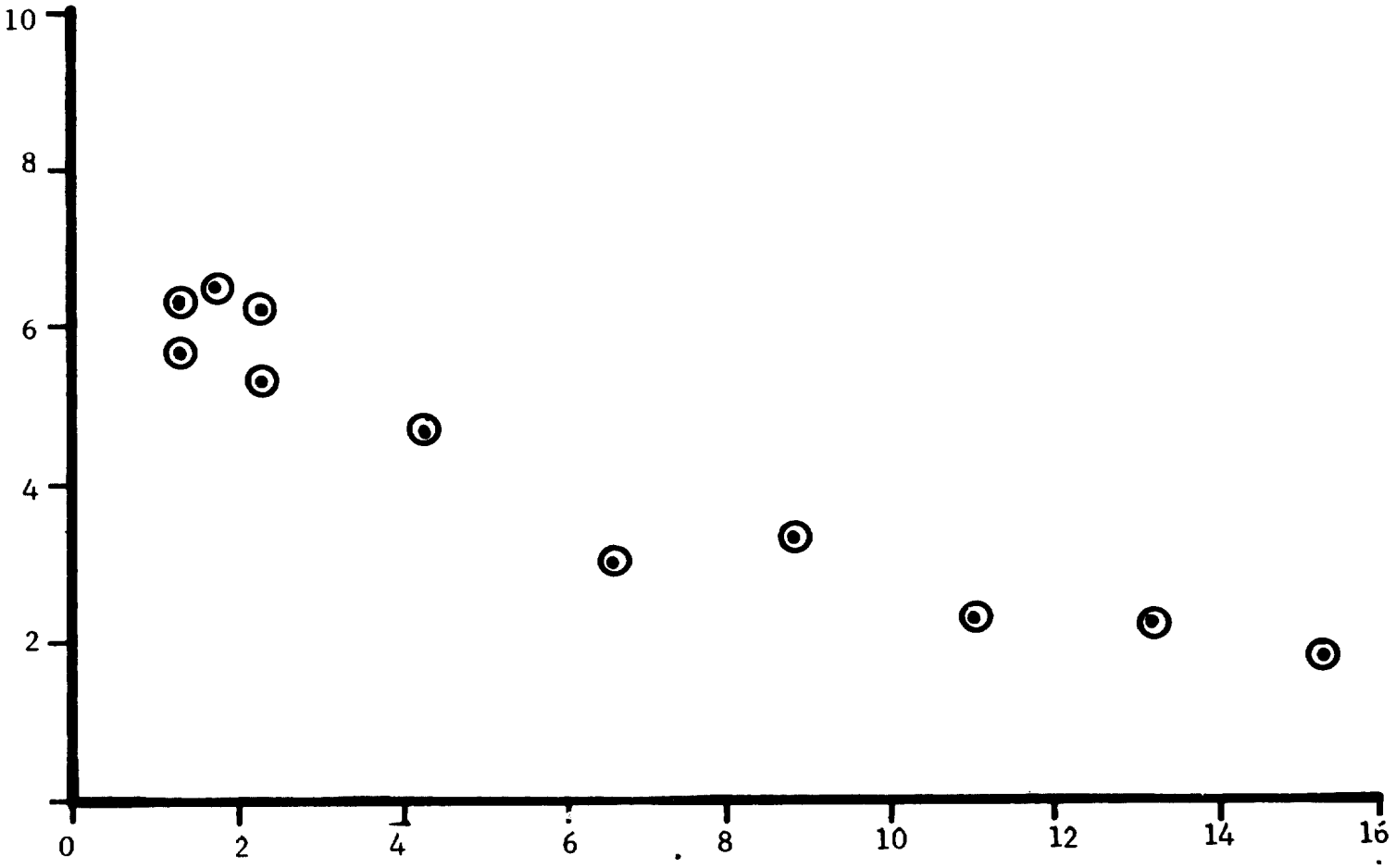

FIGURE 36. $\Delta t_{weak}/\Delta t_{osc}$ VS. D.P. FREQUENCY SPLITTING FOR AN EXPERIMENT IN WHICH THE LASER CAVITY LENGTH WAS SINUSOIDALLY SWEPT.
Δt_{osc} IS THE TIME INTERVAL OVER WHICH A SINGLE VIBRATIONAL-ROTATION TRANSITION OSCILLATED.
Δt_{weak} IS THE INTERVAL OVER WHICH WEAK COUPLING OCCURRED.
THE TOTAL GAS PRESSURE IN DISCHARGE TUBE IS 12.5 TORR.

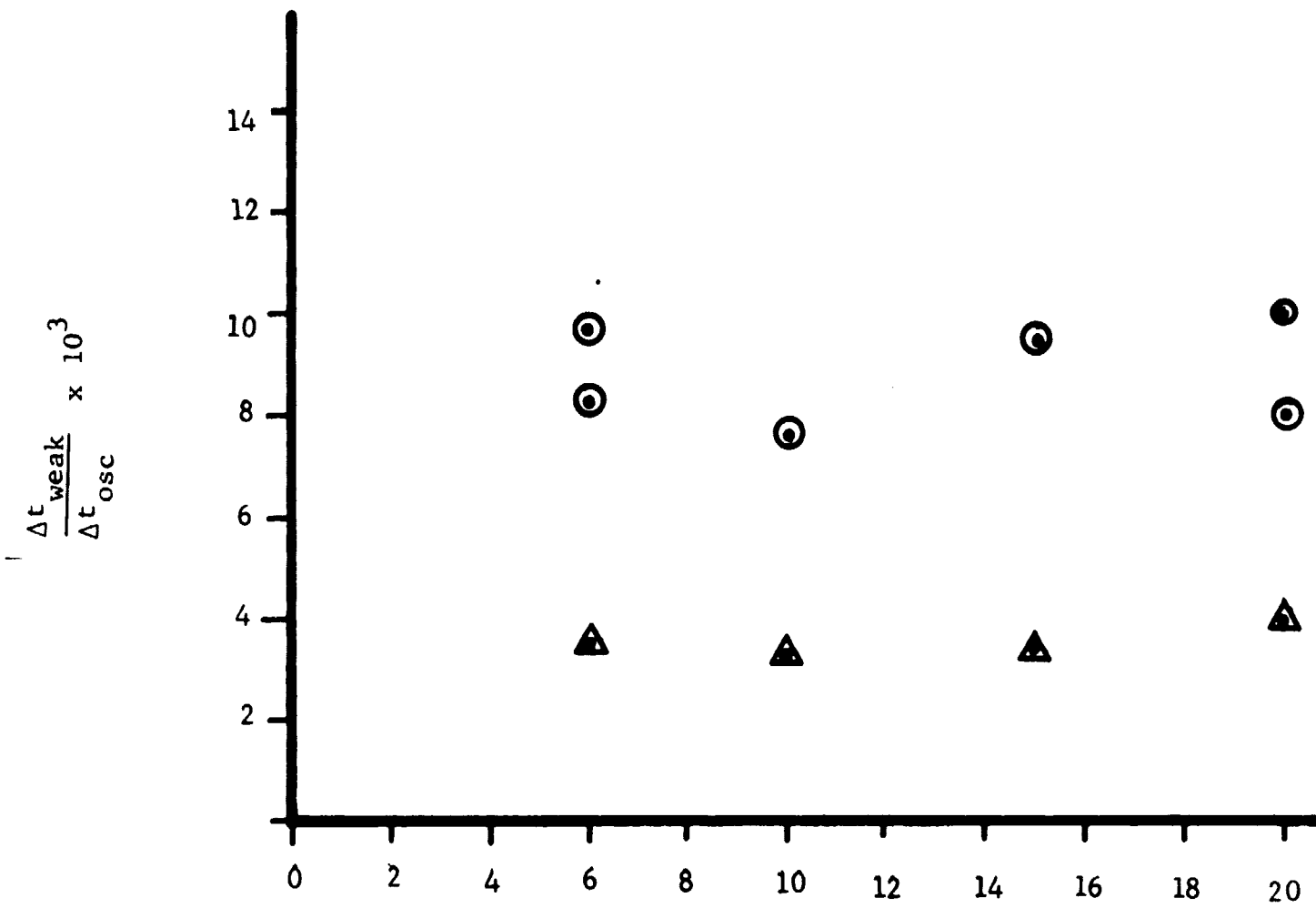

FIGURE 37. $\Delta t_{weak}/\Delta t_{osc}$ VS. TOTAL GAS PRESSURE IN DISCHARGE TUBE FOR AN EXPERIMENT IN WHICH THE LASER CAVITY LENGTH WAS SINUSOIDALLY SWEPT. Δt_{osc} IS THE TIME INTERVAL OVER WHICH A SINGLE VIBRATIONAL-ROTATIONAL TRANSITION OSCILLATED. Δt_{weak} IS THE TIME INTERVAL OVER WHICH WEAK COUPLING OCCURRED.

● ⇒ D.P. FREQUENCY SPLITTING = 1 MHz

▲ ⇒ D.P. FREQUENCY SPLITTING = 11 MHz

5.4 FREQUENCY STABILIZATION

In view of the very sharp crossover in the intensities of orthogonally polarized modes which occurs for the CO_2 laser near central tuning, it would seem that the frequency stabilization system described in Section 4 would be particularly well suited for use in conjunction with this laser. This fact motivated a preliminary attempt to frequency stabilize our continuous flow CO_2 laser. During this attempt the same apparatus as was described above in Section 4.2 was used except that the two photomultipliers were replaced by Barnes Engineering Thermistor Bolsometers and a Brewster angle, polarization dependent beam-splitter was used rather than a Wollaston prism.

It was found that the output of the CO_2 laser could be quite easily locked to a condition where a single linearily polarized oscillation with a stabilized intensity was obtained. Furthermore, a stabilization condition was achieved in which two orthogonally polarized modes oscillated simultaneously on two different vibrational-rotational transitions. However, a stabilization condition involving two stable orthogonally polarized modes oscillating on a single vibrational-rotational transition could not be obtained.

We attribute our initial inability to obtain a normal DP stabilization of our CO_2 laser to its poor free-running stability. Figure 36 and the discussions of Section 5.3 indicate that under the most favorable conditions weak coupling persists over a frequency interval which is less than 1% of the total frequency range for oscillation on a sirgle vibrational rotational transition. It is furthermore indicated in Section 5.3 that the total frequency range for oscillation on a single transition corresponds to less than 1/3 of the intermode beat frequency (that is 1/3 c/2L). These facts suggest that a cavity length change of less than $\lambda/600$ would cause the cavity tuning to sweep completely through the weak coupling region. It is thus apparent that a fairly high degree of passive stabilization would be necessary before a crossover lock-on could be achieved using our rather slow feedback circuitry. A program aimed at the design and construction of a sufficiently stable CO_2 laser of the static variety is currently underway at our laboratory. Since the narrowness of the weak coupling region necessitates the use of some form of active stabilization in order to retain weak coupling for any appreciable period of time, practical DP frequency modulation of the CO_2 laser appears to be contingent upon the successful completion of this stabilization program.

5.5 DISCUSSION

The experimental results presented above indicate that dual-polarization operation of a CO_2 laser can be achieved over a large range of frequency splittings. As would be expected, the upper limit on the obtainable frequency

splitting is set by the frequency range over which laser oscillation can be achieved on a single vibrational-rotational line. For a properly designed high gain CO_2 laser system this frequency range could easily exceed 50 MHz. On the other hand, the lowest achievable frequency splitting is determined by DP mode competition effects. These effects are apparently not well understood for the CO_2 laser. The existing theory of gas laser operation outlined in Section 2 seems to indicate that for the CO_2 laser weak coupling between orthogonal linear polarized modes should not prevail at frequency splittings much less than the pressure broadened linewidth. However, we have observed weak coupling at splittings of less than .25 MHz under conditions where the pressure broadened linewidth should have been well over 200 MHz. Current theory furthermore indicates that mode coupling for a DP gas laser should become weaker as the frequency splitting is increased and stronger as the pressure broadened line width becomes greater. In the case of the CO_2 laser, however, the competition appears to be essentially independent of both these parameters and to be almost solely dependent upon the excess laser gain. It seems clear that a good deal of theoretical work remains to be done before an adequate understanding of the dual-polarization CO_2 laser will be realized.

It was noted during the experimental observations discussed above, that whenever two vibrational-rotational transitions oscillated simultaneously, these transitions tended to oscillate in mutually orthogonal states of linear polarization. Hence, dual-polarization competition effects were evident even when the only interaction between the mutually orthogonal oscillations was through collisions of the participating molecules. This phenomenon is of considerable theoretical interest since it implies that the directional characteristics of a molecule can in some sense be preserved during a collision, even though its total angular momentum state is altered.

All of our experimental results indicate that even though linearly polarized DP output can be quite easily obtained from a properly designed CO_2 laser, this type output prevails only over a very restricted range of cavity tunings. This situation has the advantage of enabling the DP stabilization technique to be used to achieve very precise frequency stabilization, but it has the disadvantage of necessitating the use of active frequency stabilization in any practical CO_2 DPFM system. Since present theory predicts weak coupling of closely spaced orthogonal circularly polarized mode in a CO_2 laser it is plausible that the mode coupling would not be as critical if a circularly birefringent element were included in the laser cavity, (See Section 2). Verification of this point obviously will require further experimental work.

SECTION 6

CO_2 DP POLARIZATION MODULATION EXPERIMENTS

6.1 INTRODUCTION

The operation of the DP Polarization Modulation System is based on the same principles as that of the DPFM System. DPPM, however, capitalizes on the extreme sensitivity of laser output to the orientation of intracavity birefringence rather than to its magnitude, and as a result, has potentially an even greater modulation sensitivity than DPFM.

Most of the previous laser modulation experiments conducted in our laboratories have been concerned with the DPFM approach. Among the reasons for this are the noise surpression capabilities of fm, the extreme linearity of the DPFM system and the probability that this system is less sensitive to cavity mode width limitations than the DPPM system. During the course of our CO_2 experiments, however, it became apparent that the pm system was particularly attractive for use at 10.6 microns. First the lack of good modulator materials at this wavelength greatly enhances the importance of the extreme sensitivity inherent in the DPPM system. Second, the experiments reported in Section 5 of this report revealed that a CO_2 laser could be very easily operated in a single, strongly coupled, Dual Polarization mode. Finally the Doppler line characteristics of CO_2 are likely to be the ultimate bandwidth limiting factor for both the DPFM and DPPM systems so that the inherent bandwidth advantages of DPFM will not be important.

The preliminary experimental results presented below clearly indicate the potential usefulness of DP polarization modulation for CO_2 laser system applications. These results furthermore lay a substantial experimental groundwork for future development of this modulation technique.

6.2 PRINCIPLES OF OPERATION

As was illustrated in Section 2, both the frequency and polarization characteristics of an appropriately designed laser can be sensitively controlled by the use of intracavity birefringent effects. We have found experimentally, in fact, that even the weakest birefringent effects which we've been able to observe ($10^{-5}\lambda$ retardation) are sufficient to completely determine the polarization states of the laser output. This suggests that a weak birefringent modulator inside the cavity of a single mode, dual-polarization CO_2 laser could be used to periodically swing the polarization of the oscillating mode through 90^{o}. With the aid of an external polarizer, this polarization modulation could then be converted to 100% amplitude modulation.

Figure 38 shows an experimental arrangement that can be used to exploit the principle discussed in the last paragraph so as to achieve broadband modulation of the CO_2 laser.

In this arrangement a CO_2 dual-polarization laser is utilized which employs an intracavity electrooptic modulator. The length of the laser cavity and the diameter of the discharge tube are such that only one axial mode can oscillate at any given time. The window of the discharge tube is chosen to have as low a residual stress birefringence as possible

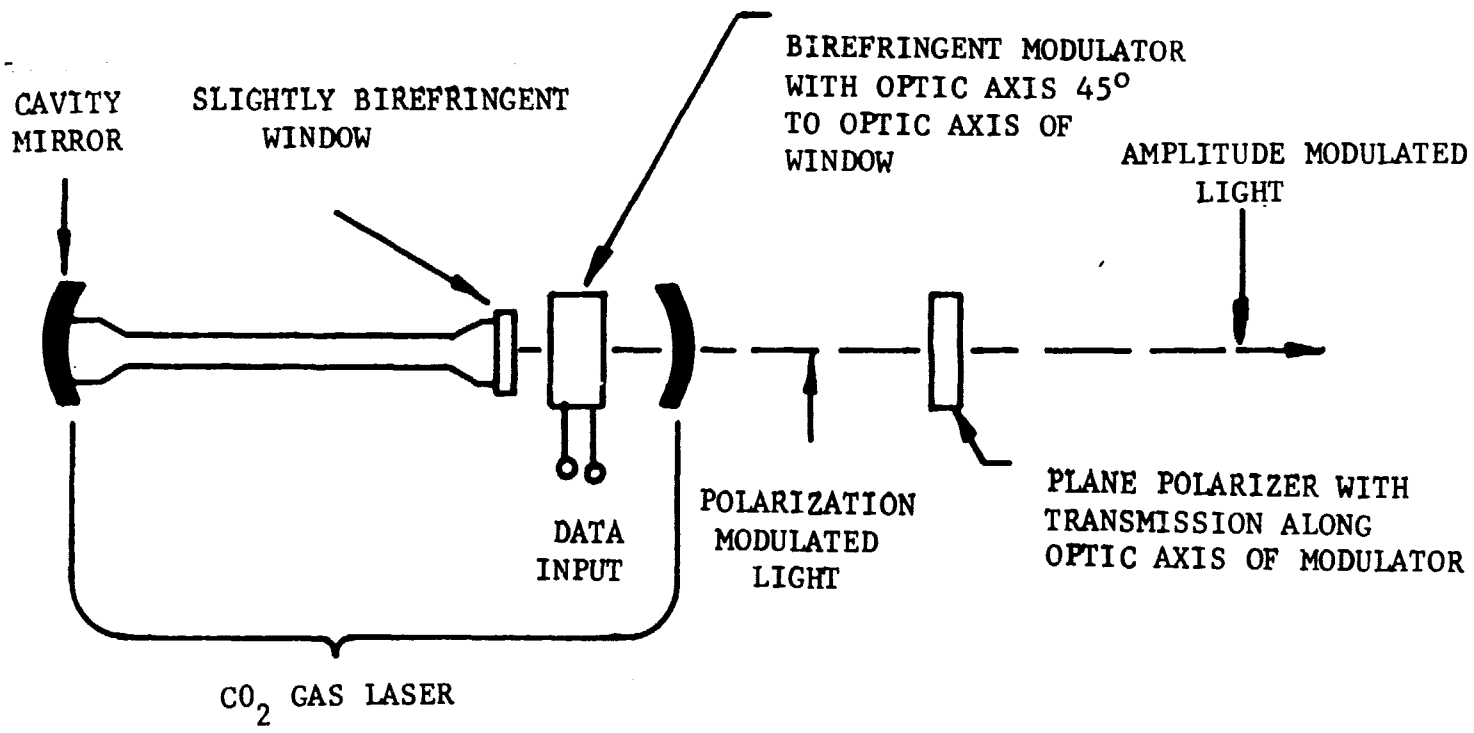

FIGURE 38. DP POLARIZATION MODULATION SYSTEM

and the electrically induced optic axis of the modulator is placed at 45^{o} with respect to the optic axis of the window.

It can be shown that, as far as dual-polarization laser operation is concerned, two intracavity birefringent components with non-parallel optic axes have the effect of a single birefringent component. A straightforward calculation indicates that if the angle between the optic axes of the elements is equal to 45^{o} and if one of the elements produces a fixed phase retardation φ_f while the other one produces a variable phase retardation φ_m, then the angle, β, between the effective optic axis of the combination and the optic axis of the element with fixed birefringence is given by:

$$\beta = \mathrm{Tan}^{-1}\left[\frac{(1 + r^2)^{\frac{1}{2}} - 1}{r}\right] \tag{37}$$

where

$$r = \frac{\varphi_m}{\varphi_f} \tag{38}$$

In the limit of $r \ll 1$ Equation (37) approaches:

$$\beta = \mathrm{Tan}^{-1}\left[\frac{r}{2}\right] \tag{39}$$

while in the limit $r \gg 1$ Eqn. (37) becomes:

$$\beta = \mathrm{Tan}^{-1}\left[\frac{r - 1}{r}\right] \tag{40}$$

If we identify φ_f with the fixed birefringent of the discharge tube window shown in Figure 38 and φ_m with the variable birefringent produced by the electrooptic modulator of that figure, then $r = 0$ when no electric field is applied to the electrooptic modulator. Hence Equation (39) and the discussion above indicates that the output of the laser will be linearly polarized along (or perpendicular to) the optic axis of the window. As the field on the modulator is increased r will increase and, according to Equation (37), so will β. Finally, a condition will be reached in which the electrooptically included birefringence will be much greater than the birefringence of the window. Under these circumstances $r \gg 1$ and Equation (40) implies that β approach 45^{o} so that the polarization direction of the laser output lies along the modulator's optic axis. As the field on the modulator decreases and passes back through zero, the polarization will reverse its behavior and at the opposite extreme of the voltage swing it will be along a direction that is perpendicular to the optic axis of the modulator. In this way, a 100% amplitude modulation can be obtained after the CO_2 laser output passes through the polarizer of Figure 38. The direction

of output polarization prior to turning on the electrooptic axis of the window, is determined by slight amplitude anisotropies in the cavity. It has been demonstrated experimentally that these anisotropies plus-non-linear hysteresis effects in the laser active medium are sufficient to prevent the polarization direction from suddenly switching through 90^{o} during the modulation process.

The modulated signal which reaches the detector of Figure 38 is given by the expression:

$$I(t) = \frac{I_o}{2}\left[1 + \sin 2\beta\ (t)\right] \tag{41}$$

Here I_o is the dc laser output power that would reach the detector if the polarizer were removed. Defining the depth of amplitude modulation as:

$$D_m = \frac{I(t)_{max} - I(t)_{min}}{I_o} \tag{42}$$

Equation (41) indicates that:

$$D_m = \sin 2\beta_{max} \tag{43}$$

where

$$\beta_{max} = \mathrm{Tan}^{-1}\left[\frac{(1 + r_{max}^2)^{\frac{1}{2}} - 1}{r_{max}}\right] \tag{44}$$

If the electrooptic modulator is driven by a sinusoidal voltage of the form:

$$V = V_p \sin \omega_m t \tag{45}$$

r_{max} assumes the form

$$r_{max} = \frac{(\varphi_m)_{max}}{\varphi_f} = \frac{(\Delta\nu_m)_{max}}{\Delta\nu_f} = \frac{V_p\, \partial(\Delta\nu_m)/\partial V}{\Delta\nu_f} \tag{46}$$

where

$(\Delta\nu_m)_{max}$ = electrooptically induced DP frequency splitting produced by modulator voltage V_p.

$\Delta\nu_f$ = DP frequency splitting due to the birefringence of the discharge tube window.

Equations (43), (44), and (46) are used in the analysis of the experimental data presented below in Section 6.3.

It is clear from Equations (40), (43) and (46) that essentially 100% amplitude modulation should be achievable using the system of Figure 38 as the maximum electrically induced birefringence of the modulator is considerably larger than the stress birefringence of the discharge tube window. In fact, an analysis carried out on the basis of these equations indicates that a $(\Delta\nu_m)_{max}/\Delta\nu_f$ equal to five is adequate to yield a 98% depth of modulation.[7] The analysis furthermore shows that the modulation process should be quite linear for modulation depths less than 75% $[(\Delta\nu_m)_{max}/\Delta\nu_f < 4]$. We have experimentally observed DP behavior in a 1 m long CO_2 laser which possessed a DP frequency splitting corresponding to a $\lambda/1250$ birefringent phase retardation in its discharge tube's window. Taking this laser as an example, the discussion above indicates that a $\lambda/250$ peak electrooptically induced phase retardation would result in 98% amplitude modulation. This figure should be compared with the $\lambda/4.5$ phase retardation that is necessary for 98% amplitude or polarization modulation outside the laser cavity.

It should be mentioned that we have found experimentally that a $\lambda/10^6$ phase shift is adequate to determine the polarization characteristics of a 1.15μ He-Ne laser. If, as is likely, this same magnitude phase shift should prove adequate for a properly designed CO_2 laser, minimizing the stress birefringence of the discharge tube's window should allow 98% amplitude modulation to be achieved through application of a $\lambda/2 \times 10^5$ peak electro-optically induced phase retardation.

6.3 EXPERIMENTAL RESULTS

The experimental arrangement used for our studies of CO_2 DP polarization modulation was identical to that shown in Figure 38. It employed a 1 m long, 1 cm ID discharge tube of the continuous flow variety and a 1.5 m long near hemispherical resonator. A 1.5 m radius of curvature gold coated cavity mirror was directly sealed to one end of the discharge tube while the other end of the tube was closed by means of a 1/8" thick NaCl optical flat. A remote, 20 m radius of curvature dielectric coated Ge mirror with 5% transmission completed the laser curvature. A 5 cm long Monsanto GaAs electrooptically induced optic axis at a 45° angle with respect to the salt window's axis.

The laser output was passed through a rotatable, Ge Brewster angle polarizer and allowed to strike the active element of a Philco-Ford Ge:Au detector. The output from the detector was fed through an appropriate amplifier and monitored by an oscilloscope. It was found that after a few minutes of initial warm-up the laser output would remain quite steady in intensity and would maintain the same state of linear polarization for periods exceeding 1/2 hour. Under these conditions the laser output power was typically about 1 Watt.

The initial quantitative experiment that was performed using our CO_2 polarization modulation apparatus involved checking (on a dc basis)[2] the dependence of laser output polarization on applied modulator voltage. During this experiment the dc voltage applied to the electro-optic modulator was set at various values and in each case the polarizer was oriented so as to give a null signal at the detector. The polarizer orientation versus voltage data are shown in Figure 39. The solid curve shown in this figure is a plot of Equations (37) with

$$r = V \frac{\partial(\Delta_m)}{\partial V} / \Delta\nu_f \tag{47}$$

where V = applied dc voltage.

At the onset of our experiment $\Delta\nu_f$ was measured and found to be equal to .710 MHz. Furthermore, a calculated value of

$$\frac{\partial(\Delta\nu_m)}{\partial V} = 11 \text{ kHz/volt} \tag{48}$$

was obtained for our experimental condition using the known electrooptic properties of the modulator crystal.

The experimental data presented in Figure 39 are obviously consistent with the theoretical predictions of Section 2. It is important to note that these data indicate a smooth variation in the direction of laser output polarization as the voltage applied to the modulator is varied from -300 volts to +300 volts. The fact that "polarization switching" does not occur during the polarization modulation process is of considerable importance for the successful operation of the modulation system under discussion.

After the theoretically predicted dependence of laser output polarization on voltage had been confirmed experimentally on a dc basis, an experiment was undertaken to check the low frequency modulation response of the system. This experiment involved driving the electro-modulator at various levels using the 60 Hz output from a line powered transformer. The polarization modulated laser output was passed through the polarizer, which was oriented with its passage directly along the electrically induced optic axis of the modulator, and was then mechanically chopped so as to enable its zero level to be established. Finally, it was allowed to strike the surface of the detector. At each modulator drive voltage, an oscilloscope photograph was taken of the detector output. A typical photograph, obtained in this way, is shown in Figure 40. The narrow striations visible on this photograph are due to the mechanical chopping of the laser beam.

In order to obtain a quantitative measure of the low frequency modulation capabilities of the DP polarization modulation system, the modulation depth (on the criterion on Equation (42)) was directly measured

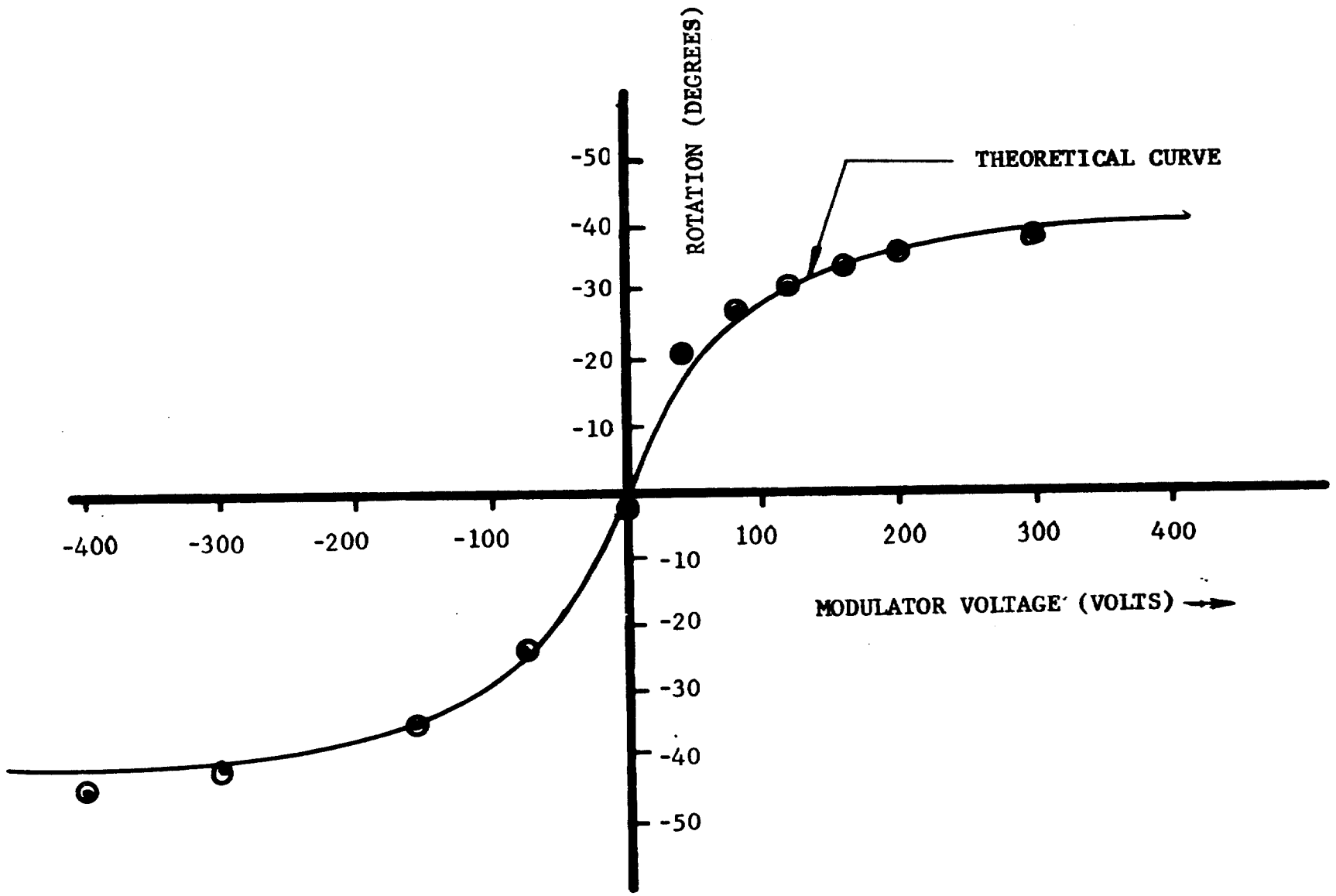

FIGURE 39. ROTATION OF LASER OUTPUT POLARIZATION VS APPLIED MODULATOR VOLTAGE. THE SOLID CURVE GIVES THE THEORETICALLY PREDICTED BEHAVIOR

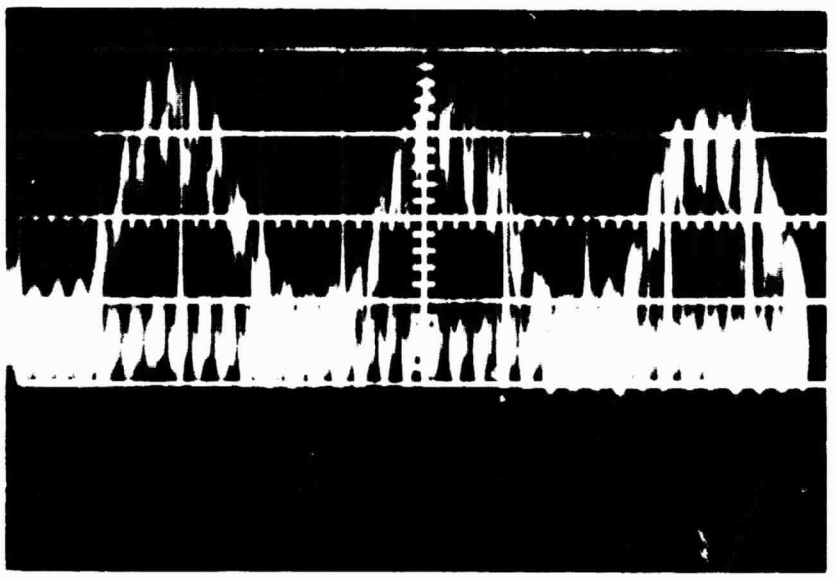

FIGURE 40. CO_2 LASER OUTPUT, AMPLITUDE MODULATED AT 60 Hz.
MODULATOR DRIVE VOLTAGE = 60 V_{rms}
DEPTH OF MODULATION $\simeq$ 70%
THE NARROW STRIATIONS ARE DUE TO MECHANICAL CHOPPING OF LASER BEAM. LITTLE OR NO HARMONIC DISTORTION IS EVIDENT.

from the oscilloscope traces mentioned above. The experimental data obtained in this way is presented in Figure 41. The depth of modulation versus modulation voltage curve that is theoretically predicted by Equations (43) through (46) under the conditions of our experiment is also plotted in this figure. This figure clearly indicates that the agreement between theory and experiment is reasonably good. It is worth noting that the theoretical curve of Figure 41 remains fairly linear up to a modulation depth of about 75%. Hence noticeable frequency distortions of the modulated output would not be expected to occur for modulation depths smaller than this value. This conclusion is substantiated by the approximately 70% modulated waveform of Figure 40. For the sake of comparison an 85% modulated waveform is shown in Figure 42. A small amount of frequency distortion is evidenced by a slight flattening out of the peaks and valleys of the waveform.

In addition to our low frequency modulation work, some effort has been devoted to observing rf amplitude modulation. Typical rf modulated waveforms, obtained at a drive frequency of 1.53 MHz and a drive voltage of 14 V_{rms}, are shown in Figure 43. Figure 43a is taken with a slow oscilloscope sweep speed so that the 1.53 MHz modulation appears as a continuous white area which fills the open portion of each chopper cycle. Figure 43b displays a portion of one of the white regions of Figure 43a

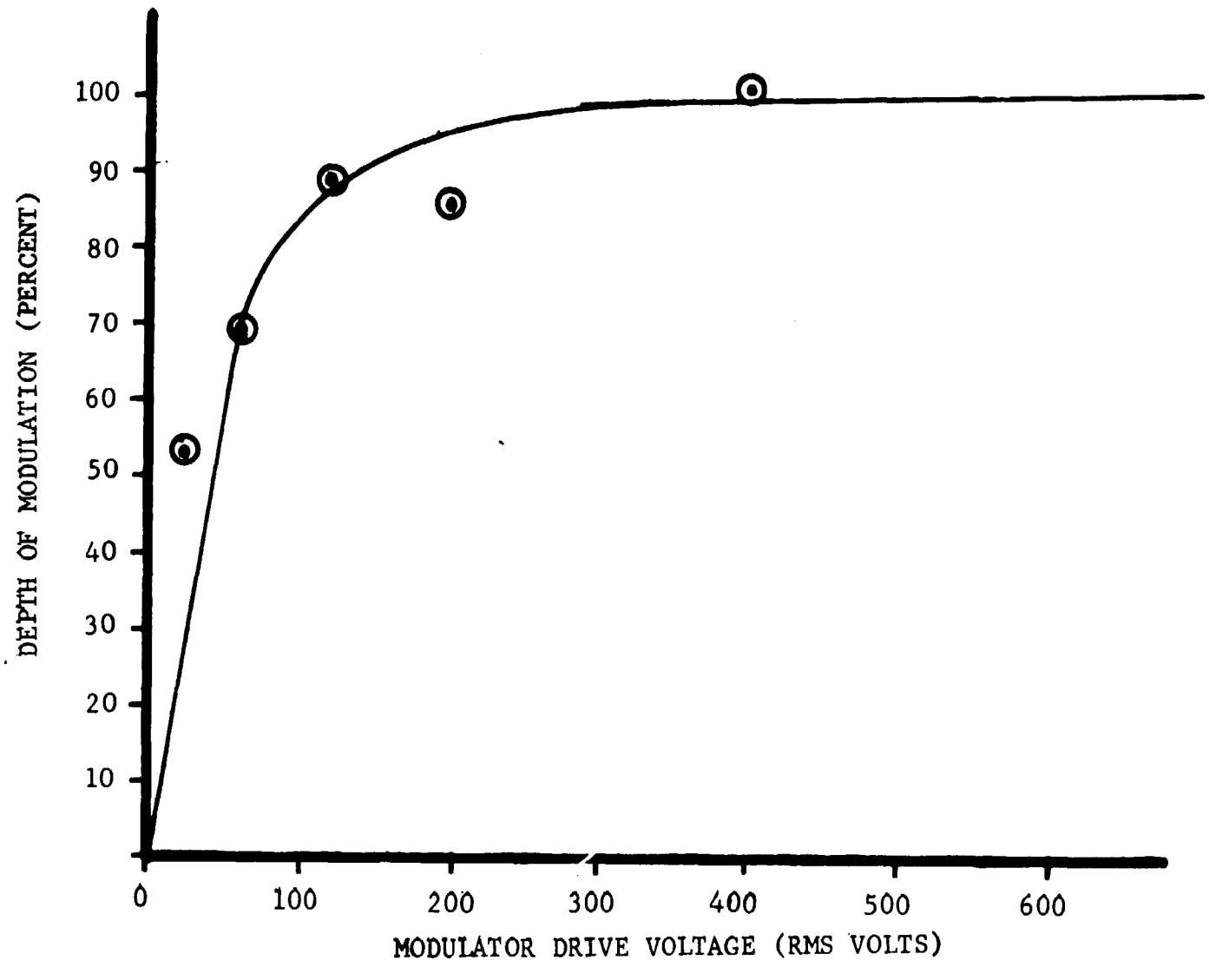

FIGURE 41. DEPTH OF AMPLITUDE MODULATION VS. MODULATOR DRIVE VOLTAGE.
MODULATION FREQUENCY = 60 HZ.
DP FREQUENCY SPLITTING = 1 MHZ.
THE SOLID CURVE GIVES THE THEORETICALLY PREDICTED BEHAVIOR.

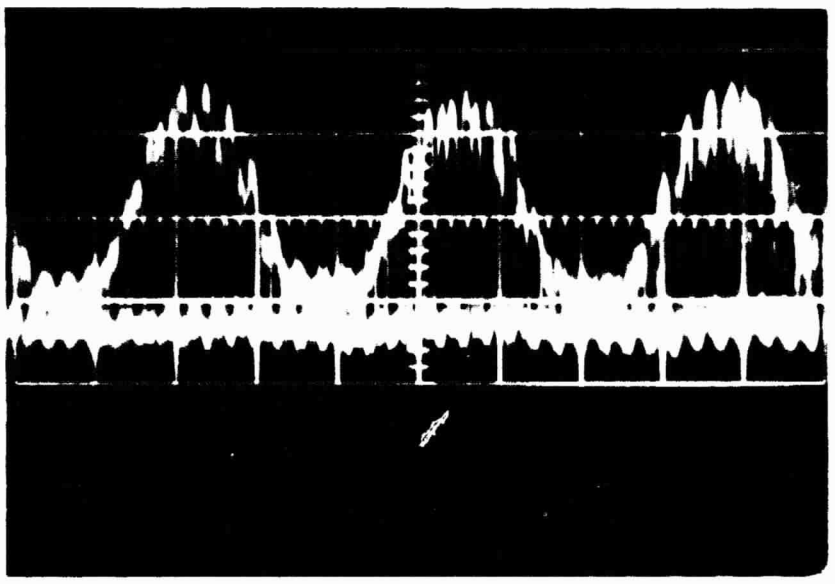

FIGURE 42. CO_2 LASER OUTPUT, AMPLITUDE MODULATED AT 60 Hz. MODULATOR DRIVE VOLTAGE = 120 V_{rms}. DEPTH OF MODULATION $\approx$ 85%. NOTICEABLE HARMONIC DISTORTION IS EVIDENT.

using a fast enough sweep speed to resolve the rf modulation. Measurements made on Figure 43a indicate that a 54% depth of modulation was achievable at the time the photographs were taken. This is considerably higher than is predicted by the theory presented above.

RF modulation was observed over a frequency range extending from about 700 kHz to over 5 MHz with drive voltages ranging from 12 V_{rms} to 140 V_{rms}. It was found that the drive voltage necessary to yield a particular depth of modulation varied widely from frequency to frequency, and that there was little correlation between the values predicted by theory and those actually observed. For example, in one measurement, at 3.05 MHz, a 140 V_{rms} drive yielded only 21% modulation while in the case illustrated in Figure 43, 14 V_{rms} yielded 54%. Furthermore, the depth of modulation seemed to be strongly dependent upon laser cavity tuning.

The reasons for the apparent departures of the measured rf voltage reaponse from the theoretical predictions are not yet known. The observed behavior could possibly arise because of: (1) resonant electrical coupling between the rf signal generator and the electrooptical crystal, (2) piezoelectric resonances in the GaAs crystal and/or (3) the inherent nature of the modulation process itself. Additional experimental work will have to be done before the actual cause can be pinned down and appropriate

(a)

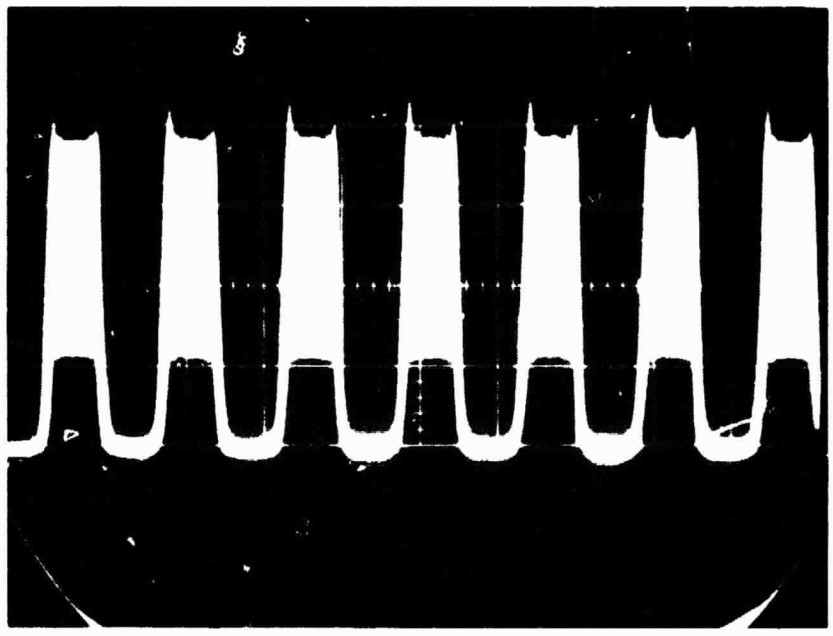

(b)

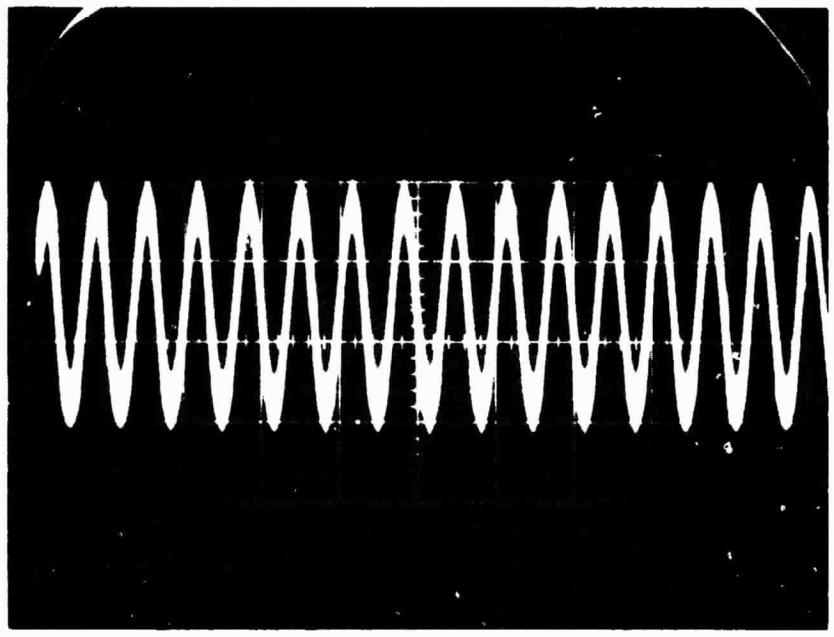

FIGURE 43. CO_2 LASER OUTPUT, AMPLITUDE MODULATED AT 1.53 MHz.
MODULATOR DRIVE VOLTAGE = 14 V_{rms}.
DEPTH OF MODULATION ≈ 54%.
(a) SWEEP SPEED = 1 msec/cm. UNRESOLVED RF MODULATION FILLS OPEN PORTIONS OF CHOPPER CYCLES.
(b) RF MODULATION WITH SWEEP SPEED INCREASED TO 1 sec/cm.

corrective steps taken. Furthermore, a more comprehensive theoretical evaluation of the modulation process will probably be necessary in order to gain an understanding of the role that cavity tuning plays in determining the achievable depth of modulation.

Because of the limited time available in the contractual period we have not attempted to directly determine the bandwidth capabilities of a CO_2 laser DPPM system. However, we have recently used the arrangement similar to that of Figure 38 to amplitude modulate the 80 MHz intermodes beat note derived from a dual-polarization He-Ne laser oscillating on two orthogonally polarized modes near 3.4μ. A 60% amplitude modulation at 50 MHz was achieved by applying 5 volts rms to an intracavity Monsanto modulator crystal. Hence, at 3.4μ the bandwidth capabilities of the modulation system under discussion seems to be at least comparable to that achievable using other optical data transmission systems. There is no ad hoc reason to believe that the situation should be any different at 10.6μ.

SECTION 7

CONCLUSIONS AND RECOMMENDATIONS

The work reported in the preceding sections has demonstrated to a considerable degree the practical advantages to be gained from the use of Dual-Polarization laser techniques in wideband optical communications. The He-Ne experiments discussed in Section 3, for example, established that highly linear fm information with bandwidths in excess of 100 MHz can be impressed on the output of a Dual-Polarization laser. The bandwidths observed are much greater than those implied by either the static laser response or the Fabry-Perot cavity characteristics. In addition, the work reported in Section 4 revealed that the operation of the Dual-Polarization Stabilization System is completely compatible with simultaneous modulation.

The CO_2 laser experiments are particularly significant since the high power and efficiency of this laser makes it quite attractive for deep space communication. The work reported in Section 5 demonstrates Dual-Polarization operation, frequency modulation, and active frequency stabilization of the CO_2 system. The results also indicated the possibility of achieving DP Polarization Modulation. Since this technique appeared to have distinct advantages over fm in the form of experimental simplicity and extreme sensitivity, it was pursued experimentally. The results given in Section 6 revealed the soundness of this approach. Modulation was accomplished at a number of frequencies from 60 Hz to 5 MHz with a typical requirement of 60 V_{rms} for 70% polarization modulation. In addition, a potential for much greater future sensitivity was experimentally indicated.

The program covered by this report has answered a large number of questions regarding the operation of Dual-Polarization lasers and their potential for practical utilization. At the same time, some quite significant new questions have been raised. The work reported in Section 5, for example,

revealed that CO_2 laser operation is inconsistent with the existing laser theories in at least two ways: (1) collision broadening apparently has little effect on nonlinear mode interactions, (2) the coupling of modes belonging to different rotational lines appears to be polarization dependent. Along more immediately practical lines, the initial success of the DPPM experiments raises obvious questions regarding the sensitivity, response linearity, and bandwidth ultimately attainable with this system.

Both the fundamental and practical questions mentioned above offer intriguing starting points for future research programs. In addition, the encouraging results of the present program suggest the desirability of undertaking the development of a CO_2 master oscillator using either the DPPM or the DPFM technique. Such a device would make possible a thorough demonstration of the capabilities of a CO_2 communication system. The above possibilities are recommended for future consideration.

In conclusion, we wish to acknowledge the general dependence of our laser research programs on continued support from Aeronutronic independent research and development funds. In particular, this support has made possible the fundamental and practical studies which laid the ground work for the present program. Some of these prerequisite studies are discussed in Sections 2, 5, and 6 of this report.

REFERENCES

1. W. M. Doyle and M. B. White, Appl. Phys. Letters 5, 193 (1964).
2. H. Hurwitz, Jr. and R. C. Jones, Jr. Opt. Soc. Am. 31, 493 (1941).
3. W. M. Doyle and M. B. White, J. Opt. Soc. Am. 55, 1221 (1965).
4. W. M. Doyle and M. B. White, Phys. Rev. 147, 359 (1966).
5. W. M. Doyle, W. D. Gerber, P. M. Sutton, and M. B. White, IEEE, J. Quant. Electronics QE-1, 181 (1965).
6. Investigation of Dual Polarization Laser Modulation, Aeronutronic Proposal No. P-16330(U).
7. P. V. Lenzo, E. G. Spencer, K. Nassau, J. Opt. Soc. Am. 56, 633 (1966).
8. S. Namba, J. Opt. Soc. Am., 51, 76 (1961).
9. F. Sterzer, D. Blattner, S. Miniter, J. Opt. Soc. Am. 34, 62 (1964).
10. K. Nassau, H. J. Levinstein, G. M. Loicono, J. Phys. Chem. Solids, 27, 989 (1966).
11. E. H. Turner, Appl. Phys. Letters, 8, 303 (1966).
12. P. H. Smakula, P. C. Claspy, 17th Annual Northeast Electronic Materials Conference, Boston, Proclaime, August 1966.
13. T. E. Walsh, R.C.A. Review, Volume XXVII, No. 3, September 1966.
14. Specification Sheet, MM40, Electro-Optic Modulator Crystal Monsanto, St. Louis, Mo., May 1968.
15. R. T. Denton, F. S. Chen, A. A. Ballman, J. Appl. Phys., 38, 1611 (1967).
16. F. A. Jenkins and H. E. White, "Fundamentals of Optics,"(McGraw-Hill Book Co. Inc., New York, 1957).
17. J. Brown and E. V. D. Glazier, "Signal Analysis," (Reinbold Publishing Corp., New York 1964).
18. R. S. Carson, "Principals of Applied Electronics," McGraw Hill Book Co., New York 1961.
19. W. B. Bennett, Jr., Appl. Optics, Supplement, 24 (1962).
20. W. M. Doyle and M. B. White, Appl. Phys. Letters 10, 224 (1967).
21. W. M. Doyle, W. D. Gerber and M. B. White, 1968 International Quantum Electronics Conference., paper P-5, to be published in IEEE, J. Quant. Electronics.
22. C. J. Savant, "Basic Feedback Control System Design, McGraw-Hill Book Co. New York, 1958.